SMOULDERING OCEANS:
ON THE PHOTOCHEMICALLY MEDIATED OXIDATION OF DISSOLVED ORGANIC CARBON IN COASTAL WATERS

by

HEATHER ERIN READER

(Under the Direction of William L. Miller)

ABSTRACT

Marine dissolved organic carbon (DOC) is one of the largest and most dynamic pools of reduced carbon on earth. Photochemical processes have the potential to significantly affect the content of this DOC pool. Photochemical oxidation to carbon monoxide and carbon dioxide are two direct pathways for the removal of DOC from the marine system. Indirectly, photochemical processes can lead to the removal of DOC through the alteration of chemical structures rendering them more biologically labile. In order to assess the influence of photochemistry on the coastal carbon cycle the variability of these processes must be well constrained. To calculate photochemical production in marine waters, it is crucial to know how light is absorbed by chromophoric dissolved organic matter (CDOM), as well as the spectral efficiency of the resulting photochemical reactions (i.e. the apparent quantum yield (AQY) spectra).

The challenges of using visible wavelength CDOM absorption data to model ultraviolet absorption data are investigated. Direct measurements of ultraviolet absorption data model photochemical processes best. When this is not possible, visible data can be used with an accuracy of +/- 10% in coastal waters. Either a hyperbolic absorption model or one using correction factors applied to a traditional exponential model will allow for similar accuracy in the ultraviolet portion of the absorption spectrum.

The variability of photochemical oxidation of dissolved organic carbon in a coastal system was studied in order to constrain remote sensing calculations. The variability of CO and CO_2 AQY spectra were relatively well constrained in three estuaries of Georgia, USA. The AQY for CO varied within +/- 12.7% year-round while CO_2 varied within +/- 33.6% year-round. Hyperspectral remote sensing reveals fine-scale hydrodynamic structure in estuarine systems and is readily adaptable to photochemical modeling applications.

Defining the variability of photochemistry's influence on the biological lability of DOC is a complex undertaking. Unlike direct photochemical oxidation of DOC to CO and CO_2, the biologically labile products (BLPs) of incomplete oxidation can themselves be photochemically reactive. Competition between production and destruction of BLPs during irradiation is a significant consideration when determining the quantitative influence of photochemistry on marine systems.

INDEX WORDS: Photochemistry; Carbon Monoxide; Carbon Dioxide; Biological Lability; Dissolved Organic Carbon; Chromophoric Dissolved Organic Matter; Remote Sensing; Estuaries

SMOULDERING OCEANS:
ON THE PHOTOCHEMICALLY MEDIATED OXIDATION OF DISSOLVED ORGANIC MATTER IN COASTAL WATERS

by

HEATHER ERIN READER

B.Sc.H., University of Calgary, Canada, 2005

A Dissertation Submitted to the Graduate Faculty of The University of Georgia in Partial Fulfillment of the Requirements for the Degree

DOCTOR OF PHILOSOPHY

ATHENS, GEORGIA

2011

SMOULDERING OCEANS:

ON THE PHOTOCHEMICALLY MEDIATED OXIDATION OF DISSOLVED ORGANIC CARBON IN COASTAL WATERS

by

HEATHER ERIN READER

Major Professor:	William L. Miller
Committee:	Mary Ann Moran Wei-Jun Cai Melissa Booth Richard Zepp

Electronic Version Approved:

Maureen Grasso
Dean of the Graduate School
The University of Georgia
May 2011

DEDICATION

To my parents, John and Sheila, whose love and support has helped me become the person I am today.

ACKNOWLEDGEMENTS

There are many people that I have encountered over the past six years of this PhD journey that I want to thank. First my advisor, Bill Miller, who has been fun to work with and who has taught me many things, about science and about everything else. I would also like to thank my committee members who have all been helpful with details and methods as well as the big picture. Thanks to the staff of the University of Georgia Marine Institute and the Georgia Coastal Ecosystems Long Term Ecological Research Project, who helped me with sampling, setting up my lab and all the other things that come along with working and living on Sapelo Island. Thanks to my Island friends, Mary D, Ruth, Brenda, Jason, Ike and Kendra, Mary P, without you guys my fieldwork would have been much harder! My lab mates, past and present and even the ones who left before I got here! Cedric, Adair, Leanne, Fang, Joanna, and Lori, you've all been great to work with! My other MarSci friends, Sylvia and Adrian, Christine, Marcia, and Jennie, Joan and Wade, you've all helped me along the way. The Seays (and now Miltiades) have been so great to me over the past six years and I can't thank you all enough for being my family away from home! Rachel, Aaron and Jonah Luther, I don't know what to say, without you guys, I would have been homeless for a least a while, haha! Thanks for everything! Finally and most importantly, I'd like to thank my family for being supportive and loving and for just being my family.

TABLE OF CONTENTS

APPENDIX

LIST OF TABLES

LIST OF FIGURES

Page

CHAPTER 1

INTRODUCTION AND LITERATURE REVIEW

1.1 Dissolved Organic Carbon

Dissolved organic carbon (DOC) in the ocean is a dynamic pool in the global carbon cycle. With a total size of 662 Pg of carbon, the oceanic DOC pool is comparable in size to the atmospheric reservoir of carbon dioxide (~800 Pg) [*Canadell et al.*, 2007; *Hansell et al.*, 2009]. Radiocarbon estimates of the age of the oceanic DOC pool suggest that the turnover time of bulk DOC in the ocean is on the scale of a few hundred years. More recent research shows evidence for a portion of the DOC pool that turns over quite rapidly, and another less labile portion that turns over on the scale of millennia [*Carlson*, 2002]. The present model has DOC on a continuum of lability, with a small portion falling on the "very labile" side of the continuum and the majority of DOC falling on the "refractory" side [*Carlson*, 2002; *Nagata*, 2008].

Rivers contribute a significant flux of DOC into the oceans. Most of this riverine DOC is thought to be soil derived from the continents, though some in situ riverine production may also occur [*Ludwig et al.*, 1996]. The total riverine flux of DOC to the ocean is estimated as ~0.2 Pg C/year [*Ludwig et al.*, 1996]. The coastal ocean therefore receives a large amount of DOC and is thereby is an important area for carbon cycling. Biological production also contributes to the DOC pool of the ocean through processes such as the release of phytoplankton exudates, viral lysates, the degradation of primary production and more, and is especially important in the open ocean [*Carlson*, 2002]. The labile portion of dissolved organic matter (DOM) supports the marine food web by providing substrate for heterotrophic bacteria [*Pomeroy*, 1974].

Structural characterization of DOC has proven difficult because of the many distinct sources and processes that affect the composition of DOC in the ocean. Traditionally, natural organic matter (NOM) has been separated into three large groups; humin, humic acids and fulvic acids. These three groups are distinguished by their solubility at different pH, with humin being the insoluble in water at all pHs, humic acids being soluble only at pH>2 and fulvic acids remaining soluble at all pHs. This working definition arose from work on soil organic matter, and while much riverine DOC is derived from soil, it is not necessarily an appropriate definition for marine systems [*Mopper and Kieber*, 2000]. Nevertheless, the word “humic” continues to be applied to marine-derived sources of DOM. Other attempts to characterize the marine DOC pool involve using techniques such as ultrafiltration and reverse osmosis where the DOC is separated into groups based on molecular size [*Mopper et al.*, 2007]. More recently, the technique of high-resolution Fourier-transform ion cyclotron resonance mass spectrometry (HR FT-ICR-MS) has been shown to be a powerful tool in the characterization of DOC [*Kujawinski et al.*, 2004; *Kujawinski et al.*, 2009; *Stubbins et al.*, 2010] and useful in the characterization of DOC transformations [*Minor et al.*, 2007; *Stubbins et al.*, 2010]. The work with high resolution mass spectrometry has revealed the presence of over 10,000 distinct mass values in some samples, confirming the complexity of the DOC [*Mopper et al.*, 2007].

1.2 Chromophoric Dissolved Organic Matter

Chromophoric dissolved organic matter (CDOM), is the fraction of the DOC pool that absorbs solar radiation. Formerly referred to as gelbstoff, gilvin, or yellow substances, it absorbs strongly in the UV and blue portions of the spectrum, and when present in high concentrations, imparts a yellowish hue to the water in which it is dissolved [*Bricaud et al.*, 1981]. CDOM, though only a fraction of total DOC, is as structurally complex as DOC, and the same issues in characterization of CDOM exist. Additionally, it requires the knowledge of its absorption characteristics, by definition. The most common property measured for CDOM is the UV-visible absorption spectrum. Because of this, a common working definition of CDOM is a measure of absorbance for that fraction of seawater passing though a 0.2 μm filter in units of m^{-1}. The UV-visible absorption spectrum of CDOM is generally characterized by a monotonically decreasing signal as wavelength increases [*Bricaud et al.*, 1981]. The cause of this featureless spectrum has been debated in recent years. One model suggests a series of individual overlapping absorption spectra, with stronger absorption in the UV and blue due to aromatic structures in the CDOM [*Blough and Del Vecchio*, 2002; *Stedmon and Markager*, 2003]. A more recent model presents evidence for an electronic charge transfer among the absorbing moieties of the CDOM, resulting in a continuum of absorption across the spectrum [*Boyle et al.*, 2009; *Del Vecchio and Blough*, 2004].

The CDOM spectrum has long been approximated by an exponentially decreasing function,

$$a_g(\lambda) = a_g(ref) * e^{-S(\lambda-\lambda_{ref})} \qquad (1.1)$$

where a_g is the absorption coefficient (m^{-1}), λ is wavelength (nm), *ref* refers to a reference wavelength, and S is the spectral slope coefficient, so called because it determines the slope of the exponential curve [*Bricaud et al.*, 1981; *Jerlov*, 1976]. The spectral slope coefficient (S) is a widely reported variable in the CDOM literature [*Blough and Del Vecchio*, 2002](and references therein). The value of S is said to increase with decreasing CDOM concentration (i.e. in the oligotrophic ocean), and decrease in coastal and dark waters, where the CDOM concentrations are higher [*Blough and Del Vecchio*, 2002]. Although this trend exists within single data sets, S is largely dependent on the instruments used and the wavelength ranges modeled, making comparison between data sets difficult [*Blough and Del Vecchio*, 2002]. The discrepancies between data sets arise in part because the absorption spectrum of CDOM only approximates an exponential shape. It is not exactly exponential over all wavelengths, and the deviations from such occur along differing portions of the spectrum, especially in the blue and UV regions of the spectrum [*Helms et al.*, 2008; *Loiselle et al.*, 2009; *Twardowski et al.*, 2004]. Recently, the specific spectral slope ratios have been suggested as more indicative of CDOM characteristics than the spectral slope alone. Helms et al. [2008] suggest a slope ratio calculated as $SR = S_{275\text{-}295}/S_{350\text{-}400}$ as a good indicator of molecular size, with the higher the value, the larger the average molecular size of the CDOM. Taking this approach further, Loiselle et al. [2009] and Bracchini et al. [2010] have developed spectral slope "curves", which are essentially a first derivative of the absorption curve, and have found them useful for indicating source material, and past processing (biotic and abiotic) of the CDOM.

Along with absorption spectroscopy, fluorescence spectroscopy also has proven to be a useful tool in the study of CDOM. Excitation-emission matrix (EEM) spectroscopy has been employed to examine the complex fluorescence of CDOM, where the emission spectrum is scanned over a range of excitation wavelengths, and the result is a 3-D matrix of fluorescent information [*Coble*, 1991; *Coble et al.*, 1993]. As may be expected from the shape of the absorption curve of CDOM, the fluorescent DOM (FDOM) EEM is rather smooth, but there are distinct excitation-emission pairings which indicate differing source material. For example, marine-type humics excite and fluoresce at lower wavelengths than terrestrially sourced DOM [*Coble*, 1991]. Early studies in EEMS focused on a qualitative assessment of where peaks of fluorescent activity fell in the matrix [*Coble*, 1991; *Coble et al.*, 1993], while more recent studies have applied a statistical approach, parallel factor analysis (PARAFAC) to the EEMs for a more quantitative analysis of the data [*Stedmon and Markager*, 2005; *Stedmon and Bro*, 2008; *Walker et al.*, 2009]. The study of EEMS is allowing for more study of the absorbing fraction of DOC, and is deepening the understanding of the sources of these compounds in the marine environment and even their history, as evidence of transformation processes, such as photobleaching can be seen in some reports [*Del Vecchio and Blough*, 2002].

1.3 Photochemical Transformations of Chromophoric Dissolved Organic Matter

Photons absorbed by CDOM can lead to various reactive transients. Energetically excited DOM can return to its ground state by internal energy conversions and energy release such as fluorescence and phosphorescence. Release of absorbed energy can also include chemical reactions such as the transfer of energy from an excited DOM molecule to ground state oxygen to create reactive oxygen species (ROS) such as superoxide, singlet oxygen or hydroxyl radical [*Mopper and Kieber*, 2000]. These can, in turn, induce further chemical reactions in the DOM. Direct photochemistry such as photodecarbonylation and photodecarboxylation of DOM moieties are also likely consequences of photon absorption by DOM [*Mopper and Kieber*, 2000].

Photochemical reactions in natural waters have been studied for many years. Early studies focused on the photoreactivity of reactive intermediates, such as hydrogen peroxide and superoxide [*Cooper et al.*, 1988; *Micinski et al.*, 1993; *Moffett and Zafiriou*, 1993; *Zika et al.*, 1985], and on production of easily identifiable low molecular weight carbon products such as pyruvate and carbon monoxide [*D J Kieber et al.*, 1989]. Many of the first studies focused on products of biological importance, such as the production of easily consumable carbon products [*D J Kieber et al.*, 1989; *R J Kieber et al.*, 1990; *Wetzel et al.*, 1995; *Zafiriou et al.*, 1984; *Zhou and Mopper*, 1997]. The ability of photochemical processes to oxidize DOC and remove it from the organic pool raised interest in the impact photochemical processes in the ocean had on the global carbon cycle [*Miller and Zepp*, 1995; *Mopper and Kieber*, 2000; *Mopper et al.*, 1991; *Zafiriou et al.*, 1984; *Zika et al.*, 1993]. The photoproduction of CO and CO_2 represent the two direct photochemical routes to the mineralization of DOC in the surface ocean. Indirectly, photochemistry can also lead to mineralization of carbon through production of biologically labile carbon products from previously refractory carbon. These three photochemically mediated pathways will be the focus of this dissertation.

1.3.1 Carbon Monoxide

Photochemical production of CO is the dominant source for the chemical in the world's oceans. CO has two strong loss terms in the surface ocean. First, CO has been shown to be an efficient energy source for certain marine bacteria [*Tolli et al.*, 2006], secondly, air-sea exchange can also be an important loss term for CO, due to its insolubility in the ocean thereby bypassing the microbial loop and contributing directly to the mineralization of DOC. In the marine environments, the concentration of CO exhibits a strong diurnal signal, with a peak in mid-late afternoon [*Zafiriou et al.*, 2008] due to its strong photochemical source and two efficient sink mechanisms. The efficiency of photoproduction and the two major loss terms described above keep the total concentration of CO low in the ocean, varying around average concentrations of 12 nM and ~2 nM in the coastal and open ocean respectively [*Zafiriou et al.*, 2003; *Zafiriou et al.*, 2008].

The analytical methods for detection of low concentrations of CO in seawater are relatively straightforward and the detection limits are quite low (nanomolar concentrations of CO in headspace injections into a gas chromatograph), and thus the photochemical production of CO has been well studied. Most studies have concentrated on the photochemical production of CO in coastal and oligotrophic waters [*Law et al.*, 2002; *Stubbins et al.*, 2006; *White et al.*, 2010; *Xie et al.*, 2009; *Zafiriou et al.*, 2003; *Ziolkowski and Miller*, 2007]. The efficiency of photochemical production of CO seems to be relatively constant from over the world's ocean waters [*Zafiriou et al.*, 2003] though some reports indicate that the efficiency of photochemical production of CO is higher inshore than offshore, indicating that the source material of the CDOM is important

[*Ziolkowski and Miller*, 2007]. Recent studies on the photochemical activity of CO show that there can also be significant dark production of CO in marine waters [*Zhang et al.*, 2008], as well as photoproduction from particulate organic matter [*Xie and Zafiriou*, 2009]. These two extra sources of CO production that have been ignored in the past could increase even further the significance of this important trace gas in the mineralization of organic matter in natural waters.

1.3.2 Carbon Dioxide

Another photochemical route to mineralization of DOM in natural waters is through the production of carbon dioxide [*Johannessen and Miller*, 2001; *Miller and Zepp*, 1995; *White et al.*, 2010]. Photochemical production of CO_2 has been studied extensively in freshwater systems [*Anesio and Graneli*, 2003; 2004; *Bertilsson and Tranvik*, 2000; *Graneli et al.*, 1998; *Salonen and Vahatalo*, 1994]. Due to analytical constraints related to the carbonate system in marine waters, the photochemical production of CO_2 has not been studied to the same extent in the oceans. Oceanic studies comparing the photochemical production of CO and CO_2 have found that the efficiency of production of CO_2 appears to be around 15-20 times higher than that of CO [*Gao and Zepp*, 1998; *Miller and Zepp*, 1995; *Miller and Moran*, 1997]. More recent studies suggest that this ratio is considerably more variable, ranging form 2- 98 depending on the source [*White et al.*, 2010]. While there is variation of this ratio among different water types, this makes CO_2 the largest identifiable photoproduct in natural waters, followed by CO. Though the ocean as a whole acts as a sink for atmospheric CO_2, some coastal areas, notably estuaries, have been shown to be seasonal, if not year-round, sources of CO_2 to the atmosphere [*Cai*, 2011; *Guo et al.*, 2009; *Jiang et al.*, 2008a; *Jiang et al.*, 2008b]. The influence of photochemistry on these systems has not yet been explicitly studied.

1.3.3 Biologically Labile Products

While CO and CO_2 are readily identifiable using conventional analytical methods, CDOM and many of its photochemical products remain largely unidentifiable due to the complex nature of the mixture. Generally, CDOM is seen as being part of the non-labile portion of DOM, with respect to biological consumption. There is evidence that exposure to ultraviolet radiation (UVR) can alter the biological lability of DOM. Many early photochemical studies showed production of low molecular weight carbon substrates [*D J Kieber et al.*, 1989; *R J Kieber et al.*, 1990; *Wetzel et al.*, 1995; *Zafiriou et al.*, 1984; *Zhou and Mopper*, 1997]. Many studies, however, concentrate on the overall effect of photochemistry on the biological lability of the entire DOC pool, rather than just the production of specific compounds [*Miller and Moran*, 1997; *Mopper and Kieber*, 2002; *Obernosterer and Benner*, 2004; *Tranvik and Bertilsson*, 2001]. These types of studies require a proxy for bacterial response to photochemical transformations, such as the effect on total microbial respiration, or bacterial production as measured by uptake radiolabeled compounds such as leucine or thymidine. Mopper and Kieber [*Mopper and Kieber*, 2002] compiled a review of 59 studies on the effect of photochemistry on biological activity, which showed a range of -75% to +200% change in biological activity depending on the source material and the proxy used to determine biological activity. Out of the total of 59 studies Mopper and Kieber [2002] found that 38 of the studies showed an enhancement of DOM lability after UVR exposure and 21 studies show no effect or a negative effect. The studies of terrestrially dominated waters, such as those in coastal marine areas, tended to show enhanced DOM lability after UVR exposure. Photochemistry can therefore be an indirect route to mineralization of DOM through increases in bacterial activity.

1.3.4 Photochemistry and the Carbon Cycle

Recent work estimates the global oceanic photoproduction of CO to be in the range of 30 – 84 Tg C /year [*Fichot and Miller*, 2010; *Stubbins et al.*, 2006; *Zafiriou et al.*, 2003]. Using an average ratio between CO_2 and CO photoproduction rates of 20, as previously stated, this translates to a low value for the CO_2 photoproduction in the global ocean of 600 Tg C /year, and an upper estimate of 1680 Tg C /year. The conservative end of this estimation would mean that around 1/1000 of the total pool of DOC in the ocean being oxidized to CO and CO_2 by photochemistry directly each year. This number is somewhat lower than previous estimates [*Mopper and Kieber*, 2000], due to better constraints on the global photoproduction of CO made in recent years. It is, however, on the order of ~10 - 20% of yearly new production in the oceans (7.2 Pg /year, [*Hansell and Carlson*, 1998]) and ~5-6% of the total yearly marine production [*Gehlen et al.*, 2006]. See Table 1.1 for a simplified comparison of these and other fluxes.

Based on various other studies of the enhancement of bacterial activity by UVR treated DOM, it is estimated that photochemically mediated oxidation of DOM through enhanced microbial activity is on the order of direct photomineralization to CO_2 [*Miller and Moran*, 1997]. Though these estimates are based on limited studies they indicate that photochemistry, through the sum of direct oxidation and photochemically mediated stimulation of bacterial consumption of DOC, has the potential to mineralize nearly half of new production in the global ocean annually.

Table 1.1 Comparative global carbon fluxes

Flux	Amount (Tg C/year)	Reference
Riverine DOC to Ocean	200	[*Ludwig et al.*, 1996]
Global oceanic new production	7200	[*Hansell and Carlson*, 1998]
Contemporary air-sea flux of CO_2 (inversion model)	1700 +/- 400	[*Gruber et al.*, 2009]
Contemporary air-sea flux of CO_2 ($p$$CO_2$ climatology)	1400 +/- 400	[*Gruber et al.*, 2009]
Global export production	~8000	[*Gehlen et al.*, 2006]
Total global oceanic production	~30000	[*Gehlen et al.*, 2006]
Global oceanic photoproduction of carbon monoxide	30 - 84	[*Fichot and Miller*, 2010; *Stubbins et al.*, 2006; *Zafiriou et al.*, 2003]
Global oceanic photoproduction of CO_2 (using CO:CO_2 1:20)	600 – 1680	[*Miller and Zepp*, 1995]
Total oceanic photochemical mineralization (CO, CO_2, BLP)	1500 - 3454	[*Miller and Zepp*, 1995; *Mopper and Kieber*, 2000]

1.4 Modeling Photochemistry

To apply a quantitative model of photochemical reactions in the ocean there are three quantities that must be known: (1) the light available in the system, (2) the fraction of light that is absorbed by the CDOM (i.e. the absorption coefficient of the CDOM) and (3) the photochemical efficiency of the reaction under consideration, or its apparent quantum yield. Each of these quantities is spectral and the general model used to calculate photochemical production in the ocean is

$$\frac{d[product]}{dt}(\lambda,z) = E_0(\lambda,z) * a_g(\lambda,z) * \Phi(\lambda,z) \tag{1.2}$$

where the concentration of product per unit time (e.g. $mol/m^3/day$) is a spectrally and depth dependent. $E_0(\lambda,Z)$ is the scalar irradiance (mol photons/m^2/day), $a_g(\lambda.z)$ is the absorption coefficient of the CDOM (m^{-1}), Φ is the AQY (unitless), and each of these quantities is spectrally and depth dependent. Integrated total photochemical production is calculated as

$$\sum_0^z \sum_{290}^{490} \frac{dP}{dt} = E_0 * a_g * \Phi \tag{1.3}$$

where dP/dt is summed over both depth and wavelength.

1.4.1 E_0, Scalar Irradiance

Scalar irradiance represents the three-dimensional light field available for absorption by CDOM present in the ocean [*Jerlov*, 1976; *Mobley*, 1994]. It can be broken down into an upwelling component, $E_{0u}(\lambda,z)$ and a downwelling component, $E_{0d}(\lambda,z)$. Though there is the possibility of particulate backscatter and in shallow locations, bottom reflectance, the magnitude of the upwelling component of irradiance is generally much smaller than that of the downwelling component, and in photochemical situations can largely be ignored [*Fichot and Miller*, 2010]. Therefore the scalar irradiance can be approximated by

$$E_0(\lambda,z) \approx E_{0d}(\lambda,z). \qquad (1.4)$$

The quantity $E_0(\lambda,0)$, the scalar irradiance at the very surface of the ocean, can be measured in various ways; both multiband instruments detecting several discrete wavelengths of interest, and spectroradiometers equipped with monochromators which allow a high resolution spectral response are employed. However, for the purposes of large regional photochemical calculations it is often more useful to employ a radiative transfer model that can take into account the latitudinal region of interest and estimate atmospheric constituents which absorb and scatter solar radiation on its transit to the earth's surface, providing irradiance values over large areas of the ocean at once.

Regardless of the method chosen to obtain surface irradiance, once that value just above the surface is known (i.e. $E_0(\lambda,0^+)$), it must be translated across the air-sea interface, to be used in oceanic photochemical calculations. Phenomena such as surface reflectance and refraction must be taken into account. Gregg and Carder [1990], performed a comprehensive analysis of various surface ocean phenomena and their interaction with light in the ocean. The effect of wind speed in creating waves and sea foam and the subsequent effects on how light reflects off the surface of the water under those were all taken into account, and indeed this approach for radiative transfer across the atmospheric-ocean boundary is what is used for further calculations in this dissertation, following the methodology laid out in Fichot and Miller [2010].

With $E_0(\lambda,0^-)$, or the downwelling scalar irradiance just below the surface of the water, one can calculate the depth resolved irradiance with the attenuation of light within the water column described as follows,

$$E_0(\lambda,z) = E_0(\lambda,0^-) * e^{-K_0(\lambda)*z} \tag{1.5}$$

where K_0 is the diffuse attenuation coefficient, and has units of m^{-1}. Attenuation of light in the water column is affected by detrital particles, biological particles including using light for photosynthesis (i.e. chlorophylls, phycobiliprotein, carotenoids). As previously mentioned, CDOM is a strong absorber of UVR in the ocean, fueling photochemistry in the ocean.

Attenuation of radiation in the water column can be measured with light profiling instruments, and the attenuation coefficients can be calculated from that data. It is important to note that K_0 is also a spectral quantity and the various wavelengths in the solar spectrum are attenuated at different rates. In the UV, the majority of light attenuation is due to absorption by CDOM [*Bricaud et al.*, 1981; *Fichot and Miller*, 2010]. The remote sensing algorithm, SeaUV [*Fichot et al.*, 2008] can retrieve attenuation coefficients from multiband remote sensing reflectance data (using data from the SeaWiFS sensor), and is employed later in this dissertation in order to perform remote sensing photochemistry calculations.

1.4.2 a_g, Absorption Coefficient

Not only is it necessary to know how solar radiation is attenuated in the ocean, by knowing K_0, it is important to know what portion of the attenuated light is absorbed by CDOM. CDOM is operationally defined as the fraction of light absorbing material that passes through a 0.2 μm filter. Determining how much of light is absorbed by CDOM in a given sample of seawater is a relatively straightforward process. The filtered sample is placed in a UV-visible spectrophotometer and the absorbance is measured. Absorbance which is defined as the log of % transmitted light is converted to Naperian absorption coefficient using the equation

$$a_g(\lambda) = \frac{2.303 * A(\lambda)}{\ell} \tag{1.6}$$

where a_g is the absorption coefficient in m^{-1}, A is absorbance (unitless), and ℓ is the path length of the spectrophotometric cell used in the measurement (m), 2.303 is the coefficient that converts from decadic absorption (i.e. log 10 scale) to Naperian absorption (i.e. natural log scale).

For larger scale calculations, it is not always possible to obtain a measured absorption spectrum, nor is it always appropriate. Because of the spectral nature of CDOM absorption, as described previously (section 1.2), the literature often reports CDOM as either the absorption at a specific wavelength [*Blough and Del Vecchio*, 2002], or as the spectral slope coefficient of an exponential fit to the spectrum [*Blough and Del Vecchio*, 2002]. In remote sensing applications, algorithms often retrieve CDOM at a single wavelength. Because the initial motivation for determining CDOM absorption in remote sensing applications was to correct for its influence when modeling chlorophyll-*a*, many remote sensing algorithms derive CDOM at 412nm, where the overlap with chlorophyll-*a* absorption is at a minimum [*Carder et al.*, 1989; *Carder et al.*, 1999; *Carder et al.*, 1991]. In these cases, in order to use these data for other calculations at other wavelengths, a spectral slope coefficient is often employed to extrapolate the 412 nm information to the rest of the spectrums [*Twardowski et al.*, 2004]. Chapter 2 of this dissertation deals with the challenges to such an approach for use in photochemical calculations.

1.4.3 Φ, Apparent Quantum Yield

The first law of photochemistry states that in order for there to be a photochemical reaction, a photon must first be absorbed. This leads to the simple description of the efficiency of a photochemical reaction, or the quantum yield as

$$\Phi = \frac{mols\ product\ \ formed\ (or\ destroyed)}{mols\ photons\ absorbed\ by\ reactant} \tag{1.7}$$

which is unitless, and almost always less than one, because of the potential of the absorbed photon to lead to non-photochemical reactions, such as fluorescence or phosphorescence, as well as inter-system transfers which lead to energy dispersal as heat. In cases of chain reactions, where the absorbed photon can create more than one bond change (such as the ferrioxalate actinometer, Φ= 1.26, [*Lee and Seliger*, 1963]), the quantum yield can exceed one. Such reactions are relatively rare.

In the ocean, the reactant is rarely a chemically defined molecule because of the complex mixture that constitutes CDOM. Many reactions are secondary; created through reaction of excited DOM, that creates reactive intermediates that consequently form products through thermal reactions [*Mopper and Kieber*, 2000]. Because of this, a true quantum yield is extremely difficult to define and the mixture we call CDOM is treated as the single absorbing moiety leading to photochemical reactions. In the ocean then, as with other natural waters, we determine an apparent quantum yield (AQY), which is defined as

$$AQY = \Phi = \frac{mol\ product\ formed\ (or\ destroyed)}{mol\ photons\ absorbed\ by\ CDOM} \tag{1.8}$$

where AQY remains unitless. Because photons of different wavelengths possess different energies, these quantities are spectral. Generally, UV and blue wavelengths facilitate more photochemical reactions than the lower energy green and red portions of the solar spectrum.

Determining the efficiency of reactions is arguably the most elusive part of the photochemical production calculation since it is not readily measured with a single instrument. Instead, a sample must be irradiated at different wavelengths, and the response over the photochemically active range must be determined, often using a different technique for each product of interest. Some products are more readily measured than others. For example, CO is easily measured at the nanomolar concentrations present in the ocean using a relatively simple gas chromatograph based analytical technique involving a mercuric oxide reactor with spectrophotometric detection. CO also partitions strongly to the gas phase due to its very low solubility in seawater, allowing it to be concentrated in a headspace equilibration. Other photochemical products such as CO_2 are much more difficult to detect in seawater, solubility of CO_2 in seawater is relatively high, and its participating in the carbonate chemistry creates a strong background signal that can interfere with the analysis. Methods that strip the carbonate system from the sample prior to irradiation [*Johannessen and Miller*, 2001; *Miller and Zepp*, 1995; *White et al.*, 2010] or use an isotope dilution methods [*Wang et al.*, 2009], can avoid the issues caused by the high background signal of the carbonate system but struggle with the limit of detection and analytical complexity.

Beyond the analytical difficulties inherent in measuring certain photochemical products, the variation in time and space of the individual AQYs is difficult to define. While the effect of source material on the efficiency of photochemical production appears to be minimal for some photochemical products, such as CO [*Ziolkowski and Miller*, 2007] the source material appears to have a much stronger effect on others, such as CO_2 [*Johannessen and Miller*, 2001; *White et al.*, 2010]. Data comparing these two is sparse, with most researchers focusing on one or the other. Spatial and temporal sampling density for most photochemical products and efficiencies in the ocean is low. This lack of data, especially for the more analytically challenging products, such as CO_2 and BLPs, makes modeling of such processes challenging. One approach, to estimate the photochemical production of the analytically challenging species is to determine its photoproduction ratio with a more easily identifiable product. One example of this approach has been CO_2:CO. Early work suggested that this ratio was ~15 to 20 [*Miller and Zepp*, 1995; *Mopper and Kieber*, 2000] though recent work [*White et al.*, 2010] shows that this ratio maybe much more variable and strongly correlated to varying DOC source material.

In order to improve the estimates of photochemical production in the ocean, and its influence on carbon cycling, more concerted efforts on improving sampling of AQYs for the three products involved with the mineralization of DOC (i.e CO, CO_2 and BLPs) must be made.

1.5 Overall Goal of the Dissertation

The aim of the current study is to improve estimates of coastal photochemical processes important to quantify and model the magnitude of the influence of such reactions on the coastal organic carbon cycle. The coastal oceans serve as the point of transition between terrestrial carbon runoff and the open ocean, the ocean margins are productive, estimated to be on the order of 8 Pg C/year [*Valiela*, 1995] and consequently have high CDOM concentrations. Though the total size of the coastal oceans is small compared to the total ocean, its area is very dynamic with regards to photochemical activity. The current study concentrates on the coastal margin in the South Atlantic Bight, featuring extensive salt marshes as well as strong seasonal freshwater DOC sources.

Three distinct sites near the University of Georgia Marine Institute (UGAMI) at Sapelo Island, GA, were chosen for the study. Sampling took place over the course of one year, in all seasons, in order to obtain insight into the variability of the system. North of Sapelo Island lies Sapelo Sound, a coastal marine dominated site, receiving little to no freshwater input over the course of the year, and as such provides a proxy for photochemistry in coastal waters. Just south of the UGAMI is Doboy Sound, largely marine dominated, though in periods of high river flow on the Altamaha River to the south, does receive some freshwater. Altamaha Sound, the southernmost site drains the largest watershed in the state of Georgia, and is heavily riverine influenced. All three sites exhibit carbon material input (both DOC and POC) from the extensive salt marshes that characterize the coast of Georgia. The salt marsh of coastal Georgia is dominated by the smooth cordgrass, *Spartina alterniflora*, which goes through periods of growth and senescence, and is known to influence the CDOM in the tidal creeks of estuaries [*Chen et al.*, 2010].

1.6 Structure of the dissertation

This dissertation is arranged in manuscript format with the following four chapters either accepted, in review, or in preparation for submittal to various journals. As mentioned previously, Chapter 2: *Effect of estimations of ultraviolet absorption spectra of chromophoric dissolved organic matter on the uncertainty of photochemical production calculations*, deals with the challenges to using modeled CDOM absorption data in UV dependent calculations such as photochemistry. Chapter 3 presents a large data set of CO and CO_2 AQY spectra determined for matching seasonal and spatial samples, and Chapter 4 examines the challenges inherent in determining quantitative spectral AQYs for the influence of photochemistry on the biological availability of carbon to the coastal microbial community. Chapter 5 presents the application of a hyperspectral remote sensing image to photochemical calculations. Chapter 6 provides a synoptic view of the entire dissertation and discusses its significance in the field.

References

Anesio, A. M., and W. Graneli (2003), Increased photoreactivity of DOC by acidification: Implications for the carbon cycle in humic lakes, *Limnology and Oceanography*, *48*(2), 735-744.

Anesio, A. M., and W. Graneli (2004), Photochemical mineralization of dissolved organic carbon in lakes of differing pH and humic content, *Archiv Fur Hydrobiologie*, *160*(1), 105-116.

Bertilsson, S., and L. J. Tranvik (2000), Photochemical transformation of dissolved organic matter in lakes, *Limnology and Oceanography*, *45*(4), 753-762.

Blough, N. V., and R. Del Vecchio (2002), Chromophoric DOM in the Coastal Environment, in *Biogeochemistry of Marine Dissolved Organic Matter*, edited by D. A.

Hansell and C. A. Carlson, pp. 509 - 546, Academic Press, San Diego.

Boyle, E. S., N. Guerriero, A. Thiallet, R. Del Vecchio, and N. V. Blough (2009), Optical Properties of Humic Substances and CDOM: Relation to Structure, *Environmental Science & Technology*, *43*(7), 2262-2268.

Bracchini, L., A. Tognazzi, A. M. Dattilo, F. Decembrini, C. Rossi, and S. A. Loiselle (2010), Sensitivity analysis of CDOM spectral slope in artificial and natural samples: an application in the central eastern Mediterranean Basin, *Aquatic Sciences*, *72*(4), 485-498.

Bricaud, A., A. Morel, and L. Prieur (1981), ABSORPTION BY DISSOLVED ORGANIC-MATTER OF THE SEA (YELLOW SUBSTANCE) IN THE UV AND VISIBLE DOMAINS, *Limnology and Oceanography*, *26*(1), 43-53.

Cai, W. J. (2011), Estuarine and Coastal Ocean Carbon Paradox: CO2 Sinks or Sites of Terrestrial Carbon Incineration?, *Annual Review of Marine Science*, *3*, 123-145.

Canadell, J. G., C. Le Quere, M. R. Raupach, C. B. Field, E. T. Buitenhuis, P. Ciais, T. J. Conway, N. P. Gillett, R. A. Houghton, and G. Marland (2007), Contributions to accelerating atmospheric CO2 growth from economic activity, carbon intensity, and efficiency of natural sinks, *Proceedings of the National Academy of Sciences of the United States of America*, *104*(47), 18866-18870.

Carder, K. L., R. G. Steward, P. B. Harvey, and P. B. Ortner (1989), Marine humic and fulvic acids: Their effects on remote sensing of chlorophyll, *Limnology and Oceanography*, *34*(1), 68-81.

Carder, K. L., F. R. Chen, Z. P. Lee, S. K. Hawes, and D. Kamykowski (1999), Semi-analytic MODIS algorithms for chlorophyll a and absorption with bio-optical domains based on nitrate depletion temperatures, *Journal of Geophysical Research-Oceans*, *104*(C3), 5403-5421.

Carder, K. L., S. K. Hawes, A. Baker, R. C. Smith, R. G. Steward, and B. G. Mitchell (1991), Relectrance model for quantifying chlorophyll a in the presence of productivity degradation products, *Journal of Geophysical Research*, *96*(20599-20611).

Carlson, C. A. (2002), Production and Removal Processes, in *Biogeochemistry of Marine Dissolved Organic Matter*, edited by D. A. Hansell and C. A. Carlson, pp. 91 - 152, Academic Press, San Diego.

Chen, R. F., M. Jiang, Y. Q. Tian, G. B. Gardner, F. Peri, W. Huang, and K. T. Cialino (2010), Understanding the Temporal Evolution of the Flux of Organic Matter from a Watershed to the Coastal Ocean, in *Ocean Sciences*, edited, Portland, Oregon.

Coble, P. G. (1991), CHARACTERIZATION OF DISSOLVED ORGANIC-MATTER USING TOTAL FLUORESCENCE SPECTROSCOPY, *Abstracts of Papers of the American Chemical Society*, *201*, 12-GEOC.

Coble, P. G., C. A. Schultz, and K. Mopper (1993), FLUORESCENCE CONTOURING ANALYSIS OF DOC INTERCALIBRATION EXPERIMENT SAMPLES - A COMPARISON OF TECHNIQUES, *Marine Chemistry*, *41*(1-3), 173-178.

Cooper, W. J., R. G. Zika, R. G. Petasne, and J. M. C. Plane (1988), PHOTOCHEMICAL FORMATION OF H2O2 IN NATURAL-WATERS EXPOSED TO SUNLIGHT, *Environmental Science & Technology*, *22*(10), 1156-1160.

Del Vecchio, R., and N. V. Blough (2002), Photobleaching of chromophoric dissolved organic matter in natural waters: kinetics and modeling, *Marine Chemistry*, *78*(4), 231-253.

Del Vecchio, R., and N. V. Blough (2004), On the origin of the optical properties of humic substances, *Environmental Science & Technology*, *38*(14), 3885-3891.

Fichot, C. G., and W. L. Miller (2010), An approach to quantify depth-resolved marine photochemical fluxes using remote sensing: Application to carbon monoxide (CO) photoproduction, *Remote Sensing of Environment*, *114*(7), 1363-1377.

Fichot, C. G., S. Sathyendranath, and W. L. Miller (2008), SeaUV and SeaUV(C): Algorithms for the retrieval of UV/Visible diffuse attenuation coefficients from ocean color, *Remote Sensing of Environment*, *112*(4), 1584-1602.

Gao, H. Z., and R. G. Zepp (1998), Factors influencing photoreactions of dissolved organic matter in a coastal river of the southeastern United States, *Environmental Science & Technology*, *32*(19), 2940-2946.

Gehlen, M., L. Bopp, N. Ernprin, O. Aumont, C. Heinze, and O. Raguencau (2006), Reconciling surface ocean productivity, export fluxes and sediment composition in a global biogeochemical ocean model, *Biogeosciences*, *3*(4), 521-537.

Graneli, W., M. Lindell, B. M. De Faria, and F. D. Esteves (1998), Photoproduction of dissolved inorganic carbon in temperate and tropical lakes - dependence on wavelength band and dissolved organic carbon concentration, *Biogeochemistry*, *43*(2), 175-195.

Gregg, W. W., and K. L. Carder (1990), A SIMPLE SPECTRAL SOLAR IRRADIANCE MODEL FOR CLOUDLESS MARITIME ATMOSPHERES, *Limnology and Oceanography*, *35*(8), 1657-1675.

Gruber, N., et al. (2009), Oceanic sources, sinks, and transport of atmospheric CO2, *Global Biogeochemical Cycles*, *23*.

Guo, X. H., M. H. Dai, W. D. Zhai, W. J. Cai, and B. S. Chen (2009), CO2 flux and seasonal variability in a large subtropical estuarine system, the Pearl River Estuary, China, *Journal of Geophysical Research-Biogeosciences*, *114*.

Hansell, D. A., and C. A. Carlson (1998), Net community production of dissolved organic carbon, *Global Biogeochemical Cycles*, *12*(3), 443-453.

Hansell, D. A., C. A. Carlson, D. J. Repeta, and R. Schlitzer (2009), DISSOLVED ORGANIC MATTER IN THE OCEAN A CONTROVERSY STIMULATES NEW INSIGHTS, *Oceanography*, *22*(4), 202-211.

Helms, J. R., A. Stubbins, J. D. Ritchie, E. C. Minor, D. J. Kieber, and K. Mopper (2008), Absorption spectral slopes and slope ratios as indicators of molecular weight, source, and photobleaching of chromophoric dissolved organic matter, *Limnology and Oceanography*, *53*(3), 955-969.

Jerlov, N. G. (1976), *Marine Optics*, Elsevier, Amsterdam.

Jiang, L. Q., W. J. Cai, and Y. C. Wang (2008a), A comparative study of carbon dioxide degassing in river- and marine-dominated estuaries, *Limnology and Oceanography*, *53*(6), 2603-2615.

Jiang, L. Q., W. J. Cai, R. Wanninkhof, Y. C. Wang, and H. Luger (2008b), Air-sea CO2 fluxes on the US South Atlantic Bight: Spatial and seasonal variability, *Journal of Geophysical Research-Oceans*, *113*(C7).

Johannessen, S. C., and W. L. Miller (2001), Quantum yield for the photochemical production of dissolved inorganic carbon in seawater, *Marine Chemistry*, *76*(4), 271-283.

Kieber, D. J., J. McDaniel, and K. Mopper (1989), PHOTOCHEMICAL SOURCE OF BIOLOGICAL SUBSTRATES IN SEA-WATER - IMPLICATIONS FOR CARBON CYCLING, *Nature*, *341*(6243), 637-639.

Kieber, R. J., X. L. Zhou, and K. Mopper (1990), FORMATION OF CARBONYL-COMPOUNDS FROM UV-INDUCED PHOTODEGRADATION OF HUMIC SUBSTANCES IN NATURAL-WATERS - FATE OF RIVERINE CARBON IN THE SEA, *Limnology and Oceanography*, *35*(7), 1503-1515.

Kujawinski, E. B., R. Del Vecchio, N. V. Blough, G. C. Klein, and A. G. Marshall (2004), Probing molecular-level transformations of dissolved organic matter: insights on photochemical degradation and protozoan modification of DOM from electrospray ionization Fourier transform ion cyclotron resonance mass spectrometry, *Marine Chemistry*, *92*(1-4), 23-37.

Kujawinski, E. B., K. Longnecker, N. V. Blough, R. Del Vecchio, L. Finlay, J. B. Kitner, and S. J. Giovannoni (2009), Identification of possible source markers in marine dissolved organic matter using ultrahigh resolution mass spectrometry, *Geochimica Et Cosmochimica Acta*, *73*(15), 4384-4399.

Law, C. S., T. N. Sjoberg, and R. D. Ling (2002), Atmospheric emission and cycling of carbon monoxide in the Scheldt Estuary, *Biogeochemistry*, *59*(1-2), 69-94.

Lee, J., and H. H. Seliger (1963), Quantum Yield of the Ferrioxalate Actinometer, *Journal of Chemical Physics*, *40*(2), 519-523.

Loiselle, S. A., L. Bracchini, A. M. Dattilo, M. Ricci, A. Tognazzi, A. Cozar, and C. Rossi (2009), Optical characterization of chromophoric dissolved organic matter using wavelength distribution of absorption spectral slopes, *Limnology and Oceanography*, *54*(2), 590-597.

Ludwig, W., J. L. Probst, and S. Kempe (1996), Predicting the oceanic input of organic carbon by continental erosion, *Global Biogeochemical Cycles*, *10*(1), 23-41.

Micinski, E., L. A. Ball, and O. C. Zafiriou (1993), PHOTOCHEMICAL OXYGEN ACTIVATION - SUPEROXIDE RADICAL DETECTION AND PRODUCTION-RATES IN THE EASTERN CARIBBEAN, *Journal of Geophysical Research-Oceans*, *98*(C2), 2299-2306.

Miller, W. L., and R. G. Zepp (1995), PHOTOCHEMICAL PRODUCTION OF DISSOLVED INORGANIC CARBON FROM TERRESTRIAL ORGANIC-MATTER - SIGNIFICANCE TO THE OCEANIC ORGANIC-CARBON CYCLE, *Geophysical Research Letters*, *22*(4), 417-420.

Miller, W. L., and M. A. Moran (1997), Interaction of photochemical and microbial processes in the degradation of refractory dissolved organic matter from a coastal marine environment, *Limnology and Oceanography*, *42*(6), 1317-1324.

Minor, E. C., B. L. Dalzell, A. Stubbins, and K. Mopper (2007), Evaluating the photoalteration of estuarine dissolved organic matter using direct temperature-resolved mass spectrometry and UV-visible spectroscopy, *Aquatic Sciences*, *69*(4), 440-455.

Mobley, C. (1994), *Light and Water*, Academic Press.

Moffett, J. W., and O. C. Zafiriou (1993), THE PHOTOCHEMICAL DECOMPOSITION OF HYDROGEN-PEROXIDE IN SURFACE WATERS OF THE EASTERN CARIBBEAN AND ORINOCO RIVER, *Journal of Geophysical Research-Oceans*, *98*(C2), 2307-2313.

Mopper, K., and D. J. Kieber (2000), Marine photochemistry and its impact on carbon cycling, in *The effects of UV radiation in the marine environment*, edited by S. J. De Mora, S. Demers and M. Vernet, pp. 101-129, Cambridge University PRess, Cambridge, UK.

Mopper, K., and D. J. Kieber (2002), Photochemistry and the Cycling of Carbon, Sulfur, Nitrogen and Phosphorus, in *Biogeochemistry of Marine Dissolved Organic Matter*, edited by D. A. Hansell and C. A. Carlson, pp. 456 - 508, Academic Press, San Diego.

Mopper, K., A. Stubbins, J. D. Ritchie, H. M. Bialk, and P. G. Hatcher (2007), Adrvanced Instrumental Approaches for Characterization of Marine Dissolved Organic Matter: Extraction Techniques, Mass Spectrometry, and Nuclear Magnetic Resonance Spectroscopy, *Chemical Reviews*, *107*(2), 419-442.

Mopper, K., X. L. Zhou, R. J. Kieber, D. J. Kieber, R. J. Sikorski, and R. D. Jones (1991), PHOTOCHEMICAL DEGRADATION OF DISSOLVED ORGANIC-CARBON AND ITS IMPACT ON THE OCEANIC CARBON-CYCLE, *Nature*, *353*(6339), 60-62.

Nagata, T. (2008), Organic Matter-Bacteria Interactions In Seawater, in *Microbial Ecology of the Oceans, Second Edition*, edited by D. L. Kirchman, pp. 207-241, John Wiley and Sons, Inc.

Obernosterer, I., and R. Benner (2004), Competition between biological and photochemical processes in the mineralization of dissolved organic carbon, *Limnology and Oceanography*, *49*(1), 117-124.

Pomeroy, L. R. (1974), OCEANS FOOD WEB, A CHANGING PARADIGM, *Bioscience*, *24*(9), 499-504.

Salonen, K., and A. Vahatalo (1994), PHOTOCHEMICAL MINERALIZATION OF DISSOLVED ORGANIC-MATTER IN LAKE SKJERVATJERN, *Environment International*, *20*(3), 307-312.

Stedmon, C. A., and S. Markager (2003), Behaviour of the optical properties of coloured dissolved organic matter under conservative mixing, *Estuarine Coastal and Shelf Science*, *57*(5-6), 973-979.

Stedmon, C. A., and S. Markager (2005), Resolving the variability in dissolved organic matter fluorescence in a temperate estuary and its catchment using PARAFAC analysis, *Limnology and Oceanography*, *50*(2), 686-697.

Stedmon, C. A., and R. Bro (2008), Characterizing dissolved organic matter fluorescence with parallel factor analysis: a tutorial, *Limnology and Oceanography-Methods*, *6*, 572-579.

Stubbins, A., G. Uher, C. S. Law, K. Mopper, C. Robinson, and R. C. Upstill-Goddard (2006), Open-ocean carbon monoxide photoproduction, *Deep-Sea Research Part Ii-Topical Studies in Oceanography*, *53*(14-16), 1695-1705.

Stubbins, A., R. G. M. Spencer, H. M. Chen, P. G. Hatcher, K. Mopper, P. J. Hernes, V. L. Mwamba, A. M. Mangangu, J. N. Wabakanghanzi, and J. Six (2010), Illuminated darkness: Molecular signatures of Congo River dissolved organic matter and its photochemical alteration as revealed by ultrahigh precision mass spectrometry, *Limnology and Oceanography*, *55*(4), 1467-1477.

Tolli, J. D., S. M. Sievert, and C. D. Taylor (2006), Unexpected diversity of bacteria capable of carbon monoxide oxidation in a coastal marine environment, and contribution of the Roseobacter-associated clade to total CO oxidation, *Applied and Environmental Microbiology*, *72*(3), 1966-1973.

Tranvik, L. J., and S. Bertilsson (2001), Contrasting effects of solar UV radiation on dissolved organic sources for bacterial growth, *Ecology Letters*, *4*(5), 458-463.

Twardowski, M. S., E. Boss, J. M. Sullivan, and P. L. Donaghay (2004), Modeling the spectral shape of absorption by chromophoric dissolved organic matter, *Marine Chemistry*, *89*(1-4), 69-88.

Valiela, I. (1995), *Marine Ecological Processes*, 686 pp., Springer, New York.

Walker, S. A., R. M. W. Amon, C. Stedmon, S. W. Duan, and P. Louchouarn (2009), The use of PARAFAC modeling to trace terrestrial dissolved organic matter and fingerprint water masses in coastal Canadian Arctic surface waters, *Journal of Geophysical Research-Biogeosciences*, *114*.

Wang, W., C. G. Johnson, K. Takeda, and O. C. Zafiriou (2009), Measuring the Photochemical Production of Carbon Dioxide from Marine Dissolved Organic Matter by Pool Isotope Exchange, *Environmental Science & Technology*, *43*(22), 8604-8609.

Wetzel, R. G., P. G. Hatcher, and T. S. Bianchi (1995), Natural photolysis by ultraviolet irradiance of recalcitrant dissolved organic matter to simple substrates for rapid bacterial metabolism, *Limnology and Oceanography*, *40*(8), 1369-1380.

White, E. M., D. J. Kieber, J. Sherrard, W. L. Miller, and K. Mopper (2010), Carbon dioxide and carbon monoxide photoproduction quantum yields in the Delaware Estuary, *Marine Chemistry*, *118*(1-2), 11-21.

Xie, H. X., and O. C. Zafiriou (2009), Evidence for significant photochemical production of carbon monoxide by particles in coastal and oligotrophic marine waters, *Geophysical Research Letters*, *36*.

Xie, H. X., S. Belanger, S. Demers, W. F. Vincent, and T. N. Papakyriakou (2009), Photobiogeochemical cycling of carbon monoxide in the southeastern Beaufort Sea in spring and autumn, *Limnology and Oceanography*, *54*(1), 234-249.

Zafiriou, O. C., S. S. Andrews, and W. Wang (2003), Concordant estimates of oceanic carbon monoxide source and sink processes in the Pacific yield a balanced global "blue-water" CO budget, *Global Biogeochemical Cycles*, *17*(1).

Zafiriou, O. C., J. Joussotdubien, R. G. Zepp, and R. G. Zika (1984), PHOTOCHEMISTRY OF NATURAL-WATERS, *Environmental Science & Technology*, *18*(12), A358-A371.

Zafiriou, O. C., H. X. Xie, N. B. Nelson, R. G. Najjar, and W. Wang (2008), Diel carbon monoxide cycling in the upper Sargasso Sea near Bermuda at the onset of spring and in midsummer, *Limnology and Oceanography*, *53*(2), 835-850.

Zhang, Y., H. X. Xie, C. G. Fichot, and G. H. Chen (2008), Dark production of carbon monoxide (CO) from dissolved organic matter in the St. Lawrence estuarine system: Implication for the global coastal and blue water CO budgets, *Journal of Geophysical Research-Oceans*, *113*(C12).

Zhou, X. L., and K. Mopper (1997), Photochemical production of low-molecular-weight carbonyl compounds in seawater and surface microlayer and their air-sea exchange, *Marine Chemistry*, *56*(3-4), 201-213.

Zika, R. G., E. S. Saltzman, and W. J. Cooper (1985), HYDROGEN-PEROXIDE CONCENTRATIONS IN THE PERU UPWELLING AREA, *Marine Chemistry*, *17*(3), 265-275.

Zika, R. G., P. J. Milne, and O. C. Zafiriou (1993), PHOTOCHEMICAL STUDIES OF THE EASTERN CARIBBEAN - AN INTRODUCTORY OVERVIEW, *Journal of Geophysical Research-Oceans*, *98*(C2), 2223-2232.

Ziolkowski, L. A., and W. L. Miller (2007), Variability of the apparent quantum efficiency of CO photoproduction in the Gulf of Maine and Northwest Atlantic, *Marine Chemistry*, *105*(3-4), 258-270.

CHAPTER 2

EFFECT OF ESTIMATIONS OF ULTRAVIOLET ABSORPTION SPECTRA OF CHROMOPHORIC DISSOLVED ORGANIC MATTER ON THE UNCERTAINTY OF PHOTOCHEMICAL PRODUCTION CALCULATIONS[1]

---

[1] Reader, H. E. and W. L. Miller. Accepted by *Journal of Geophysical Research – Oceans*.

Reprinted here with permission of American Geophysical Union, 04/29/2011.

Abstract

The UV-visible absorption spectrum of chromophoric dissolved organic matter (CDOM) is crucial for accurate calculation of photochemical reaction rates in the ocean. The literature contains considerable variability for quantifying CDOM absorption spectra and it is unclear how these different approaches affect subsequent photochemical calculations. Using 128 surface ocean samples collected during coastal transects from Texas to Maine (USA), we examine the ability of four simple models to reconstruct the measured UV absorption spectra and examine the accuracy of photochemical production calculations made using the reconstructed spectra. Three exponential models are based on determination of a spectral slope coefficient (SSC) over distinct wavelength ranges (412-560nm, 290-412nm, 290-650nm) and one is based on the absorption only at 412nm. Including UV wavelengths in determination of SSC resulted in reconstruction of UV absorption spectra with high accuracy, underestimating measured absorption integrated over the UV by only -1.5 to -4.3% at worst for the 128 samples. The 412nm model estimated UV-integrated absorption ranged between -4.3 to +6.5% of measured spectra for coastal stations. The 412-560nm SSC model underestimated measured UV absorption at all wavelengths by up to 60%. A spectral correction factor based on the average percent underestimation for all samples was found to improve reconstruction of UV absorption and photochemical estimates. Without the correction factor, photoproduction from this model underestimates values calculated from measured UV spectra ranged from -13 to -20% for coastal stations. Corrected estimates improve this to between -1.4 and +6.8%.

1. Introduction

Chromophoric dissolved organic matter (CDOM) absorbs ultraviolet (UV) and visible radiation, and alters the optical properties of natural waters. CDOM is the fuel for photochemical transformations in natural waters. Photochemical transformations of CDOM are a dynamic part of DOM transformations in the marine environment. In coastal systems, where CDOM concentrations are high, photochemistry has potential to significantly impact the carbon cycle. [*Mopper and Kieber,* 2002]. Most photochemical activity is largely driven by higher energy photons in the blue and UV wavelengths of the solar spectrum. In order to drive photochemical production models, it is essential to know the efficiency of the reaction of interest (i.e. apparent quantum yield, AQY) as well as the energy and quantity of photons are absorbed by CDOM. The UV-visible absorption spectrum of the CDOM is thus a crucial piece of information required when attempting to implement photochemical models.

CDOM is a complex mixture of various compounds [*Kujawinski et al,* 2004; *Mopper et al,* 2007] and the shape of the UV-visible absorption spectrum has long been approximated by an exponential curve [*Jerlov,* 1976*; Bricaud et al.*, 1981; *Blough and Del Vecchio,* 2002 (and references therein)]. Various mechanistic models have been postulated to explain the shape of the CDOM absorption spectrum, from overlapping many individual single compound absorption spectra, which absorb fewer photons as the energy of the radiation decreases towards the visible [*Blough and Del Vecchio,* 2002; *Stedmon et al,* 2003] to an intramolecular electronic interaction model resulting in a relatively smooth decrease in absorption as the wavelength increases [*Blough and Del*

Vecchio 2004; *Boyle et al.,* 2009]. In the literature, CDOM absorption is often reported using its "spectral slope" (S), which is the slope coefficient of an exponential decay function used to describe the spectral shape of absorption (i.e S in Equation 2.1 below). Many methods have been used in the past to model spectral slope, and many of these depend on the instrumentation and wavelengths used to determine the absorption spectrum [*Carder et al.,* 1989; *Stedmon et al.,* 2000 *Blough and Del Vecchio*, 2002]. The addition of an offset, O, to an exponential decay function has been suggested as a better fit to the shape of CDOM absorption, than the single exponential decay alone:

$$a_g(\lambda) = Ae^{-S\lambda} + O, \tag{2.1}$$

where $a_g(\lambda)$ is the spectral absorption coefficient of CDOM, A is a fitting coefficient, S is the spectral slope, and λ is the wavelength. The primary cause of this offset has been ascribed to the difference in refractive index between pure water and salt water, and arises from the common use of a pure water as a blank, in spectrophotometric measurements [*Green and Blough,* 1994]. *Twardowski et al.* [2004] did a comprehensive survey of various mathematical models used to determine spectral slope in the literature. They found that while the single exponential function with an offset described the shape of absorption better than the single exponential alone, a hyperbolic function performed statistically better than both.

Because many remote sensing applications retrieve CDOM at only one wavelength, typically 412nm, *Twardowski et al.* [2004] suggested a single wavelength version of the hyperbolic model to describe spectral shape, derived from their extensive data set:

$$a_g(\lambda) = a_g(412)(\frac{\lambda}{412})^{-6.92}. \tag{2.2}$$

They found that for the visible wavelengths from 400 nm to 650 nm these two methods of describing spectral absorption by CDOM were able to model the absorption spectrum with less than 12% error. Because of the complexity of CDOM, the exponential shape is still only an approximation for the spectral shape of the absorption of light by CDOM, and deviations from exponential can occur differently in different portions of the spectrum. More recent studies [*Helms et al* 2008, *Loiselle et al* 2009] have shown that the spectral slope varies considerably when applied to different portions of the absorption spectrum, and that these variations occur differently in varying water types. These variations in concentration of CDOM as well as CDOM spectral slopes have been suggested as a semi-conservative tracer for water masses [*Nelson et al, 2007*].

Because the most critical wavelengths for CDOM absorption with respect to photochemical processes are the blue and UV wavelengths of light, it is crucial to know the absorption accurately at those wavelengths. Many literature values for spectral slope coefficients are not determined using absorption over UV wavelengths, due to either instrument limitations, or to the intentions of the authors in applying the data to non-photochemical problems, and thus not needing the information in the UV. While the fit of a particular model to optical data may be appropriate within certain statistical bounds and over certain wavelength ranges, due to the spectral nature of all of the components involved in calculating photochemical production these statistical parameters can be misleading depending on the range of active wavelengths for different chemical species. In this paper we assess the usefulness of various approaches for the determination of spectral slope coefficients from visible data specifically for use in UV-dependant (i.e. photochemical) calculations, by applying the single wavelength with offset model

(Equation 2.1) calculated using various wavelength ranges, as well as Twardowski et al.'s [2004] generalized hyperbolic function (the single wavelength extrapolation) (Equation 2.2), to a large coastal water data set from the Gulf of Mexico and Northwestern Atlantic Ocean.

2. Methods

2.1 Sample Collection

The data used to test the utility of various CDOM models were from 128 surface (between 2-4 m depth, avoiding the surface stagnant layer) samples collected from July 10 – August 4 2007 as part of the Gulf of Mexico East Coast Carbon Cruise (GOMECC; R/V Ronald H. Brown, NOAA) (Figure 2.1). This includes a wide variety of coastal and blue waters stations covering the eastern Gulf of Mexico and the United States east coast from Texas to Maine. Samples were 0.2 μm filtered (Whatman Polycap AS75) into 150mL acid washed amber glass bottles and stored at 0-4 °C until returned to the lab for processing. UV-visible absorption spectra were taken from 190 nm -700 nm at 1 nm resolution in 10 cm quartz cells using a Perkin Elmer Lambda-40 spectrophotometer. Pure water (Milli-Q, Millipore) was used as a blank.

2.2 Data Processing

Using the non-linear fitting routine *nlinfit*, in the MATLAB ® Statistics Toolbox, the raw absorbance spectra were fit to a 3-part exponential equation (Equation 2.1) over the wavelength range 380-700 nm in order to determine the offset created by the differences in refractive index between seawater and the Milli-Q blank. The respective offsets were then subtracted from the individual spectra, and absorbance was converted to naperian (natural log scale) absorption coefficient using Equation 2.3:

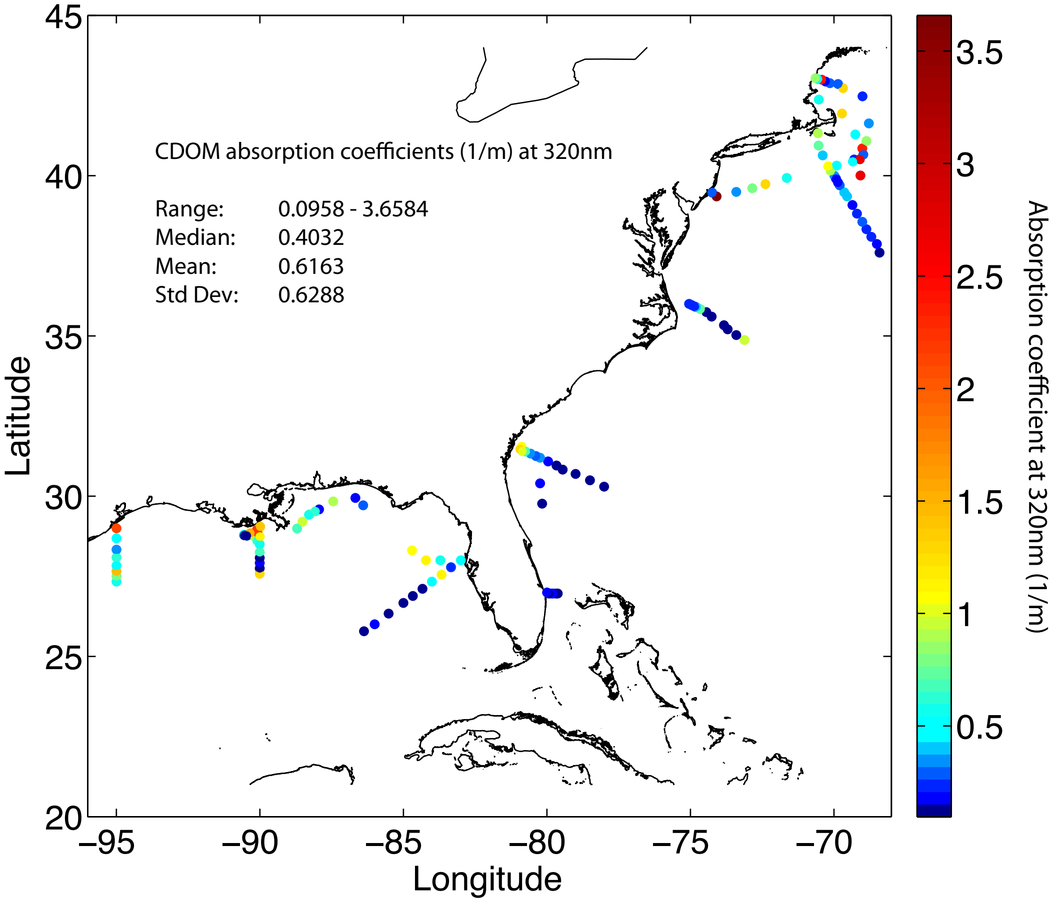

Figure 2.1: CDOM absorption at 320nm for the surface CDOM samples collected during the 2007 GOMECC Cruise. Station colors show absorption coefficients as indicated with the color bar at the right.

$$a_g = \frac{2.303 * A}{l}, \tag{2.3}$$

where l is the path length of the spectrophotometer cell (m), A is unitless absorbance, resulting in absorption coefficients, a_g with units of m^{-1}. The absorption curves were modeled again using a single exponential curve model, with the offset removed, in order to determine the spectral slope,

$$a_g(\lambda) = Ae^{-S\lambda}. \tag{2.4}$$

Spectral slope was calculated over three different wavelength ranges: 290-412 nm (Model A) encompassing the entire UV portion of the solar spectrum reaching the Earth's surface, 412-560 nm (Model B) in the visible [*Twardowski et al,* 1999], and 290-650 nm (Model C) covering the entire UV-visible spectrum. In addition to the single exponential models, the spectra were also reconstructed using the single point model (Equation 2.2) (Model D) as reported by *Twardowski et al.* [2004].

3. Assessment

3.1 Spectral Slope Assessment

After determining the spectral slope coefficient over the given ranges, each UV spectra was then reconstructed using the modeled coefficient. The spectral percent difference between the measured absorption spectrum and modeled absorption spectrum was calculated for each station and an average percent difference spectrum (+/- 1 standard deviation) was created using the whole data set in order to assess the goodness of fit for each model in the UV (Figure 2.2). The average percent difference spectrum was then used as a potential UV correction factor for each model. A set of seven distinct stations (Table 2.1) were selected to provide a range of CDOM concentrations ($a_g(320)$ between 0.0958 – 3.6584) and geographic locations in order to examine how each model

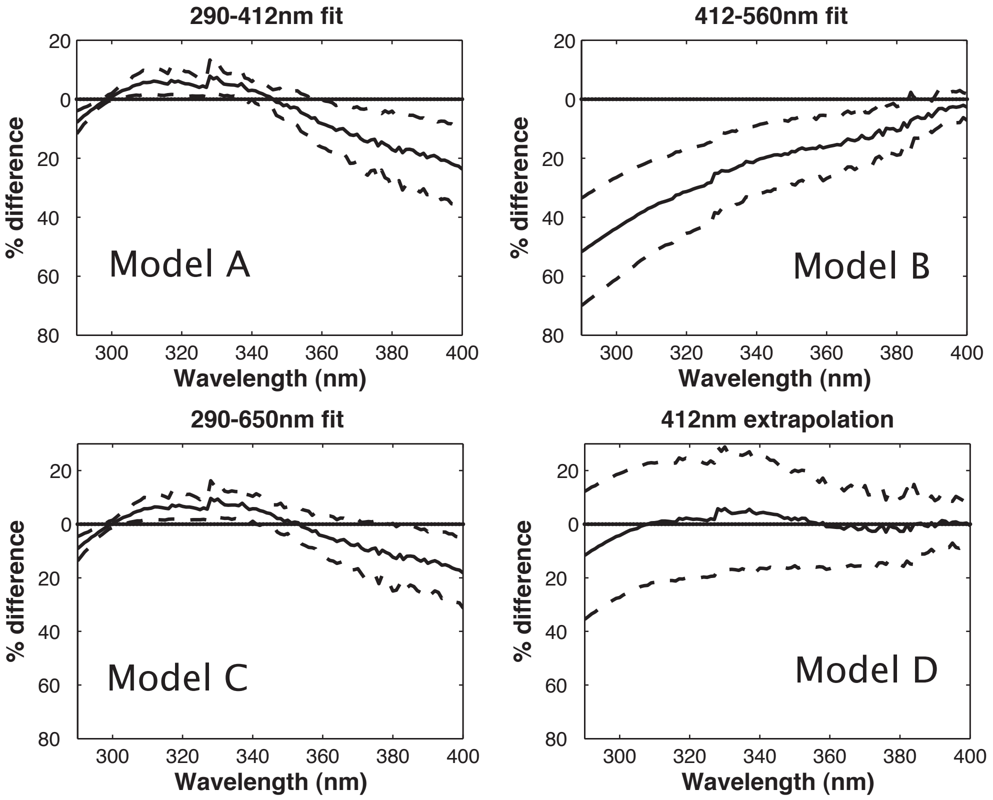

Figure 2.2: Average percent deviation of modeled CDOM absorption from measured CDOM absorption

Table 2.1: Sample stations chosen for analysis of models.

Station Number	**Latitude**	**Longitude**	**Basin**	**$a_g(320)$**
43	30.8332	-79.4540	SAB	0.0958
28	25.7840	-86.3695	GOM	0.1050
35	31.4013	-80.8582	SAB	1.0197
18	27.5827	-90.0040	GOM	1.3097
10	28.8442	-90.3360	GOM	1.4885
71	40.8472	-69.0117	MAB	2.3637
60	39.3492	-74.0852	MAB	3.6584

reconstructs different absorption spectra. The seven stations were also used to examine the effectiveness of using the average percent difference spectrum to correct for deviations from measured absorption arising from the different spectral models.

The range of spectral slope coefficients was larger for Models A and C than for Model B (Table 2.2). When using the spectral slope to then reconstruct the UV absorption curves over the wavelengths of interest (290-400nm) the blue water stations (43, 28; Figure 2.3a,b), which are in the Gulf Stream and Loop Current, respectively, had the largest deviations from the measured spectra for all models. For models A and C the spectra were overestimated by between 13 and 18% at 320 nm, though when integrated over the entire UV spectrum (290-400nm), the absorption was underestimated by -1.5 to -4.3% (Table 2.3). This highlights the difficulty inherent in using statistical values to measure goodness of fit along a spectrum such as this. Model D underestimated the UV spectrum for the blue water stations by -10 and -19%, as expected, *Twardowski et al*. [2004] do not recommend use of this model for blue waters.

Models A and C, which used UV wavelengths in the determination of spectral slope coefficient, showed higher accuracy in modeling the UV absorption spectra of the coastal stations (Figure 2.3 c-g). Percent differences between the measured spectra and the modeled spectra at 320 nm showed small overestimation by these two models, on the order of 1.0-2.7% (Table 2.3). When the absorption is integrated over the entire UV portion of the spectrum, these models deviated from the measured absorption between -0.4 and +0.6%. The ability of Model D to accurately reconstruct the UV spectrum was more variable than Models A and C with deviations between -4.7% and 7.7% at 320 nm and similarly when integrated over the UV, 290-400 nm (-4.3% to 6.5%).

Table 2.2: Spectral Slope coefficients for the various fitting models used.

Spectral Fit	**Model A 290-412 (all spectra)**	**Model C 290 – 650 (all spectra)**	**Model B 412 - 560 (all spectra)**	**Model B 412 - 560 ($a_g(412)>0.077$)**
Minimum	0.0186	0.0174	0.0072	0.0131
Maximum	0.0316	0.0312	0.0272	0.0178
Mean	0.0235	0.0227	0.0146	0.0159
Median	0.0223	0.0217	0.0151	0.0159

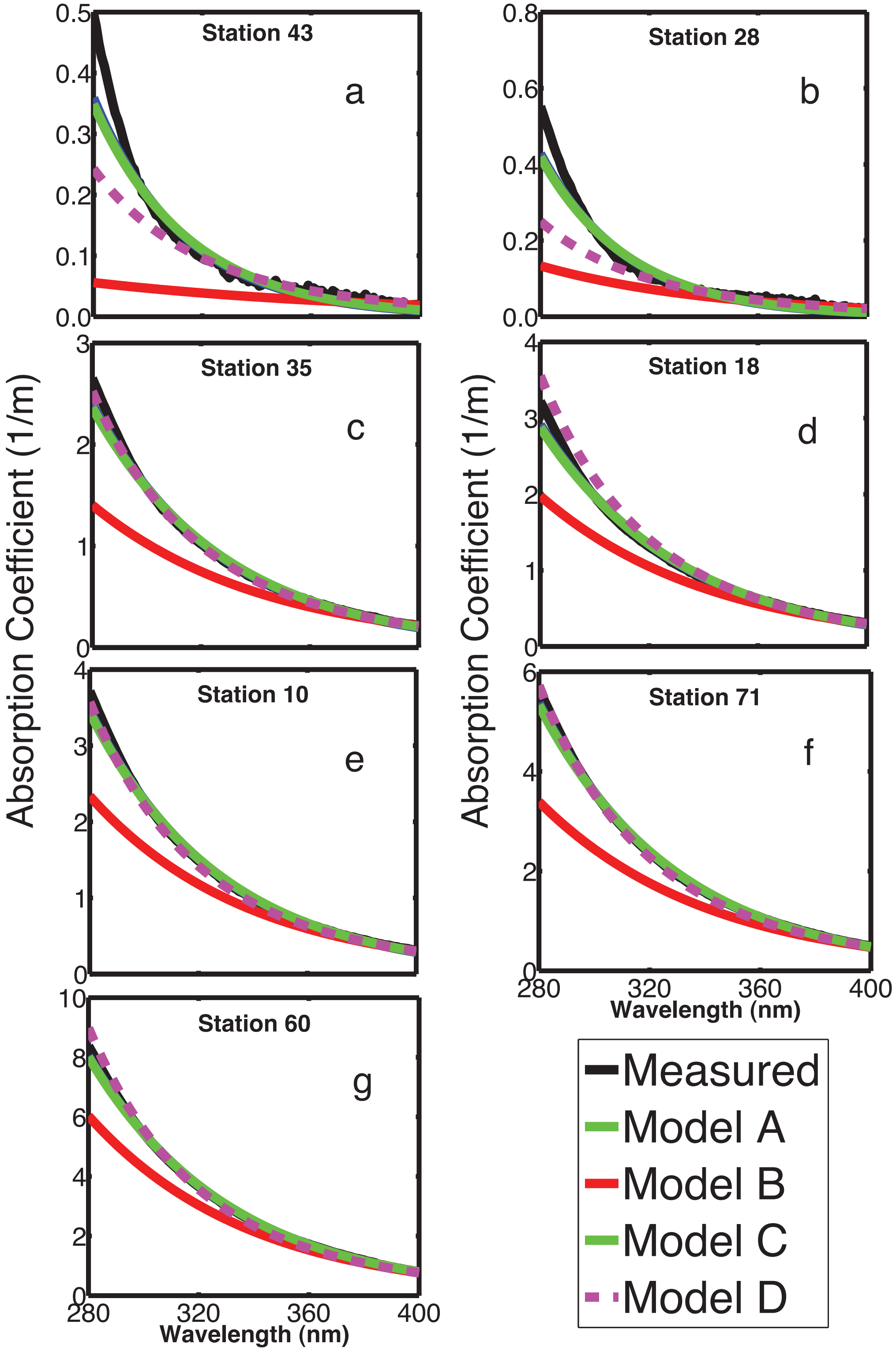

Figure 2.3: UV-visible absorption spectra for the various models as fit to seven stations representing the transition from blue to dark water (a – g). In all cases, the difference between Models A and C was less than the thickness of the line and so both are represented by the green line.

Table 2.3: Percent deviations of modeled spectra from the measured spectra, at one point (a_g320) and integrated over the UV.

MODEL	**A (290-412)**		**B (412-560)**		**C (290-650)**		**D (single wavelength)**	
STATION	**percent difference at 320nm**	**UV integrated percent difference**	**percent difference at 320nm**	**UV integrated percent difference**	**percent difference at 320nm**	**UV integrated percent difference**	**Percent difference at 320nm**	**UV integrated percent difference**
43	13.1	-3.1	-59.4	-59.8	15.1	-1.5	0.6	-10.1
28	16.4	-4.3	-30.8	-39.4	17.9	-3.2	-5.5	-19.1
35	2.1	-0.2	-26.7	-25.3	2.6	0.6	-1.8	-1.9
10	1.5	-0.1	-20.6	-19.9	1.9	-0.4	-4.7	-4.3
18	2.3	-0.1	-19.7	-19.2	2.7	0.5	7.7	6.5
71	1.1	-0.1	-25.5	-24.1	1.4	0.3	-3.9	-3.3
60	1	-0.1	-17.1	-16.5	1.1	0.1	-2.6	-2.3

Model B, which uses the spectral slope coefficient determined over visible wavelengths only, showed underestimation of the true absorption spectrum for all stations. In this case, the deviation at 320nm tracks closely to the deviation over the integrated spectrum (-17% to -59% at 320nm, -17 to -60% integrated, Table 2.3), because the spectrum is underestimated at all wavelengths, for all stations.

In order to evaluate the possibility of correcting the underestimation of absorption in the UV for cases where visible absorption data is the only data available, the average percent difference between the measured and modeled spectra (Figure 2.2b) was used to create a correction factor (Equation 2.5) for Model B at each wavelength.

$$a_{gcorrected}(\lambda) = \frac{a_{gcalculated}(\lambda)}{1+(\frac{\%difference(\lambda)}{100})} \tag{2.5}$$

Using the correction factor in conjunction with Model B, the modeled spectra were recalculated (Figure 2.4). While the correction factor did increase the modeled absorption for all stations, the absorption for blue water stations continued to be underestimated in the UV. Because the data set included a large number of blue water stations, which tend to deviate the most from exponential shape [*Helms et al,* 2008], the bluest stations ($a_g(412)$ <0.077) were removed from the data set and Model B was reapplied. When the new correction factor was applied the standard deviation of the corrected spectra showed a 50% improvement, from +/-21% to +/-11% for the entire data set (Figure 2.5).

3.2 Photochemical Production Assessment

Due to the spectral nature of photochemical production, assessing the overall deviations of the absorption spectrum can overlook issues arising from the spectral

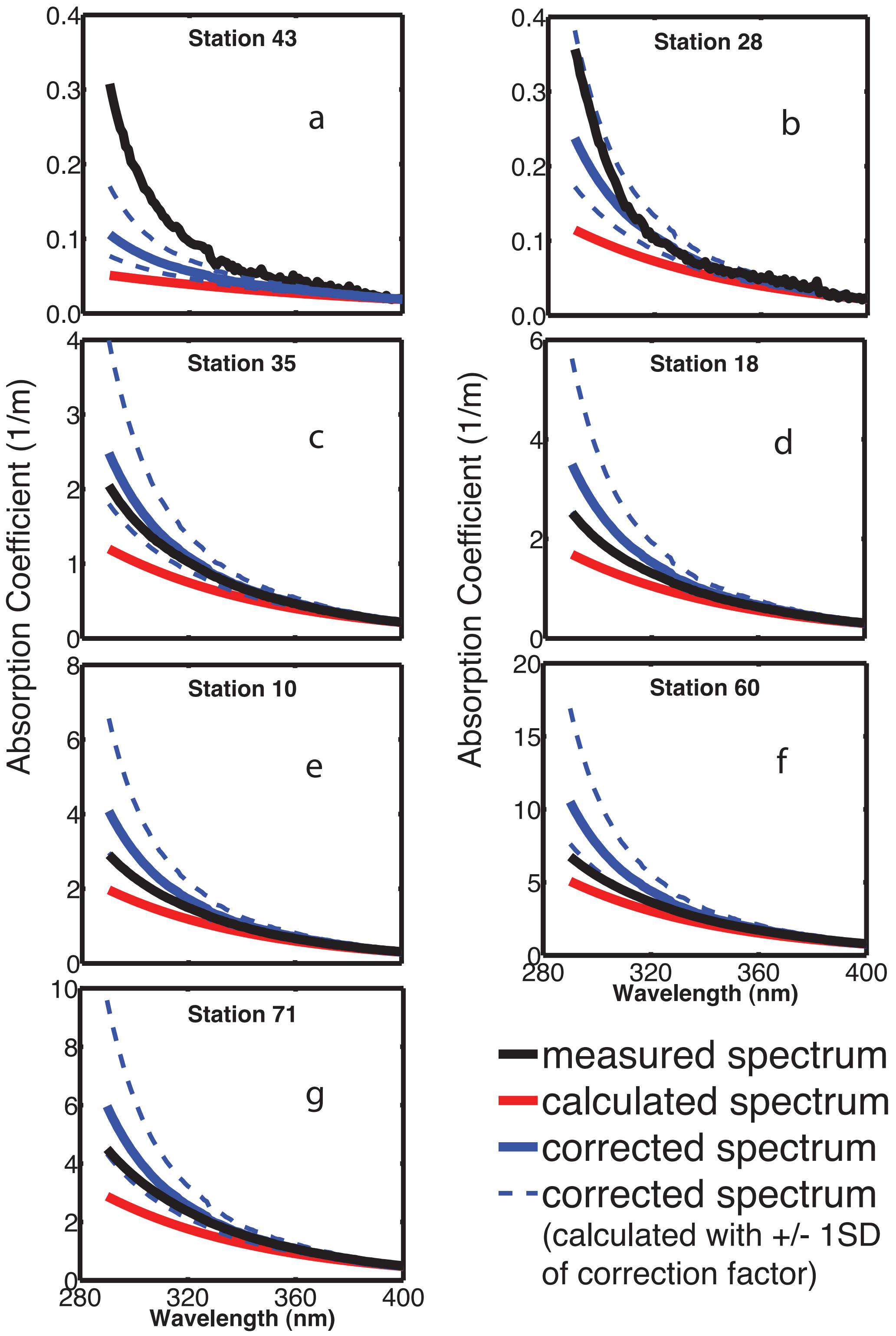

Figure 2.4: Model B (visible) spectral reconstructions with corrected spectra. The dashed lines are the corrected spectra calculated with +/- 1S.D. of the average spectral percent difference, illustrating the envelope of error. The seven stations are in order representing the transition from blue to dark water (a – g).

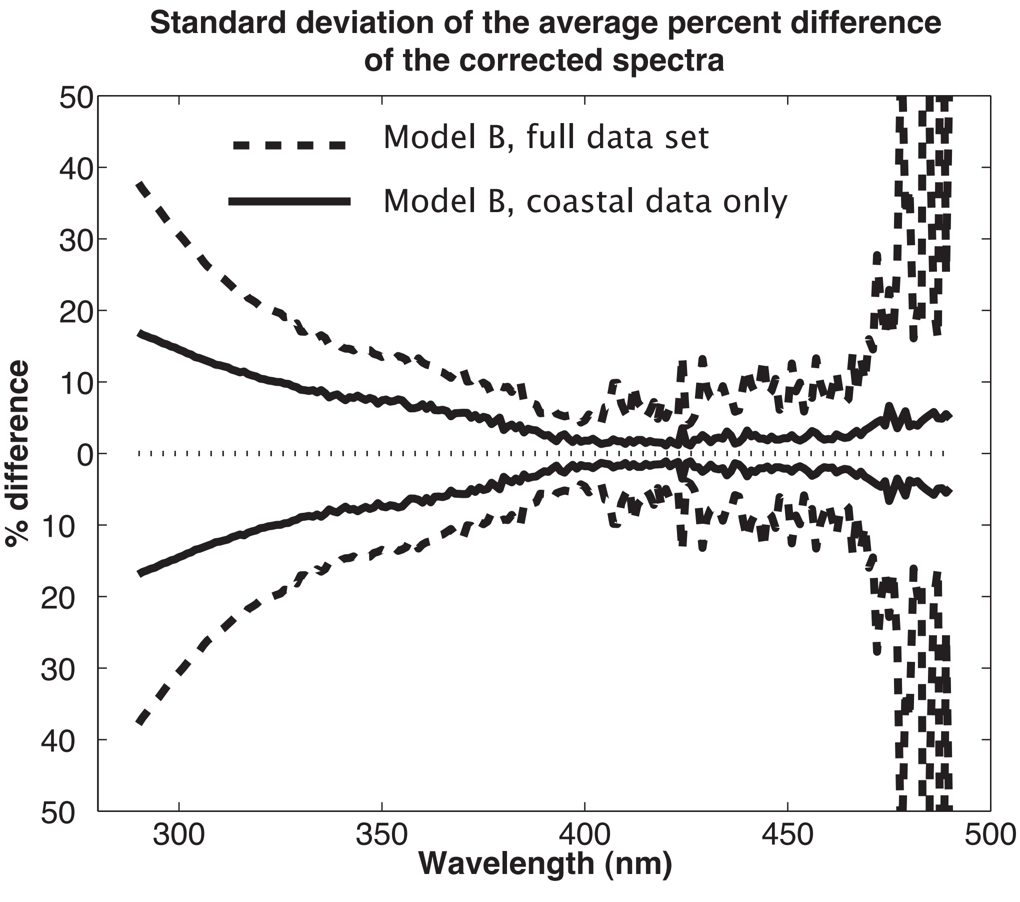

Figure 2.5: Standard deviation of the corrected fits (by percent difference) for the entire data set, and for the data set with the clearest waters removed.

distribution of the photochemically active wavelengths for a particular product. To assess the effect of different modeled UV-visible absorption spectra on photochemical production modeling, two distinct photochemical reactions were chosen: photoproduction of carbon monoxide and formaldehyde. Equation 2.6 [*Johannessen and Miller,* 2001] is used to calculate surface photochemical production rate, P(λ) (mol/m^3/day), and is defined as the change in concentration of product over time;

$$P(\lambda) = \frac{d[product]}{dt}(\lambda) = E_0(\lambda) * a_g(\lambda) * \Phi(\lambda) \tag{2.6}$$

where E_0 is the irradiance (mol photons/m^2/day), a_g is the absorption coefficient (m^{-1}) of the CDOM and Φ is the apparent quantum yield (or spectral efficiency of photochemical production, mol product/mol photons). Each term is calculated at each wavelength from 290 nm to 490 nm and the product is summed over this range to give a spectrally integrated result. Surface daily photochemical production (integrated spectrally 290-490 nm) was calculated for each station and each model, using a modeled solar spectrum for one day in August, at Sapelo Island, GA (Latitude 31.464°, Longitude -81.244°) (System for Transfer of Atmospheric Radiation, STAR model) as a constant radiance spectrum for all calculations. The STAR model was developed at the University of Munich, is based on the work of Ruggaber et al [1994] and was implemented here following the methodology of Fichot and Miller [2010]. Figure 2.6 shows the cross product of spectral irradiance, E_0, and the apparent quantum yield, for both reactions (from Equation 2.6) to show the active wavelength ranges where errors in the estimation of absorption coefficient will be most critical. While the active wavelengths for photochemical formaldehyde production are centered in the UV –B [*Kieber,* 1989], the photochemical production of carbon monoxide [*Zafiriou et al.,* 2003; *Ziolkowski and Miller,* 2007;

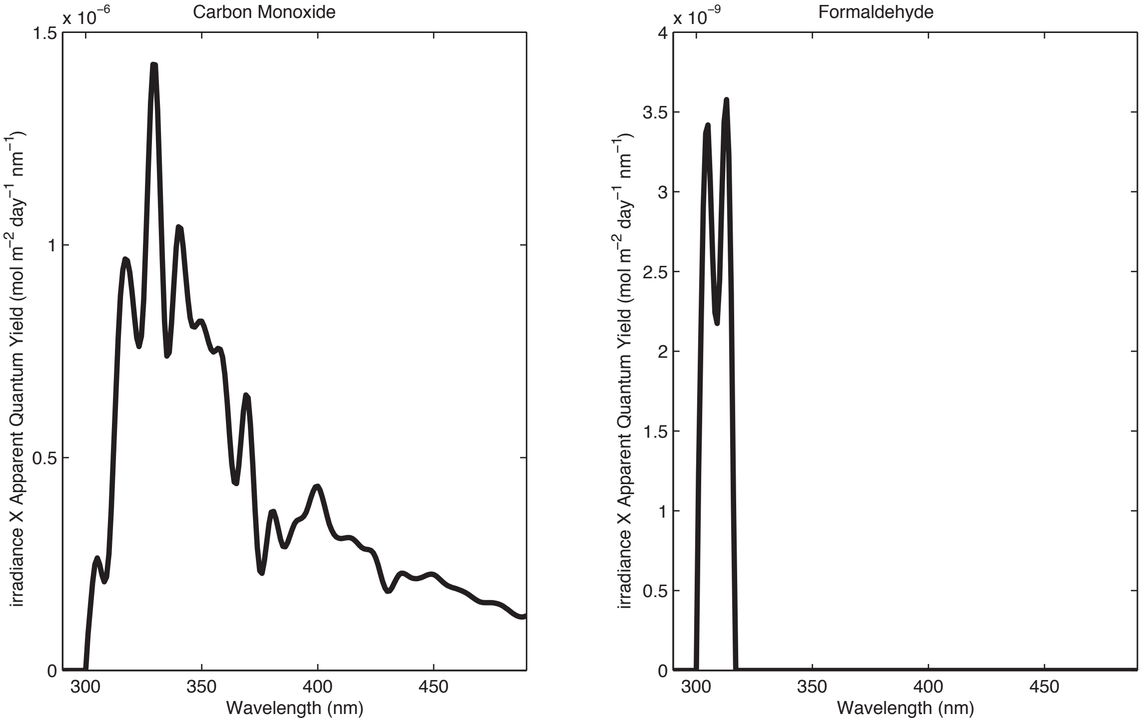

Figure 2.6: Cross product of the spectral irradiance and the apparent quantum yield for formaldehyde and carbon monoxide, revealing photochemically active wavelengths, to show where errors in absorption estimations will have the most impact.

Fichot and Miller, 2010] extends much further into the visible, with a maximum of production ~330-350 nm (Figure 2.6).

Spectrally integrated formaldehyde (CHHO) photoproduction numbers for Models A and C agreed with the CHHO photoproduction numbers calculated from the measured CDOM spectra for the coastal stations, within +/- 2%. The blue waters stations performed much worse, as expected, with a 9-12% error. This is expected because over the active wavelengths for formaldehyde production (300-320 nm), Models A and C tend to over-estimate absorption. Model D returned errors of -4 – 11%, for the coastal stations. Similar to the results of Twardowski et al. [2004], the single wavelength extrapolation returned large errors for the blue water stations (-12 to -19%). Model B severely underestimated photoproduction of CHHO by up to 31% for the coastal stations, and 70% for the blue water stations (Figure 2.7 a,b). When adjusted with the correction factor for the entire data set, Model B overestimated the production by 11 to 30% for the coastal waters, and continued to underestimate the blue waters (-11 to -50%). After removing the blue water stations from the analysis, application of the new correction factor for Model B improved the estimates of coastal photoproduction of CHHO to between -2% and +14% error, performing as well as Model D.

The active wavelengths for the photoproduction of carbon monoxide (CO) extend much further towards the visible than do those for CHHO. This serves to minimize the photoproduction error caused by misestimation of the absorption of CDOM in the UV-B. The patterns of estimation of photoproduction for CO remained the same as for CHHO, however the errors were generally lower. For Models A and C the errors ranged from -0.37 to -0.02% and 0.48 to 1.1%, respectively for the coastal stations. For the blue water

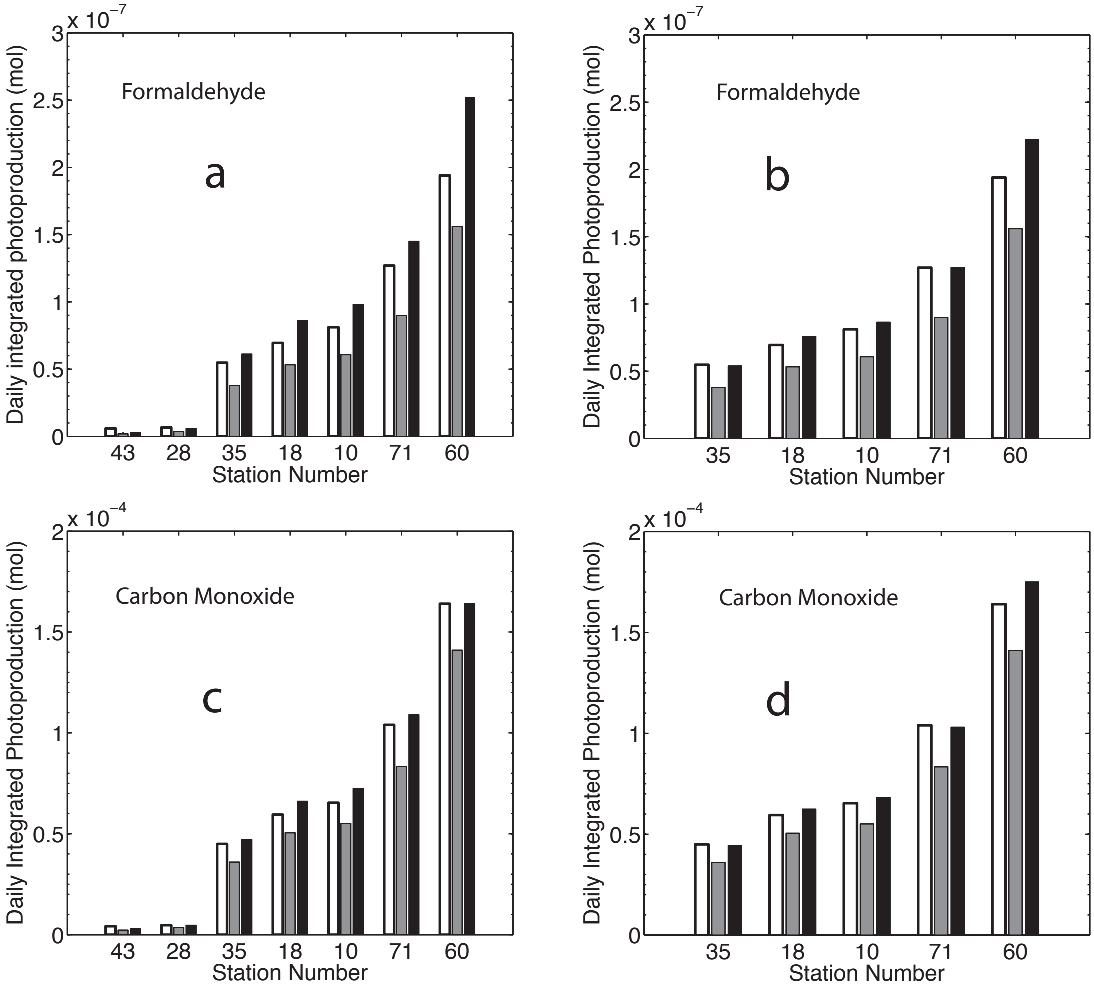

Figure 2.7: Surface photoproduction estimates for Model B, measured (white left hand bar) , calculated Model B (grey middle bar) and corrected Model B (black right hand bar). Panels a and c represent the Model B correction factor calculated with the entire data set, and the panels b and d are for the coastal application of Model B correction factor. Stations are in the order of bluest (most oligotrophic) to darkest (most coastal).

stations the errors were ~ -4.5% and ~ -2.0%, for those models. The Model D errors ranged between -4.5 and 4.5% for the coastal stations, and between -7 and 0% for the blue water stations. Using Model B applied to the full data set returned errors between -13 to -20% for the coastal stations, increasing to 0 to 11% after correction (Figure 2.7c). Photoproduction for the blue water stations (43 and 28) were underestimated by between -25 and -50%, with the correction factor improving the estimation to between -2.0% and -30%. After the removal of the blue water stations (Figure 2.7d), the new Model B correction factor improved the estimates to between -1.4 and 6.8%, again putting it on the order of Model D.

4. Discussion

While calculated predictions of photochemical reaction rates in surface waters can contain errors from AQY and irradiance uncertainties, it is also clear from Equation 2.6 that they are equally susceptible to erroneous estimates for the absorption of solar radiation by CDOM. Published papers reporting the distribution and variability of CDOM absorption spectra continue to show considerable variability among the ways that CDOM absorption spectra are reported. It is clear from the results here that the methodology chosen to describe CDOM absorption can significantly affect resulting photochemical calculations.

Looking first at the fit of the exponential models, we note that Model B exhibits a strong spectral bias of increasing error towards the shorter wavelengths of the UVB portion of the spectrum (Figure 2.2). Models A and C also show a spectral bias in their error distribution, though this is much smaller (<20%). Taken together, this argues that the practice of fitting the CDOM absorption spectrum to a single exponential curve [e.g.

Jerlov, 1976*; Bricaud et al.*, 1981; *Blough and Del Vecchio,* 2002 (and references therein)] may be a fundamentally flawed approach. Using UV wavelengths in calculating the spectral slope coefficient results in a better fit, though none of the models we evaluated are able to accurately fit the shape of the absorption in the UVB for the blue water stations (Figure 2.3), suggesting that single exponentials are not appropriate in open ocean waters. Coastal waters, with higher concentrations of CDOM, have absorption spectra that tend to approximate an exponential curve better than blue waters.

Indeed, other studies have shown that the source of CDOM [*Helms et al,* 2008; *Loiselle et al,* 2009] as well as the concentration of CDOM [*Bracchini et al,* 2010] have a strong effect on the distribution of spectral slopes across the UV and visible wavelengths. Marine derived CDOM tends to have higher spectral slope values over the UV as well as increased variability in these spectral slope values, potentially due to the lower overall concentrations of CDOM [*Nelson et al, 2007; Swan et al 2009*]. Terrestrially derived CDOM and samples with higher concentrations of CDOM tend to have less variable spectral slope distributions as well as lower overall slope coefficients. Interestingly, Model D, which uses the absorption at 412nm to extrapolate the absorption in the UV shows no spectral bias (Figure 2.2) except for a slight decrease below 300nm. This is particularly surprising because the equation was developed from visible absorption data only [*Twardowski et al,* 2004]. The sharper inflection of a hyperbolic curve relative to an exponential curve could explain the ability of this equation to fit the UV portion of the absorbance spectrum where the spectral slopes are generally higher than those in the visible [*Helms et al,* 2008]. Though the standard deviation of this model is higher than obtained with the spectral slope derived models, this lack of spectral bias is encouraging for use in photochemical calculations.

Obviously, the best option for calculating photochemical production for all cases is to use the true absorption coefficients measured over the photochemically active wavelengths in the UV and visible. When this is not possible, such as cases where only spectral slope coefficients are available, spectral slope coefficients that were determined over the UV allow for fairly accurate estimates of photoproduction in coastal waters. Due to the deviation of bluer waters from exponential, the error for these depends highly upon the range of photochemically active wavelengths (i.e. the response spectrum of the product in question). A photochemical production reaction such as that seen for formaldehyde, with its narrow range of active wavelengths (Figure 2.6), has higher potential errors in photoproduction calculations than for a reaction like carbon monoxide, where the photochemically active wavelengths extend much farther into the visible. Because the entire photoproduction of formaldehyde is driven by absorbed radiation in the UVB (300 to 320nm), it is crucial to know the absorption of CDOM accurately over these wavelengths. Carbon monoxide photoproduction is maximal between 330nm and 350nm with significant photoproduction driven by visible radiation, making it necessary to know the CDOM absorption accurately over a different, and larger range than for formaldehyde. The lower errors found for the modeled photoproduction of carbon monoxide relative to that of formaldehyde are due to the more accurate estimation of UV-visible absorption as the wavelengths increase towards the visible. Despite the differences in the response spectra of different photochemical products, errors for photochemical production can range from -10% to +10% for blue waters, when the UV is used as part of the spectral slope determination. However, it is important to be aware of the active wavelengths of the photochemical product in any photochemical modeling.

When visible data for CDOM absorption is the only data available, using the single wavelength extrapolation reported by *Twardowski et al.* [2004] (Equation 2.2) is a good option to estimate the UV absorption spectrum in coastal waters, with relatively small errors for photochemical production and no spectral bias (Figure 2.2). Conversely, reconstructing the UV absorption spectrum from spectral slope coefficients determined using only visible wavelengths severely underestimates the absorption with the strong spectral bias of increasing error towards the shorter UVB wavelengths, and thus the photochemical production for coastal waters is also underestimated. The spectral correction factor for Model B, developed from our data set by fitting a quadratic equation to the spectral percent deviation and inserting it into the generalized Equation 2.5, resulting in Equation 2.7 may be successfully applied to the reconstructed absorption spectra for coastal waters from the US Gulf of Mexico and the US east coast and results in significant improvement for photochemical production estimates. In cases where visible spectral slopes are the only data available (e.g. using previously published CDOM data), this may be the best method for minimizing error in photochemical calculations. Given that the geographic extent of the data set used to evaluate UV spectral reconstruction was large, spanning the Gulf of Mexico as well as the south and mid Atlantic bights, it was suspected that geographical location might play a role in the effectiveness of any general model to predict the CDOM UV absorption spectrum. This did not prove to be the case and the main driver for differences in the effectiveness of the models was the “concentration” of CDOM as estimated from $a_g(412)$. The correction factor for extrapolation of visible S determinations developed in this paper, therefore, can best be used to correct CDOM absorption spectra derived from visible data in many coastal ($a_g(412)>0.077$) waters;

$$a_g(\lambda) = \frac{a_{g_{calculated}}(\lambda)}{1+(-1.4*10^{-5}*\lambda^2+1.3*10^{-2}*\lambda-2.9)}. \tag{2.7}$$

After reconstructing the spectral slope over the photochemically active wavelengths of 290-490 nm, Equation 2.7 can be applied to the calculated absorption spectrum. After correction the resulting spectrum estimates coastal photoproduction with similar accuracy to the single wavelength extrapolation (Model D). In the case where only visible data is available, either of these options provides an estimate of coastal ($a_g412 > 0.077$) photochemical production within +/-10 % error. Without correction of the absorption curve, errors in photochemical production are always underestimated by 20% or more.

Because the UV reflectance spectrum in the surface ocean cannot be directly measured remotely from space, visible optical data must be used to reconstruct the CDOM absorption spectra required for photochemical calculations. Many remote sensing methods determine CDOM absorption spectra by defining a spectral slope coefficient based on the spectral reflectance of visible radiation, often and using the absorption at a single "blue" wavelength in the visible (i.e. a_g412), and applying Equation 2.8,

$$a_g(\lambda) = a_{g(ref)}e^{-S(\lambda-\lambda_{ref})} \tag{2.8}$$

which is an alternative expression of Equation 2.4 [*Twardowski et al.,* 2004]. Indeed, the inclusion of a measurement of radiation in a band located at 412nm on sensors such as SeaWiFS (400nm on MODIS) has allowed determination of the absorption of CDOM in the visible, greatly improving the model determinations of chlorophyll-a in many locations [*Carder et al.,* 1991, *Carder et al,* 1999]. Though global models for photoproduction use different methods to determine a_g, such using average spectra [*Stubbins et al,* 2006], or the assumption that all absorption is CDOM [*Johannessen,* 2000], when attempting to use these same sensors for UV applications such as photochemical production models, spectral slope values are used to obtain UV spectral absorption values [*Fichot and Miller,* 2010]. There is a larger variability of spectral slope coefficient values in coastal waters when determined over the UV (i.e. Models A and C, Table 2.2) as opposed to the visible (Model B) and the mean S values are higher for Models A and C than those determined using Model B. Because of this variability, the use of a single spectral slope for coastal photoproduction calculations raises the errors inherent in such calculations. Given the relative accuracy of Model D in predicting the UV absorption spectrum from $a_g(412)$, this model may be the best choice for photochemical calculations using remote sensing techniques.

CDOM is a dynamic component of the carbon cycle in the coastal ocean. Photochemical transformations of carbon in coastal waters have the potential for significant contributions to the oceanic carbon cycle. Improving the accuracy of estimates for photochemical rates requires accurate spectral values for all of the components involved in the calculation of each photochemical reaction under consideration (i.e. the elements in Equation 2.6). Improving the confidence with which the CDOM absorption spectra used in photochemical production calculations can be estimated in general models will make these calculations more accurate. Remote sensing techniques are powerful tools for the observation of oceanic processes. They also hold great potential for estimating the significance of photochemistry in the oceanic carbon cycle over spatial and temporal scales that cannot be achieved with other technology. The accuracy of the spectral data required for calculating photochemical rates must be well defined to realize this potential.

Acknowledgments

The authors would like to thank the captain and crew of NOAA ship R/V Ronald H. Brown. This work was supported by NASA grant number NNX07AD85G, as part of the North American Carbon Project.

References

Blough, N. V. and R. Del Vecchio (2002), Chromophoric DOM in the Coastal Environment, in *Biogeochemistry of Marine Dissolved Organic Matter,* edited by D. A. Hansell and C. A. Carlson, pp. 509-546. Academic Press, San Diego, Calif.

Blough, N. V. and R. Del Vecchio (2004), On the Origin of the Optical Properties of Humic Substances. *Environ. Sci. Technol.* 38, 3995-3891, doi:10.1021/es049912h

Boyle, R. S., N. Guerriero, A. Thiallet, R. Del Vecchio, N. V. Blough. (2009), Optical Properties of Humic Substances and CDOM: Relation to Structure. *Environ. Sci. Technol.* 43, 2262-2268, doi: 10.1021/es803264g

Bracchini, L., A. Tognazzi, A. M. Dattilo, F. Decembrini, C. Rossi, S. A. Loiselle. (2010), Sensitivity analysis of CDOM spectral slope in artificial and natural samples: an application in the central eastern Mediterranean Basin. *Aquatic Sciences – Research Across Boundaries.* 72(4), 485-498, doi: 10.1007/s00027-010-0150-y

Bricaud, A., A. Morel, L. Prieur. (1981), Absorption by dissolved organic matter of the sea (yellow substance) in the UV and visible domains. *Limnol Oceanogr.* 26(1) 43-53.

Carder, K. L., R. G. Steward, G. R. Harvey, P. B. Ortner. (1989), Marine humic and fulvic acids: Their effects on remote sensing of ocean chlorophyll. *Limnol. Oceanogr.* 34(1) 68-81.

Carder, K. L., S. K. Hawes, K. A. Baker, R. C. Smith, R. G. Steward, B. G. Mitchell. (1991), Relectrance model for quantifying chlorophyll a in the presence of productivity degradation products. *J. Geophys. Res.* 96, 20599-20611.

Carder, K. L., F. R. Chen, Z. P. Lee, S. K. Hawes, D. Kamykowski. (1999), Semi-analytic MODIS algorithms for chlorophyll a and absorption with bio-optical domains based on nitrate-depletion temperatures. *J. Geophys. Res.* 104 (C3), 5403-5421.

Fichot, C. G., W. L. Miller. (2010), An approach to quantify depth-resolved marine photochemical fluxes using remote sensing: Application to carbon monoxide (CO) photoproduction. *Remote Sensing of Environment.* 114, 1363-1377. Doi: 10.1016/j.rse.2010.01.019

Green, S. A., N. V. Blough. (1994), Optical absorption and fluorescence properties of chromophoric dissolved organic matter in natural waters. *Limnol. Oceanogr.* 39(8), 1903-1916.

Helms, J. R., A. Stubbins, J. D. Ritchie, E. C. Minor, D. J. Kieber, and K. Mopper. (2008), Absorption spectral slopes and slope ratios as indicators of molecular weight, source, and photobleaching of chromophoric dissolved organic matter. *Limnol. Oceanogr*. 53, 955-969.

Jerlov, N. G. (1976), *Marine Optics.* Elsevier, Amsterdam.

Johannessen, S. C. (2000), A photochemical sink for dissolved organic carbon in the ocean. PhD Thesis, Department of Oceanography, Dalhousie University, Halifax, Nova Scotia, Canada.

Johannessen, S. C., W. L. Miller. (2001), Quantum yield for the photochemical production of dissolved inorganic carbon in seawater. *Marine Chemistry.* 76(4) 271-283.

Kieber, R. J., X. Zhou, K. Mopper. (1990), Formation of carbonyl compounds form UV-induced photodegradation of humic substances in natural waters: Fate of riverine carbon in the sea. *Limnol. Oceanogr.* 35(7) 1503-1515.

Kujawinski, E. B., R. Del Vecchio, N. V. Blough, G. C. Klein, A. G. Marshall. (2004), Probing molecular-level transformations of dissolved organic matter: insights on photochemical degradation and protozoan modification of DOM from electrospray ionization Fourier transform ion cyclotron resonance mass spectrometry. *Marine Chemistry.* 92 23-37

Loiselle, S. A., L. Bracchini, A. M. Dattilo, M. Ricci, A. Tognazzi, A. Cózar, C. Rossi. (2009), The optical characterization of chromophoric dissolved organic matter using wavelength distribution of absorption spectral slopes
Limnol. Oceanogr., 54(2), 590-597 doi: 10.4319/lo.2009.54.2.0590

Mopper, K., D. J. Kieber. (2002), Photochemistry and the Cycling of Carbon, Sulfur, Nitrogen and Phosophorus, in *Biogeochemistry of Marine Dissolved Organic Matter,* edited by D. A. Hansell and C. A. Carlson, pp. 509-546. Academic Press, San Diego, Calif.

Mopper, K., A. Stubbins, J. D. Ritchie, H. M. Bialk, P. G. Hatcher. (2007), Advanced instrumental approaches for characterization of marine dissolved organic matter: Extraction techniques, mass spectrometry, and nuclear magnetic resonance spectroscopy. *Chemical Reviews* 107(2), 419-442 doi 10.1021/cr050359b

Nelson, N. B., D. A. Siegel, C. A. Carlson, C. Swan, W. M. Smethie, S. Khatiwala. (2007), Hydrography of chromophoric dissolved organic matter in the North Atlantic. *Deep-Sea Research I* 54, 710-731.

Ruggaber, R., R. A. Dlugi, T. Nakajima. (1994), Modelling of radiation quantities and photolysis frequencies in the troposphere. *Journal of Atmospheric Chemistry.* 171-210.

Stedmon, C. A., S. Markager, H. Kaas. (2000), Optical Properties and Signatures of Chromophoric Dissolved Organic Matter (CDOM) in Danish Coastal Waters. *Estuarine, Coastal and Shelf Science.* 51, 267-278. doi:10.1006/ecss2000.0645

Stedmon, C. A., S. Markager, R. Bro. (2003), Tracing dissolved organic matter in aquatic environments using a new approach to fluorescence spectroscopy. *Marine Chemistry.* 82, 239-254, doi:10.1016/S0304-4203(03)00072-0

Stubbins, A., G. Uher, C.S. Law, K. Mopper, C. Robinson, R.C. Upstill-Goddard. (2006), Open-ocean carbon monoxide photoproduction. *Deep-Sea Research II*. 53 1695-1705.

Swan, C. M., D. A. Siegel, N. B. Nelson, C. A. Carlson, E. Nasir. (2009), Biogeochemical and hydrographic controls on chromophoric dissolved organic matter distribution in the Pacific Ocean. *Deep-Sea Research I.* 56 2175-2192.

Twardowski, M. S., J. M. Sullivan, P. L. Donaghay, J. R. V. Zanefeld. (1999), Microscale Quantification of the Absorption by Dissolved and Particulate Material in Coastal Waters with an ac-9. *Journal of Atmospheric and Oceanic Technology.* 16, 691-707.

Twardowski, M. S., E. Boss, J. M. Sullivan, P. L. Donaghay. (2004), Modeling the spectral shape of absorption by chromophoric dissolved organic matter. *Marine Chemistry.* 89, 69-88. doi: 10.1016/j.marchem/2004.02.008

Zafiriou O.C., S.S. Andrews, and W. Wang. (2003), Concordant estimates of oceanic carbon monoxide source and sink processes in the Pacific yield a balanced global “blue-water” CO budget. *Global Biogeochemical Cycles*. 17 (1) 15-1 – 15-13.

Ziolkowski, L.A. and W.L. Miller. (2007), Variability of the apparent quantum efficiency of CO photoproduction in the Gulf of Maine and Northwest Atlantic. *Marine Chemistry*. 118 (3-4) 258-270. 2007.

CHAPTER 3

VARIABILITY OF CARBON MONOXIDE AND CARBON DIOXIDE APPARENT QUANTUM YIELD SPECTRA IN THREE COASTAL ESTUARIES OF THE SOUTH ATLANTIC BIGHT[1]

---

[1] Reader, H. E. and W. L. Miller. To be submitted to *Marine Chemistry*.

Abstract

Carbon monoxide and carbon dioxide are the two largest identifiable photochemical products in the surface ocean. While CO is not considered a greenhouse gas, it contributes to greenhouse gas concentrations in the atmosphere by scavenging the hydroxyl radical that otherwise consumes other greenhouse gasses. CO_2 on the other hand, is a greenhouse gas, and the main contributor to ocean acidification. With estimated oceanic photoproduction on the order of petagrams of carbon annually, these two photoproducts are important to the cycling of marine dissolved organic carbon. 38 paired apparent quantum yield (AQY) spectra for CO and CO_2 were determined over the course of one year, at three locations off the coast of Georgia, USA. The AQY spectra for CO and CO_2 were variable throughout the year and sampling locations. In each case, the marine dominated site experienced a gradual seasonal shift in spectrally integrated (260 nm – 490 nm) AQY, with less efficient photoproduction in the summer and higher efficiency in the fall. Photoproduction in both cases correlates with the concentration of CDOM present in the system, as determined by the UV-B absorption of the sample prior to irradiation. Molecular size is approximated using the spectral slope ratio of the samples prior to the irradiation and not correlated with the efficiency of photoproduction in either data set. The ratio between CO_2 and CO photoproduction is determined using several methods and is ~2 +/- 1.5 for each method. The ratio is lower than previously reported in the literature and is likely due to the increased photoproduction of carbon monoxide from UVA and visible wavelengths relative to other studies. The increased efficiency of photoproduction in the blue wavelengths of the visible spectrum may be due to the strong influence of marsh-derived carbon present at all sample sites throughout the year.

1. Introduction

The ocean represents one of the largest and most dynamic reservoirs for reduced carbon on Earth. Its pool of dissolved organic carbon (DOC) is on the order of 600 Pg/C [*Canadell et al.*, 2007; *Hansell et al.*, 2009]. The coastal oceans are a very dynamic oceanic subset, with large carbon inputs from both terrestrial and in-situ sources. Rivers contribute up to 0.2Pg/C as DOC per year and most has had little exposure to sunlight before its arrival in coastal waters [*Ludwig et al.*, 1996]. Terrestrially derived carbon is generally strongly absorbing of solar radiation, and is largely biologically refractory [*Bricaud et al.*, 1981; *Carlson*, 2002]. The sunlight absorbing fraction of DOC regardless of source is referred to as chromophoric dissolved organic matter (CDOM) and acts as a sunscreen for the biological community in the ocean absorbing much of the harmful UV radiation entering the water column. Because CDOM absorbs in the blue end of the visible spectrum, it interferes with the remote sensing of chlorophyll in the ocean, and much work has gone into estimating CDOM to improve chlorophyll and primary production estimates using remote sensing of the worlds ocean [*Carder et al.*, 1989; *Carder et al.*, 1999].

Despite the continuous input of CDOM to the coastal ocean via continental sources, ocean water as a whole is not highly coloured and photochemical transformations are known to break down this coloured material [*Andrews et al.*, 2000; *Del Vecchio and Blough*, 2002; *Goldstone et al.*, 2004; *Osburn et al.*, 2009]. The absorption of solar radiation by CDOM can lead to a whole host of chemical reactions, including reactive oxygen species formation, such as hydroxyl radical (OH•) and superoxide (O_2^-) [*Blough and Zepp*, 1995; *Micinski et al.*, 1993; *Moffett and Zafiriou*, 1993; *Zika et al.*, 1985], breakdown of large molecules of carbon forming smaller organic molecules [*D J Kieber et al.*, 1989; *R J Kieber et al.*, 1990; *Wetzel et al.*, 1995], transformation of metal species [*Barbeau*, 2006; *Barbeau et al.*, 2003; *White et al.*, 2003], as well as the formation of inorganic carbon species, such as CO and CO_2 [*Clark et al.*, 2004; *Johannessen and Miller*, 2001; *Miller and Zepp*, 1995; *W Wang et al.*, 2009; *White et al.*, 2010; *Xie et al.*, 2004; *Zafiriou et al.*, 2003; *Ziolkowski and Miller*, 2007].

Photochemical production is the major source of CO in seawater. Importantly, it is a relatively insoluble gas, and can be transferred from the ocean water via air-sea exchange to the lower atmosphere where it scavenges hydroxyl radical, and thus indirectly contributes to greenhouse gas concentrations, by removing the main scavenger of methane gas [*Shindell et al.*, 2009]. Conversely, CO can also be used as a substrate for marine bacteria [*Tolli et al.*, 2006] efficiently competing with gas transfer to lessen its source to the atmosphere. Even with two removal pathways and a single production mechanism, concentrations in the surface ocean of carbon monoxide are supersaturated with respect to the atmosphere and are on the order of 2 nM in the open ocean and 12 nM in the coastal ocean [*Zafiriou et al.*, 2003; *Zafiriou et al.*, 2008]. Sun-driven production causes CO concentrations to vary with a distinct diurnal signal. Though the two removal mechanisms are fairly efficient, the photoinhibition of CO uptake by bacteria may also contribute to the late afternoon peak, with increasing bacterial drawdown when the solar radiation is less intense [*Tolli and Taylor*, 2005]. The photochemical production of CO in the oceans has been well studied in the recent past [*Day and Faloona*, 2009; *Miller and Moran*, 1997; *Stubbins et al.*, 2006; *Stubbins et al.*, 2008; *White et al.*, 2010; *Xie et al.*, 2009; *Zafiriou et al.*, 2003; *Zafiriou et al.*, 2008; *Ziolkowski and Miller*, 2007] and global annual production of CO in the worlds oceans is currently estimated at between 30 and 84 Tg C/year [*Fichot and Miller*, 2010; *Stubbins et al.*, 2006; *Zafiriou et al.*, 2003].

Carbon dioxide is a major component of the carbonate system in the ocean. As atmospheric concentrations of CO_2 continue to increase, the ocean continues to act as a buffer, absorbing CO_2 out of the atmosphere. Increased CO_2 concentrations in the surface oceans are pushing the carbonate system's equilibrium to a more acidic pH, raising concerns for the health of calcareous organisms critical to carbonate balance in the oceans in changing ocean conditions [*Fabry et al.*, 2008; *Moy et al.*, 2009]. Overall, the ocean acts as a sink for atmospheric CO_2. However, some areas of the coastal ocean, such as the terrestrially influenced South Atlantic Bight and the Pearl River Estuary, China, have been reported as seasonal sources of CO_2 to the atmosphere [*Guo et al.*, 2009; *Jiang et al.*, 2008b; *Z A Wang et al.*, 2005], with the inner shelf and estuary being the strongest sources [*Cai*, 2011; *Jiang et al.*, 2008a] presumably due to heterotrophic production in these regions.

The photochemical production of CO_2 has been studied in freshwater systems [*Anesio and Graneli*, 2003; 2004; *Bertilsson and Tranvik*, 2000; *Graneli et al.*, 1998; *Salonen and Vahatalo*, 1994] as well as marine systems [*Belanger et al.*, 2006; *Gao and Zepp*, 1998; *Johannessen and Miller*, 2001; *Miller and Zepp*, 1995], though the extent of coverage in marine systems is considerably less. Nonetheless, several noteworthy studies have found that there is indeed a strong photochemical signal of DIC production in the world's oceans [*Johannessen and Miller*, 2001; *Miller and Zepp*, 1995; *White et al.*, 2010].

Because of the analytical constraints to measuring photochemical production of CO_2 in seawater, there has been some focus on establishing a ratio of production between CO_2 and CO, for use with more prevalent CO data to estimate the magnitude of photochemical CO_2 production in the oceans. Early estimates put the CO_2:CO photochemical production ratio on the order of 15-20 [*Miller and Zepp*, 1995; *Mopper and Kieber*, 2000], however more recent studies have shown that this ratio is much more variable, ranging from ~2 to 98 in some cases [*White et al.*, 2010]. This ratio appears to be dependent on the source material comprising the CDOM. There is evidence that the photochemical efficiencies for both CO and CO_2 (i.e. Apparent Quantum Yield spectra, AQY) vary depending on the carbon source [*Johannessen and Miller*, 2001; *Ziolkowski and Miller*, 2007], though the CO AQY spectra appear to be more constant than those for CO_2. Regardless, CO and CO_2 are the two largest analytically identifiable carbon photoproducts in the ocean, and as such, have potential to affect the cycling of DOC in the oceans.

To better constrain the variability and the magnitude of the effect of photochemical production of both CO and CO_2 on the cycling of DOC in the coastal ocean, as well as examine potential environmental drivers of these photochemical processes, a study of CO and CO_2 photochemistry was performed. Thirty-eight (38) samples were collected from three sites off the coast of Georgia, USA for paired CO and CO_2 AQY spectra determinations. This provides the most extensive paired CO/CO_2 AQY data set to date, allowing a more robust consideration of not only the total photoproduction of the two species but the efficiencies of the processes as well.

2. Methods

2.1 Sample collection

Samples were collected for both CO and CO_2 photochemical experiments, monthly during spring high tides and quarterly during spring low tides. Three sites were chosen within the Georgia Coastal Ecosystems Long Term Ecological Research (GCE LTER) area, representing three coastal estuarine systems (Figure 3.1). Sapelo Sound is a coastal marine dominated site, with little freshwater input over the year. Altamaha Sound drains the largest watershed in the state of Georgia, and is a mixed riverine and marsh site. Doboy Sound is mainly a coastally dominated site, which receives some freshwater input from the Altamaha River during periods of high flow. Samples were collected during the GCE LTER monthly mini-cruise. Samples were collected in acid-washed polycarbonate bottles (Nalgene, 2L) and stored on ice until returned to the laboratory (<3 hours). Upon return to the laboratory samples were immediately filtered using a 0.2 μm nylon cartridge filter (Whatman Polycap AS75). Samples were then stored in the dark at 4°C until the experimental processing (0-6 months).

2.2 Sample Preparation

To allow analysis of micromolar concentrations of DIC photoproduction in seawater, the DIC in marine samples (i.e. the carbonate system) was stripped out of the sample prior to irradiation, following the method used in Johannessen and Miller [2001]. Briefly, 1 L of sample was transferred to a clean glass kettle, acidified to pH 2-3, using concentrated HCl (Fisher Scientific) and was bubbled overnight (~8 hours) under positive pressure with air scrubbed of CO_2 (soda lime column, 12"X1.5", Fisher Scientific, indicating grade) to ensure complete removal of dissolved carbonate species. Low

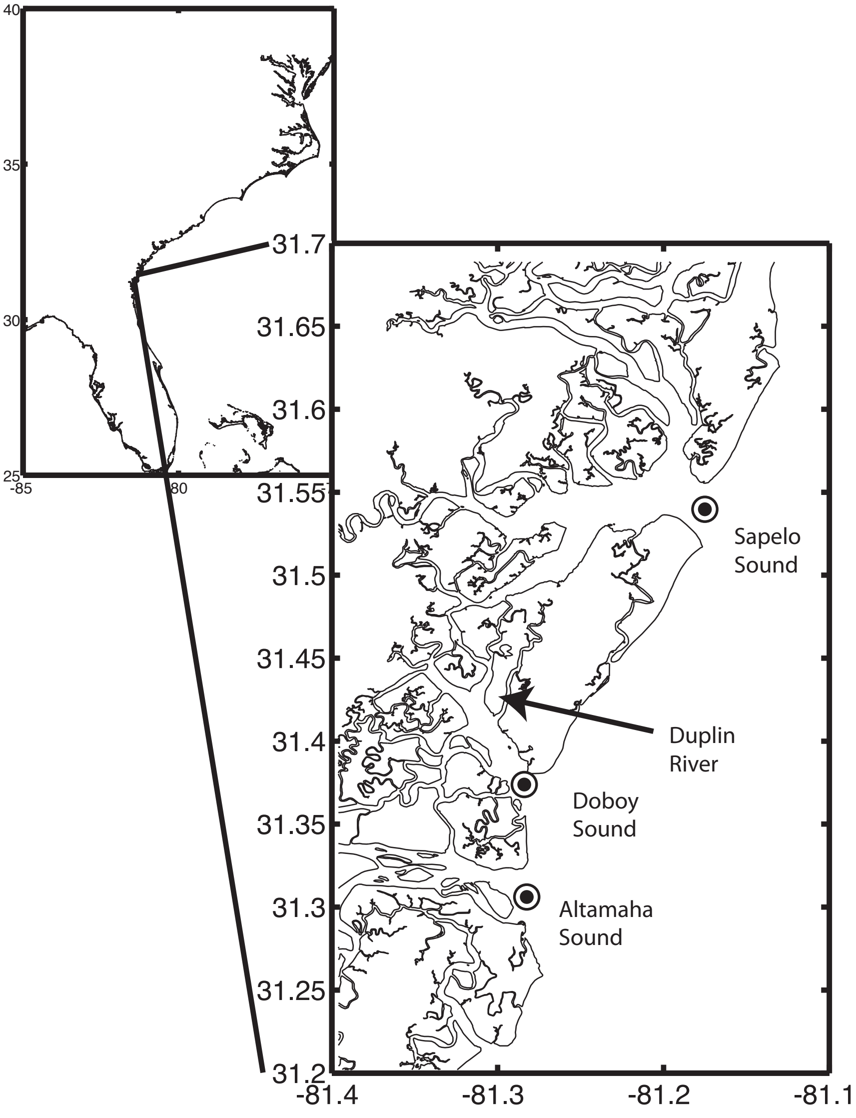

Figure 3.1: Sample sites for the seasonal study

concentration of CO_2 (area of peak at or below the Limit of Detection 0.014 μM) in the sample was confirmed via direct analysis using a Shimadzu TOC V-CPN in DIC mode.

Quartz spectrophotometric cells (10 cm pathlength, Spectrocell) for use in DIC photochemical experiments were sterilized with a UV-C lamp at close range (less than 30 cm) for an hour before filling. UV sterilization ensured that any CO_2 produced during the course of an irradiation is due to photochemical production rather than biological respiration. After sterilization and stripping of sample was complete, the sample was rebuffered to the initial pH of the sample (~7-8 pH) using crystalline sodium borate (ACS grade, Fisher Scientific). Immediately after raising the pH, the cells were filled using a glass dispenser while keeping the sample under positive pressure with CO_2 free air. Spectrophotometric cells were sealed, headspace-free, using 13 mm diameter, 1 mm thick Teflon-faced butyl rubber septa, and placed in a chilled aluminum block (held at 15°C), in a Suntest solar simulator (Suntest CPS).

Samples for CO photochemistry were refiltered (0.2 μm Whatman Polycap AS75) directly into acid washed and oven dried spectrophotometric cells, filled and sealed the same as the CO_2 experiments.

2.3 Photochemical Irradiations

Photochemical irradiations were performed following the multispectral methods of Johannessen and Miller [2001]. To create distinct irradiation conditions for each spectrophotometric cell, duplicates of Schott-glass long-pass cutoff filters (280 nm, 295 nm, 305 nm, 320 nm, 380 nm, 425 nm, 480 nm) were used. An opaque disk was used for the 15th cell in order to create a dark control. The spectral irradiance under each filter with 1nm resolution was measured using an Olis 756 spectroradiometer, using a 2-inch integrating sphere, attached with a 60 cm fiber optical cable. The spectroradiometer was calibrated using a OL 752-10 tungsten halogen standard lamp. Irradiations were either 4 or 6 hours in length for CO_2 and 3 hours for CO, resulting in a total photon dose of either 12.3 mols photons/cm^2 or 18.5 mols photons/cm^2 for CO_2 and $9.25X10^{-4}$ mols photons/cm^2 for CO under the 305 nm cutoff filter. The UV-visible absorbance of each sample was measured directly in the spectrophotometric cells on a Perkin-Elmer Lambda-40 spectrophotometer before and after each irradiation. The absorbance spectrum was converted to absorption for use in apparent quantum yield calculations using the equation

$$a(\lambda) = \frac{A(\lambda) * 2.303}{\ell} \tag{3.1}$$

where a is the Naperian absorption coefficient (m^{-1}), A is the absorbance measured by the spectrophotometer and is unitless, ℓ is the length of the spectrophotometric cell (m), and 2.303 converts from log 10 scale to natural log scale (i.e. Naperian). In all experiments, photochemical fading was minimal (less than 1% at all wavelengths). In order to account for minor effects of fading in apparent quantum yield calculations, linear fading was assumed and the linear average between the starting and ending absorption spectra was used.

Photochemically produced CO_2 was measured on a Shimadzu TOC V-CPN configured for IC analysis. The TOC was calibrated daily using a Na_2CO_3 primary standard (Na_2CO_3, ACS Grade, Fisher Scientific), which was prepared daily. The samples were drawn directly into the sample syringe from the bottom of the spectrophotometric cells, while venting room air into the top through a needle. Drawing from the bottom directly into the sample syringe minimized contact with room air prior to analysis. While waiting to be processed, spectrophotometric cells were stored under water (Millipore Milli-Q Gradient System), in order to slow potential gas transfer from the atmosphere across the septa.

Photochemically produced CO was measured with a head-space equilibration [*Xie et al.*, 2002] on a SRI 8610C gas chromatograph fitted with a reduced gas analyzer, using a mercuric oxide (HgO, Fisher Scientific) reactor bed and photometric detection of the resulting mercury gas. The gas chromatograph was equipped with a 30 cm long 5 Å molecular sieve column (SRI), and was operated at 20 psi, which ensured a flow rate of the N_2 carrier gas of ~11 mL/min. To ensure an initial CO-free headspace for equilibration, room air was drawn slowly through a 50 cc column of Schutze Reagent (Fisher Scientific). The gas chromatograph was calibrated daily using a 1 ppm CO primary standard (Scott Specialty Gas, Air Liquide), and a successive dilution with CO-free air (Limit of Quantification 7.8 ppb). In all experiments, a blank of CO-free air drawn through the Schutze Reagent column contained undetectable levels of CO, and all calibration curves necessarily had intercepts of zero.

2.4 Apparent Quantum Yield Spectra

In natural waters, photochemical production of CO and CO_2 is defined by their respective Apparent Quantum Yield (AQY):

$$AQY(\lambda) = \frac{mol\ product\ formed(\lambda)}{mol\ photons\ absorbed\ by\ CDOM(\lambda)} . \tag{3.2}$$

The AQY is unitless and all quantities are spectral. Thus, in order to describe these photoreactions, the two quantities that must be known are the amount of product formed over the course of the experiment, and the total amount of photons absorbed by the

CDOM in the sample. The amount of product produced in a given experiment is measured by the analytical techniques described above. The number of photons absorbed over the course of an experiment for optically thick samples is calculated using the following equation from Hu et al. [2002]

$$Q_a(\lambda) = E(0)_\lambda \times (a_{CDOM(\lambda)} / a_{t(\lambda)}) \times S \times [1 - \exp(-a_{t(\lambda)} \times L)] \tag{3.3}$$

where Q_a is the mol photons absorbed/second by the sample, E(0) is the irradiance entering the top of the cell (mols photons/m^2/sec), S is the irradiated surface area of the spectrophotometric cell (m^2), a_{CDOM} and a_t are the absorption coefficients for CDOM and for the total solution, respectively (m^{-1}), and L is the pathlength of the spectrophotometric cell (m). Making the assumption that essentially all of the absorption in the cell occurs due to CDOM, i.e. $a_{CDOM} \approx a_t$, this equation is simplified to

$$Q_a(\lambda) = E(0)_\lambda \times S \times [1 - \exp(-a_{CDOM(\lambda)} \times L)]\,. \tag{3.4}$$

This rigorous treatment of Q_a is necessary to avoid overestimating the absorption of photons by samples that experience varying light fields over the length of the spectrophotometric cell due to inner filter effects (i.e. self shading) [*Hu et al.*, 2002].

Due to the multispectral nature of these irradiations an iterative non-linear fitting routine must be used [*Johannessen and Miller*, 2001; *White et al.*, 2010; *Xie et al.*, 2009; *Ziolkowski and Miller*, 2007]. The experimental photochemical production under each cutoff filter is calculated according to the equation

$$\frac{dP}{dt} = AQY * Q_a \tag{3.5}$$

where the $\frac{dP}{dt}$ is the production rate of the species in question (CO or CO$_2$) per experiment. The spectral equation of the AQY is defined *a priori* as

$$AQY_{\lambda} = e^{-(m_1 + m_2(\lambda - m_3))} \tag{3.6}$$

and initial estimates for the fitting coefficients, m_1, m_2, and m_3 are from literature values [*Johannessen and Miller*, 2001; *Ziolkowski and Miller*, 2007]. The *nlinfit* routine iteratively fits the defined AQY equation adjusting the m coefficients and providing the single AQY spectrum that best describes the production measured under all of the cutoff filters for a single experiment.

2.5 CDOM Normalized Production Rates

In this experimental set up, the irradiance spectrum under the 305nm cutoff filter is equivalent to that of the solar spectrum, and photoproduction of either product under this cutoff filter is equivalent to photoproduction in the natural system for an equivalent photon dose. For certain comparisons, this number (referred to as in-cell production) can yield useful data about the variation of photoproduction in the system, but intrinsically linked to this number is the absorption coefficient of the CDOM in the system.

In order to assess the variation of the entire apparent quantum yield spectrum, independently from the CDOM in the original sample, CDOM normalized production is calculated, using the photoproduction equation:

$$\frac{d[product]}{dt}(\lambda) = E_0(\lambda) * a_g(\lambda) * \Phi(\lambda)$$

where the concentration of product per unit time (e.g. mol/s) is a spectrally dependent. $E_0(\lambda)$ is the scalar irradiance (mol photons/m^2/s), $a_g(\lambda)$ is the absorption coefficient of the CDOM (m^{-1}), Φ is the AQY (unitless), and each of these quantities is spectral. To assess only the variation in efficiency, i.e. AQY, we employ a standard absorption spectrum (absorption of the November 2008 Altamaha high tide sample) as well as a standard irradiance spectrum, while the AQY spectrum varies, and we integrate over the active wavelengths (260 nm – 450 nm). This allows an evaluation of the efficiency taking in both the slope of the AQY spectrum and its relative magnitude. For consistency, the spectral irradiance used was the same as in the experimental setup, leading to units of production in the spectrophotometric cell of nmol product/s/cell (~30 mL).

2.6 Spectral Slope Determinations

Spectral "slope" is in fact the slope coefficient of exponential fit to the CDOM absorption curve of a natural water sample, defined over a given wavelength range. Helms et al [2008] have shown that the spectral slope coefficient for the wavelength ranges 275 nm -295 nm ($S_{275\text{-}295}$) correlates with the molecular mass of the CDOM in the sample in seawater. Shallow spectral slopes in the UV, indicate smaller molecular size . Conversely, a steep $S_{275\text{-}295}$ indicates high molecular size.

Spectral slope was determined by using a non-linear to the CDOM absorption curve over the prescribed wavelengths, 275-295 nm. Using Matlab's® *nlinfit* routine, similarly to the AQY determination, the CDOM spectra were fit to the equation

$$a_g(\lambda) = A * e^{-S\lambda} \tag{3.7}$$

where a_g is absorption in m^{-1}, A is a fitting constant, λ is wavelength in nm, and S is the spectral slope coefficient.

2.7 Specific Ultraviolet Absorption

Specific ultraviolet absorbance (SUVA) is the absorbance of CDOM at a specific UV wavelength relative to the total dissolved organic carbon (DOC) concentration of the sample. When highly absorbing moieties such as those with aromatic structures make up a large fraction of the total DOC, SUVA will be higher. Indeed, Weishaar et al [2003] found a strong positive correlation between % aromatic content and SUVA at 254 nm (i.e. $SUVA_{254}$), in a variety of natural organic matter samples.

DOC is regularly measured as part of the GCE-LTER nutrient monitoring program, and DOC samples were collected at the same time as the photochemical samples were collected (www.gce-lter.marsci.uga.edu). The UV absorption at 254 nm was taken from the absorption spectrum of the sample prior to irradiation and $SUVA_{254}$ - was calculated using the equation

$$SUVA_{254} = \frac{a_g(254)}{DOC} \tag{3.8}$$

where $a_g(254)$ is the absorption coefficient of the sample prior to irradiation, and DOC is the concentration of DOC in the system in mg C/L.

2.8 Annual Photochemical Production

To extrapolate our AQY data set to photoproduction of CO and CO_2 in coastal waters total annual photoproduction in the South Atlantic Bight was calculated using the photoproduction equation, adapted from Fichot and Miller [2010] and Stubbins et al [2006] was used as shown,

$$\sum_{area} \int_{290}^{490} P(\lambda) = E_{d0-}(\lambda) * R(\lambda) * AQY(\lambda) * 12 \tag{3.9}$$

where P is the annual photoproduction rate (g C/year/m^2) summed over the area of interest, E_{d0-} is the downwelling spectral irradiance, for 30°N latitude (mol photons/year/m^2) calculated using the STAR model (System for Transfer of Atmospheric Radiation, University of Munich,[*Ruggaber et al.*, 1994]) following the methodology laid out in [*Fichot and Miller*, 2010], AQY is the apparent quantum yield in question (unitless), 12 is the molecular mass of carbon (g/mol), λ is wavelength (nm) and R is the ratio of CDOM absorption to total light attenuation (unitless), and is derived from a large coastal and oceanic data set [*Fichot*, 2004]. The ratio follows a linear relationship spectrally,

$$R(\lambda) = \frac{a_g}{K_D} = -0.0028(\lambda) + 1.575 \tag{3.10}$$

where a_g is absorption (m^{-1}), K_D is the downwelling attenuation coefficient (m^{-1}) and the ratio itself is unitless.

Mean apparent quantum yield spectra were determined by averaging the individual coefficients (i.e. m_1, m_2, m_3) of the AQY equation (equation 3.6) for all experiments.

3. Results

3.1 Apparent Quantum Yield Spectra and CDOM Normalized Photoproduction Rates

Examining the entire AQY data set shows a much tighter distribution between samples for carbon monoxide than for carbon dioxide, as can be seen in Figure 3.2. Overall, the efficiency of production of CO in the visible wavelengths is higher and of a smaller range than for CO_2, i.e. 10^{-5} to 10^{-9} at 550nm compared 10^{-5} to 10^{-12} at 550 nm.

The CDOM normalized photoproduction rates for CO and CO_2 can be seen in Figure 3.3. For both products there is no clear seasonal pattern between sites, though there appears to be more variation among the terrestrially influenced sites (i.e. Doboy Sound and Altamaha Sound) for CO_2. Both products appear to have a slight seasonal signal in Sapelo Sound, the most coastally marine influenced source, lower efficiency of production in the spring and summer months, with higher efficiency of production in the fall and winter months. The slightly lower efficiency in the spring and summer months is mirrored for all three stations at high tide for CO, though not for CO_2.

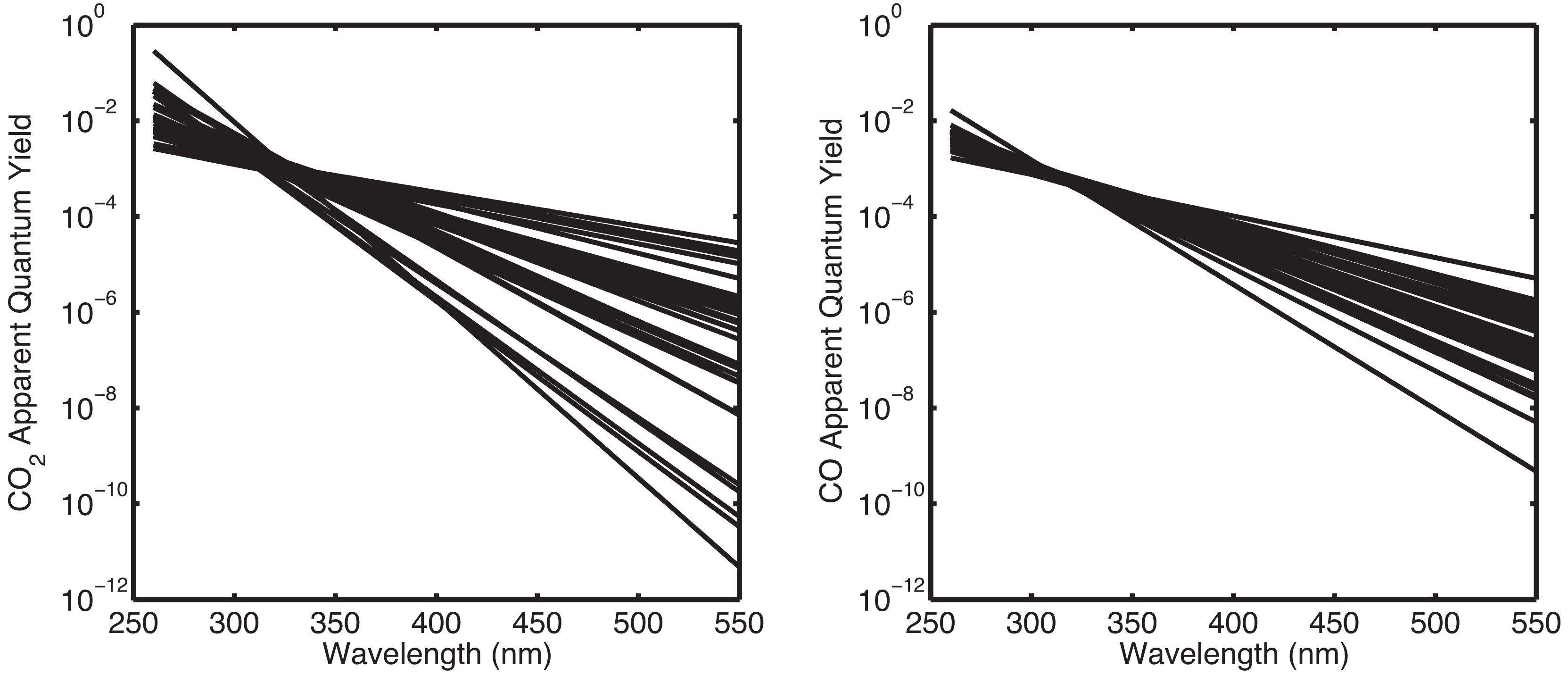

Figure 3.2: Apparent Quantum Yield Spectra for CO_2 and CO.

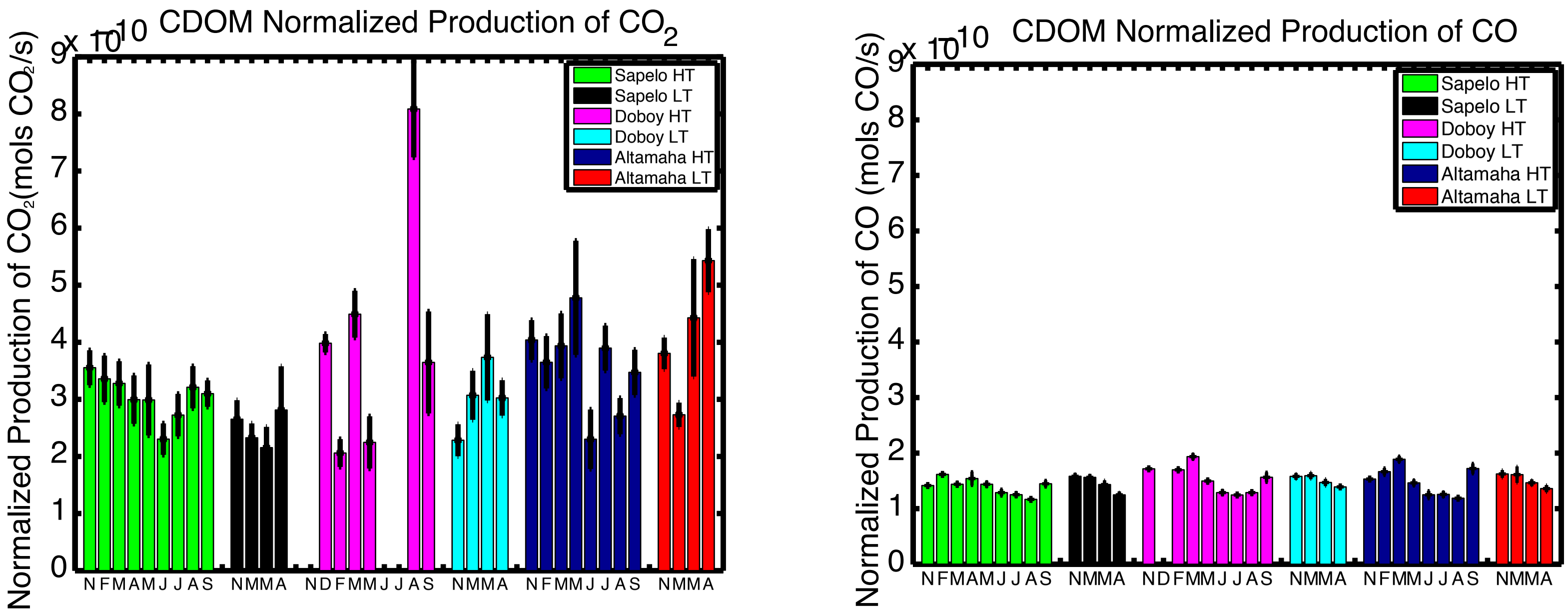

Figure 3.3: CDOM Normalized Production for CO_2 and CO. Error bars represent standard error of AQY.

3.2 Production Ratios

The ratio between photochemical production of CO_2 and CO is of interest because of the analytical difficulty of measuring photochemical CO_2 production in marine systems. In this study the ratio between photochemical production of CO_2 and CO was examined in three separate ways. First the in-cell production ratio was calculated (CO_2:$CO_{in\text{-}cell}$), second the ratio of the AQY at two different wavelengths was computed (300nm and 400nm, $RAQY_{300}$ and $RAQY_{400}$), and finally the ratio of CDOM normalized production was used (CO_2:$CO_{simualated}$). The results of this can be seen in Table 3.1. For all methods, the results were not statistically unique, though there is a larger standard deviation for $RAQY_{400}$.

3.3 Photochemical production and CDOM

Chromophoric dissolved organic matter (CDOM) is considered to be the carbon fuel for the production of both CO and CO_2. The relationship between CDOM "concentration", using the absorption coefficient of the sample at 320 nm (a_g320, m^{-1}) as a proxy, and in-cell production is shown in Figure 3.4a. The relationship between a_g320 and CDOM normalized production is shown in Figure 3.4b. Samples with higher a_g320 absorb more photons and it follows that there would be corresponding higher production of any photochemical product, as is seen in Figure 3.4a, however the scatter in the CO_2 data set does not allow for a statistically significant evaluation of this. CDOM normalized production, as a proxy for the integrated AQY spectrum, shows no trend for either product with a_g320.

Table 3.1: CO_2:CO mean production ratios

CO_2:CO ratio	**Ratio standard deviation**	**Method used**
2.25	1.26	In cell production
2.53	1.50	AQY 300nm
3.50	5.05	AQY 400nm
2.32	0.90	Simulated production

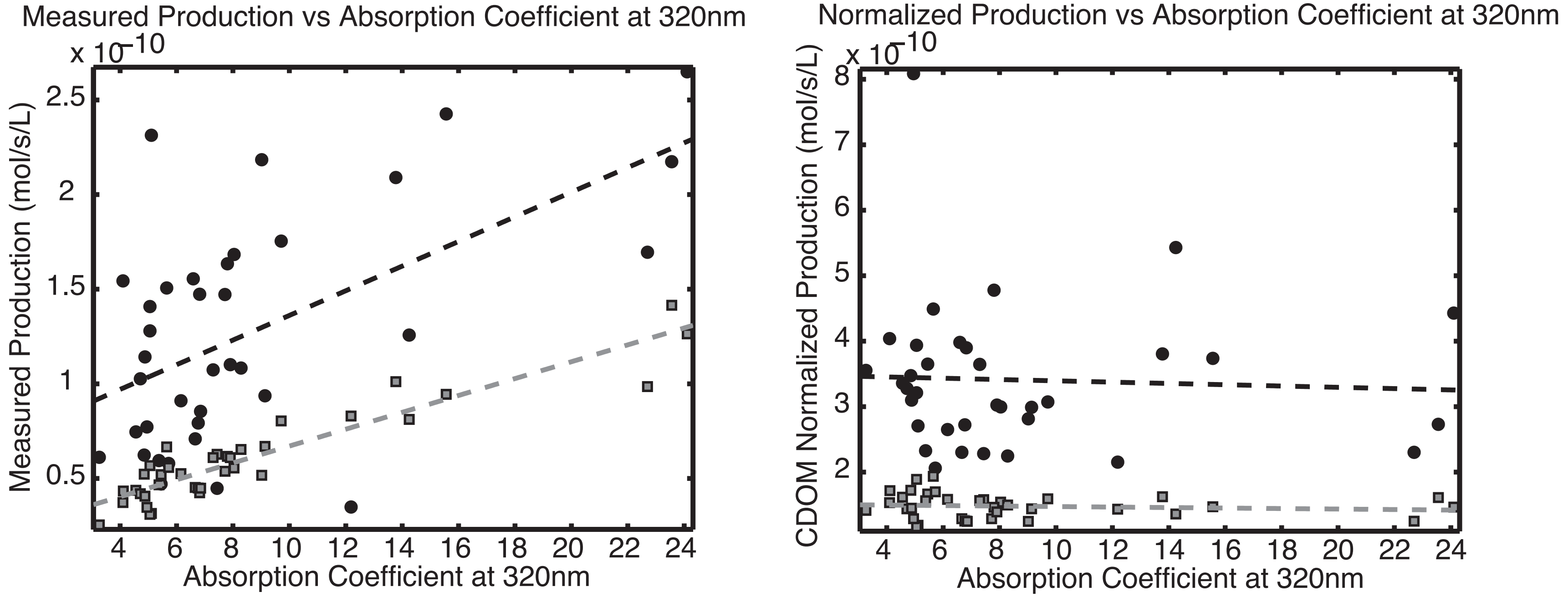

Figure 3.4: Measured production and CDOM normalized production with respect to absorption coefficient of sample at 320nm. Black circles representCO_2 and grey squares represent CO.

3.4 Photochemical production and spectral slope

The in-cell production of both products shows a large amount of scatter with relation to spectral slope and no discernable trends, as can be seen in Figure 3.5a. CDOM normalized production shows no less scatter than in-cell production, but no trend with respect to spectral slope (Figure 3.5b).

3.5 Photochemical production and specific ultraviolet absorbance

In-cell production showed a large amount of scatter with a slight indication of increasing trend with increasing $SUVA_{254}$, however, this is not statistically significant (Figure 3.6a). Evaluating how the efficiency of production changes by using CDOM normalized production shows less scatter than in cell production, but no trend for either CO or CO_2, suggesting that higher aromatic content CDOM is equally efficient at producing CO and CO_2 through photochemical processes as CDOM with lower aromatic content (Figure 3.6b).

3.6 Estimated Photochemical Production

Table 3.2 shows annual photochemical production estimates for the South Atlantic Bight) estuaries and inner shelf (SABi) using the areal extent values from Cai (2011) ($37.7\text{X}10^9$ m^2). Photochemical production of CO_2 was calculated using both the mean ratio of CO_2 to CO production, as well as the mean AQY derived from our CO_2 data set. Using the production ratio annual SABi photoproduction of CO_2 is $1.58\text{X}10^{11}$ gC/year, while using our mean AQY, annual SABi photoproduction is $1.05\text{X}10^{10}$ gC/year. Annual photoproduction of CO in the SABi is $6.03\text{X}10^{10}$ gC/year, using the mean AQY from our CO data set.

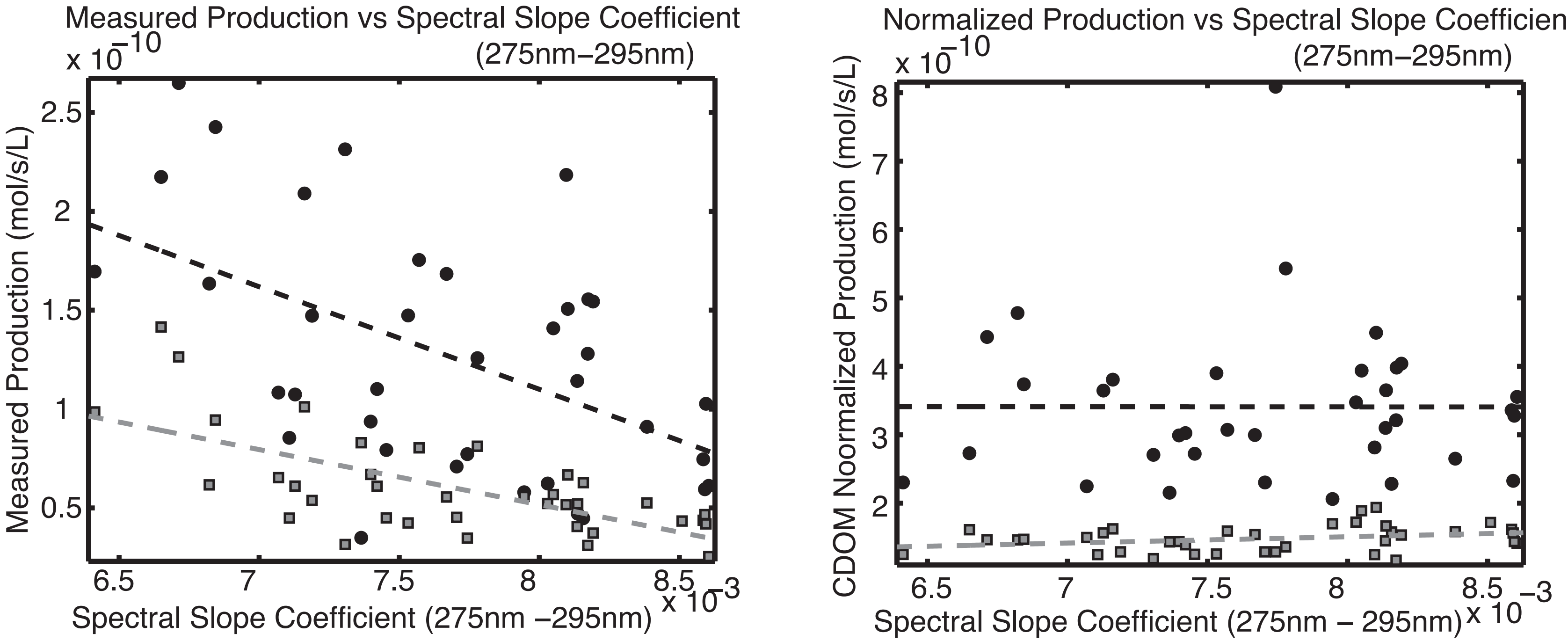

Figure 3.5: Measured production and CDOM normalized production with respect to the spectral slope coefficient (275-295nm). Black circles represent CO_2 and grey squares represent CO.

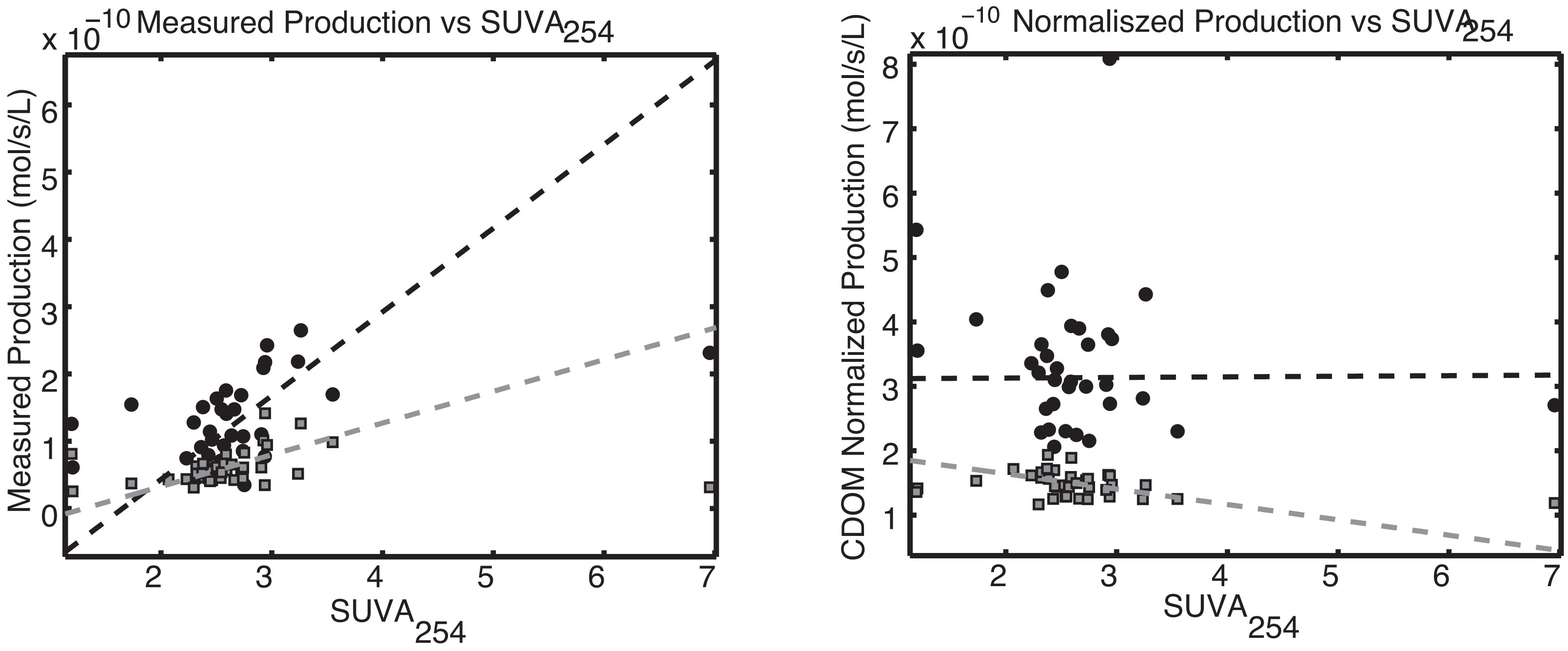

Figure 3.6: Measured production and CDOM normalized production with respect to the specific UV absorbance (254nm) of the sample. Black circles represent CO_2 and grey squares represent CO.

Table 3.2: Annual photoproduction calculated for the South Atlantic Bight (SAB) for CO and CO_2

Photoproduct	Annual SAB production (gC/year)	Method used
CO	$6.03X10^{10}$	Mean AQY
CO_2	$1.05X10^{10}$	Mean AQY
CO_2	$1.58X10^{10}$	CO_2:CO in cell production ratio

4. Discussion

4.1 Seasonal changes in photoproduction efficiency

The two sites that experience significant freshwater flow during the year (Doboy and Altamaha Sounds) exhibit considerable seasonal variability in their AQY spectra (as seen with CDOM normalized production, Figure 3.3) for CO_2. The Sapelo Sound samples show considerably less variability, likely due to the homogeneity of the carbon source material (CDOM). Sapelo Sound is a tidally dominated system, with no significant fresh water influence throughout the year with its major DOC source from tidal exchange with coastal waters and the surrounding marshes, this is unlike the mixed influence of marsh and riverine DOC as seen in the Doboy and Altamaha Sounds were the Altamaha river delivers upland (i.e. not marsh-derived) DOC with a seasonal and thus creates an inherently more complex system.

CDOM normalized production of CO shows less variability than does CO_2 across all samples. All three sites for CO as well as Sapelo Sound for CO_2 show a decrease in efficiency in the spring and summer months with and increase in efficiency in the fall and winter months. While the total change is small (21.7% November to August for CO [all sites], 9.6% November to August CO_2 [Sapelo Sound]) the fact that the trend appears for both photoproducts suggests that it is real. In Georgia, the marshes are dominated by the smooth cordgrass, *Spartina alterniflora*. Spring and summer months represent high productivity in the marsh, with senescence beginning in September and October. The fall represents a period of increased organic matter input from the marshes and this increased flux of newly formed organic carbon could explain the higher efficiency in of photoproduction of both CO and CO_2 in the fall and winter months. Interestingly, this trend is seen at all three sites for CO, which suggests that the marsh-derived carbon is the dominant source for CO photoproduction, while the carbon driving CO_2 photoproduction is dominated by a mix of both riverine and marsh derived carbon.

4.2 Production Ratios

The production ratio between CO_2 and CO is of interest because of the analytical complexity of determining the CO_2 AQY spectra. While some estimates of regional and global photochemical production of CO_2 have been made [*Miller and Zepp*, 1995; *Mopper and Kieber*, 2000], these are generally based on ratios between CO_2 and CO photoproduction, together with the relatively more well-defined CO photoproduction estimates. The first study to define a ratio between CO_2 and CO photoproduction showed a ratio between 15 and 20 (CO_2:CO) [*Miller and Zepp*, 1995], which suggested that CO_2 is by far the largest inorganic photoproduct in the worlds oceans. This was the only study where CO and CO_2 were measured from the same cell at the same time, and raises the question of whether the absence of the carbonate system and differing pH could affect the photoproduction of CO. More recent studies have shown that the ratio between CO_2 and CO photoproduction is more variable and that it could range from 2 to 98 depending on the water type [*White et al.*, 2010]. In this study, the ratio of CO_2 to CO was calculated in 4 different ways. In all cases, the ratio between CO_2 and CO was much lower than most previous estimates. All four methods give mean ratios of ~2. None of the methods is statistically different from the others.

Regardless of the method used to calculate the photoproduction ratio in this study, the ratio is considerably less than seen in previous studies [*Miller and Zepp*, 1995; *White* *et al.*, 2010]. Figure 3.2 shows that there is relatively high photoproduction in the blue wavelengths for CO, where the CO_2 is more variable and has lower visible production. While the CO AQY spectra fall in the same range seen in other studies [*Valentine and Zepp*, 1993; *Xie et al.*, 2009], the efficiency overall generally is somewhat higher than some other studies [*Ziolkowski and Miller*, 2007]. Tables 3.3 and 3.4 show the AQY spectra for several literature values as well as this study for CO_2 and CO, respectively. CO_2 AQY spectra are also within range of literature values [*Johannessen and Miller*, 2001; *Skalski*, 2006; *White et al.*, 2010], though smaller in the visible wavelengths than the more open ocean values [*Johannessen and Miller*, 2001]. While the overall AQY spectra fall in the same range as other literature reported values, the CO AQY spectra are slightly higher than seen in previous studies. The higher production of CO is likely the driver behind the lower CO_2 to CO photoproduction. The three sampling sites in this study are highly marsh influenced as mentioned above. This strong non-point source of DOC to the coastal ocean off the Georgia Bight is possibly the reason for such strong production of CO, and the resulting lower ratio between CO_2 and CO photoproduction.

4.3 Optical signals as indicators of molecular characteristics and their relationship to photoproduction efficiencies

The increase in photoproduction with increasing absorption suggests that darker waters are more efficient at producing CO and CO_2. However, the CDOM normalized production shows no trend with increasing absorption which shows that the carbon in these darker waters is actually neither more or less efficient at producing CO and CO_2 and that the increase of true production seen is just a result of more photons being absorbed and thus being able to cause a photoreaction (Figure 3.4).

Table 3.3: Comparative CO_2 AQYs from the literature

AQY 300nm	AQY 400nm	AQY 500nm	Location	Study
2.63E-03	9.09E-05	8.59E-06	Georgia Estuaries	This study (mean)
2.24E-03	8.25E-04	3.04E-04	Mid Atlantic Bight	[*Johannessen and Miller*, 2001]
3.74E-03	1.52E-03	6.17E-04	Mid Atlantic Bight	[*Johannessen and Miller*, 2001]
6.76E-04	3.36E-05	1.67E-06	Mid Atlantic Bight	[*Johannessen and Miller*, 2001]
2.96E-03	2.40E-03	1.95E-03	Medway Harbour, NS	[*Skalski*, 2006]
6.49E-04	2.17E-05	7.23E-07	Delaware River Estuary	[*White et al.*, 2010]
7.03E-04	1.92E-05	5.25E-07	Delaware River Estuary	[*White et al.*, 2010]
6.30E-04	4.23E-05	2.84E-06	Delaware River Estuary	[*White et al.*, 2010]

Table 3.4: CO AQYs from the literature

AQY 300nm	AQY 400nm	AQY 500nm	Location	Study
1.06E-03	4.03E-05	2.26E-06	Georgia Estuaries	This study (mean)
1.25E-05	1.18E-06	2.66E-07	Beaufort Sea	[*Xie et al.*, 2009]
9.50E-05	3.80E-06	5.68E-07	Beaufort Sea	[*Xie et al.*, 2009]
8.68E-06	9.49E-07	2.30E-07	Beaufort Sea	[*Xie et al.*, 2009]
8.37E-06	9.28E-07	2.26E-07	Beaufort Sea	[*Xie et al.*, 2009]
5.91E-06	7.49E-07	1.96E-07	Beaufort Sea	[*Xie et al.*, 2009]
2.65E-01	1.63E-04	5.09E-06	Beaufort Sea	[*Xie et al.*, 2009]
4.28E-02	7.56E-05	3.35E-06	Beaufort Sea	[*Xie et al.*, 2009]
3.56E-01	1.83E-04	5.43E-06	Beaufort Sea	[*Xie et al.*, 2009]
5.17E-04	9.36E-06	9.93E-07	Beaufort Sea	[*Xie et al.*, 2009]
6.93E-06	8.27E-07	2.09E-07	Beaufort Sea	[*Xie et al.*, 2009]
6.01E-05	2.94E-06	4.83E-07	Beaufort Sea	[*Xie et al.*, 2009]
8.19E-05	1.36E-06	2.25E-08	Gulf of Maine	[*Ziolkowski and Miller*, 2007]
2.31E-04	5.72E-06	1.41E-07	Sapelo Sound	[*Miller et al.*, 2002]
1.85E-04	5.07E-07	1.39E-09	Altamaha River	[*Miller et al.*, 2002]
2.00E-04	1.80E-05	6.00E-06	Okefenokee Swamp	[*Valentine and Zepp*, 1993]

Stubbins et al. [2008] showed that the aromaticity of a sample was positively correlated with increased photoproduction of carbon monoxide. While aromatic content was not directly measured in this study, Weishaar et al. [2003] showed a very strong positive linear relationship between $SUVA_{254}$ and aromatic content of natural carbon samples. Using $SUVA_{254}$ as a proxy for aromatic content, both CO and CO_2 lacks any distinct trend, likely due to the scatter in the data and the small range of $SUVA_{254}$ in this study (Figure 3.6). When focusing on efficiency of the photoreactions, both CO and CO_2 show no trend with increasing aromaticity. This results shows that though aromatic content may be an indicator of high photoproduction of CO, as shown by Stubbins et al. [2008], and possibly CO_2 as well, the aromatic carbon in our samples is not more efficient at producing either photoproduct. As with the correlation with the absorption of the sample, the increase in production is not due to these samples being more efficient at producing CO or CO_2, but rather they absorb more photons leading to more photoreactions.

In-cell production shows a slight decreasing trend with spectral slope for both CO and CO_2, but there is no trend with CDOM normalized production for both photoproducts (Figure 3.5). The lack of trend with CDOM normalized photoproduction suggests that over the range of carbon seen in this study neither the high molecular size nor the low molecular size carbon is more efficient at producing either photoproduct.

The similarity of the response between CO and CO_2 photoproduction for all of these optical indicators suggests that in this marsh-dominated system, the drivers of this photochemical activity are similar.

4.4 Contribution of photochemistry to the coastal system

The coastal ocean is a dynamic area where many transformations of carbon take place, be they biotically mediated or abiotically mediated. The contribution of photochemistry to the cycling of carbon from the organic DOC pool to the inorganic forms of CO and CO_2 in the coastal ocean has the potential to impact global carbon pools. In this study, photochemistry was found to contribute $6.03X10^{10}$ gC/year to the estuaries and inner shelf of the SAB as CO, along with $1.58X10^{11}$ gC/year in the form of CO_2. Calculating using our mean AQY gives a smaller estimate for the contribution of photochemistry in the form of CO_2. The ratio method of calculating CO_2 photoproduction is most often used due to the lack of AQY data for CO_2 in marine systems. In this case can be considered a high-end estimate for CO_2 photoproduction, with the mean AQY being a low estimate. Adding the CO and CO_2 together, the contribution of photochemistry to formation inorganic carbon products in this region is between $1.65X10^{11}$gC/year and $2.18X10^{11}$gC/year in the estuaries and inner shelf of the SAB. Cai [2011] and Jiang et al [2008a] found that the estuaries and inner shelf of the SAB are sources of CO_2 to the atmosphere. Combined, these two areas degas $2.29X10^{12}$gC/year to the atmosphere, and this is supported by remineralisation processes in the heterotrophic ecosystem [*Cai*, 2011]. Photochemical production of inorganic carbon products in this system could contribute 7.2% to 9.5% of the total annually. Total DOC input into the SAB annually is $5.1X10^{12}$gC/year ([*Cai*, 2011], based on numbers from [*Alberts and Takacs*, 1999; *Hopkinson*, 1988; *Moran et al.*, 1999]), with the vast majority of that being marsh derived (~86%). A significant portion of this DOC is transformed throughout the transit from marsh and river to open ocean [*Cauwet*, 2002]. Photochemistry could then mineralize between 3.2% and 4.3% of this carbon annually.

Estimates of global annual photochemical production of CO are fairly well constrained, with total photoproduction on the order of $47X10^{12}$ g C/year [*Fichot and Miller*, 2010; *Stubbins et al.*, 2006; *Zafiriou et al.*, 2003]. Cai [2011] found that though estuaries are a small area of the total global ocean ($1.05X10^{12}$ m^2, 0.3%), they are strong sources of CO_2 to the atmosphere. Similarly, estuaries, while relatively small are strong sources of photochemically produced CO. Per meter, the estuaries of the SAB produce 1.60 gC/m^2/year in the form of CO; using the methodology of Fichot and Miller [2010], the open ocean at the same latitude (30°N) produce 0.14 gC/m^2/year. Assuming that this ratio holds for all estuaries and open ocean realms of the earth, global estuaries produce 11.4X more CO per unit area than the rest of the ocean, and though their total area is only 0.3% of the total ocean area, this contribution can be significant. This difference of one order of magnitude mirrors the difference between previous estimates of CO_2:CO photoproduction (i.e. ~20 [*Miller and Zepp*, 1995; *Mopper and Kieber*, 2000]), and the results seen in this study with a ratio of ~2. Enhanced estuarine CO photochemical production could explain this variation.

Estuaries are dynamic areas, in terms of both production and turnover of organic carbon. The total areas of estuaries are small but they are important parts of the global ocean. Enhanced DOC inputs may lead to enhanced photoproduction, especially of CO. The photochemical impact on carbon cycling in these systems is significant, and it must be included in global models.

Acknowledgments

The authors would like to thank the GCE-LTER, S. B. Joye, and K. S. Hunter for the use of the dissolved organic carbon data.

References

Alberts, J. J., and M. Takacs (1999), Importance of humic substances for carbon and nitrogen transport into southeastern United States estuaris, *Organic Geochemistry*, *30*, 385 - 395.

Andrews, S. S., S. Caron, and O. C. Zafiriou (2000), Photochemical oxygen consumption in marine waters: A major sink for colored dissolved organic matter?, *Limnology and Oceanography*, *45*(2), 267-277.

Anesio, A. M., and W. Graneli (2003), Increased photoreactivity of DOC by acidification: Implications for the carbon cycle in humic lakes, *Limnology and Oceanography*, *48*(2), 735-744.

Anesio, A. M., and W. Graneli (2004), Photochemical mineralization of dissolved organic carbon in lakes of differing pH and humic content, *Archiv Fur Hydrobiologie*, *160*(1), 105-116.

Barbeau, K. (2006), Photochemistry of organic iron(III) complexing ligands in oceanic systems, *Photochemistry and Photobiology*, *82*(6), 1505-1516.

Barbeau, K., E. L. Rue, C. G. Trick, K. T. Bruland, and A. Butler (2003), Photochemical reactivity of siderophores produced by marine heterotrophic bacteria and cyanobacteria based on characteristic Fe(III) binding groups, *Limnology and Oceanography*, *48*(3), 1069-1078.

Belanger, S., H. X. Xie, N. Krotkov, P. Larouche, W. F. Vincent, and M. Babin (2006), Photomineralization of terrigenous dissolved organic matter in Arctic coastal waters from 1979 to 2003: Interannual variability and implications of climate change, *Global Biogeochemical Cycles*, *20*(4).

Bertilsson, S., and L. J. Tranvik (2000), Photochemical transformation of dissolved organic matter in lakes, *Limnology and Oceanography*, *45*(4), 753-762.

Blough, N. V., and R. G. Zepp (1995), Reactive oxygen species in natural waters, in *Active oxygen: Reactive oxygen species in chemistry*, edited by C. S. Foote, pp. 280-333, Chapman and Hall.

Bricaud, A., A. Morel, and L. Prieur (1981), ABSORPTION BY DISSOLVED ORGANIC-MATTER OF THE SEA (YELLOW SUBSTANCE) IN THE UV AND VISIBLE DOMAINS, *Limnology and Oceanography*, *26*(1), 43-53.

Cai, W. J. (2011), Estuarine and Coastal Ocean Carbon Paradox: CO2 Sinks or Sites of Terrestrial Carbon Incineration?, *Annual Review of Marine Science*, *3*, 123-145.

Canadell, J. G., C. Le Quere, M. R. Raupach, C. B. Field, E. T. Buitenhuis, P. Ciais, T. J. Conway, N. P. Gillett, R. A. Houghton, and G. Marland (2007), Contributions to accelerating atmospheric CO2 growth from economic activity, carbon intensity, and efficiency of natural sinks, *Proceedings of the National Academy of Sciences of the United States of America*, *104*(47), 18866-18870.

Carder, K. L., R. G. Steward, P. B. Harvey, and P. B. Ortner (1989), Marine humic and fulvic acids: Their effects on remote sensing of chlorophyll, *Limnology and Oceanography*, *34*(1), 68-81.

Carder, K. L., F. R. Chen, Z. P. Lee, S. K. Hawes, and D. Kamykowski (1999), Semi-analytic MODIS algorithms for chlorophyll a and absorption with bio-optical domains based on nitrate depletion temperatures, *Journal of Geophysical Research-Oceans*, *104*(C3), 5403-5421.

Carlson, C. A. (2002), Production and Removal Processes, in *Biogeochemistry of Marine Dissolved Organic Matter*, edited by D. A. Hansell and C. A. Carlson, pp. 91 - 152, Academic Press, San Diego.

Cauwet, G. (2002), DOM in the Coastal Zone, in *Biogeochemistry of Marine Dissolved Organic Matter*, edited by D. A. Hansell and C. A. Carlson, pp. 579 - 609, Academic Press, San Diego.

Clark, C. D., W. T. Hiscock, F. J. Millero, G. Hitchcock, L. Brand, W. L. Miller, L. Ziolkowski, R. F. Chen, and R. G. Zika (2004), CDOM distribution and CO2 production on the southwest Florida shelf, *Marine Chemistry*, *89*(1-4), 145-167.

Day, D. A., and I. Faloona (2009), Carbon monoxide and chromophoric dissolved organic matter cycles in the shelf waters of the northern California upwelling system, *Journal of Geophysical Research-Oceans*, *114*.

Del Vecchio, R., and N. V. Blough (2002), Photobleaching of chromophoric dissolved organic matter in natural waters: kinetics and modeling, *Marine Chemistry*, *78*(4), 231-253.

Fabry, V. J., B. A. Seibel, R. A. Feely, and J. C. Orr (2008), Impacts of ocean acidification on marine fauna and ecosystem processes, *Ices Journal of Marine Science*, *65*(3), 414-432.

Fichot, C. G. (2004), Marine Photochemistry From Space: Algorithms for the Retrieval of Diffuse Attenuation and CDOM Absorption Coefficients (320 - 490nm) from Ocean Color and Estimation of Depth-resolved Photoproduction Rates of Carbon Monoxide (CO) at Global Scales using SeaWiFS Imagery, 230 pp, Dalhousie University, Halifax, Nova Scotia.

Fichot, C. G., and W. L. Miller (2010), An approach to quantify depth-resolved marine photochemical fluxes using remote sensing: Application to carbon monoxide (CO) photoproduction, *Remote Sensing of Environment*, *114*(7), 1363-1377.

Gao, H. Z., and R. G. Zepp (1998), Factors influencing photoreactions of dissolved organic matter in a coastal river of the southeastern United States, *Environmental Science & Technology*, *32*(19), 2940-2946.

Goldstone, J. V., R. Del Vecchio, N. V. Blough, and B. M. Voelker (2004), A multicomponent model of chromophoric dissolved organic matter photobleaching, *Photochemistry and Photobiology*, *80*(1), 52-60.

Graneli, W., M. Lindell, B. M. De Faria, and F. D. Esteves (1998), Photoproduction of dissolved inorganic carbon in temperate and tropical lakes - dependence on wavelength band and dissolved organic carbon concentration, *Biogeochemistry*, *43*(2), 175-195.

Guo, X. H., M. H. Dai, W. D. Zhai, W. J. Cai, and B. S. Chen (2009), CO2 flux and seasonal variability in a large subtropical estuarine system, the Pearl River Estuary, China, *Journal of Geophysical Research-Biogeosciences*, *114*.

Hansell, D. A., C. A. Carlson, D. J. Repeta, and R. Schlitzer (2009), DISSOLVED ORGANIC MATTER IN THE OCEAN A CONTROVERSY STIMULATES NEW INSIGHTS, *Oceanography*, *22*(4), 202-211.

Helms, J. R., A. Stubbins, J. D. Ritchie, E. C. Minor, D. J. Kieber, and K. Mopper (2008), Absorption spectral slopes and slope ratios as indicators of molecular weight, source, and photobleaching of chromophoric dissolved organic matter, *Limnology and Oceanography*, *53*(3), 955-969.

Hopkinson, C. S. (1988), Patterns of organic carbon exchange between coastal ecosystems - the mass balance approach in salt marsh ecosystems, in *Coastal Offshore Ecosystem Interactions.Lecture Notes on Coastal and Estuarine Studies*, edited by B. O. Jansson, pp. 122 - 154, Springer, Berlin.

Hu, C. M., F. E. Muller-Karger, and R. G. Zepp (2002), Absorbance, absorption coefficient, and apparent quantum yield: A comment on common ambiguity in the use of these optical concepts, *Limnology and Oceanography*, *47*(4), 1261-1267.

Jiang, L. Q., W. J. Cai, and Y. C. Wang (2008a), A comparative study of carbon dioxide degassing in river- and marine-dominated estuaries, *Limnology and Oceanography*, *53*(6), 2603-2615.

Jiang, L. Q., W. J. Cai, R. Wanninkhof, Y. C. Wang, and H. Luger (2008b), Air-sea CO2 fluxes on the US South Atlantic Bight: Spatial and seasonal variability, *Journal of Geophysical Research-Oceans*, *113*(C7).

Johannessen, S. C., and W. L. Miller (2001), Quantum yield for the photochemical production of dissolved inorganic carbon in seawater, *Marine Chemistry*, *76*(4), 271-283.

Kieber, D. J., J. McDaniel, and K. Mopper (1989), PHOTOCHEMICAL SOURCE OF BIOLOGICAL SUBSTRATES IN SEA-WATER - IMPLICATIONS FOR CARBON CYCLING, *Nature*, *341*(6243), 637-639.

Kieber, R. J., X. L. Zhou, and K. Mopper (1990), FORMATION OF CARBONYL-COMPOUNDS FROM UV-INDUCED PHOTODEGRADATION OF HUMIC SUBSTANCES IN NATURAL-WATERS - FATE OF RIVERINE CARBON IN THE SEA, *Limnology and Oceanography*, *35*(7), 1503-1515.

Ludwig, W., J. L. Probst, and S. Kempe (1996), Predicting the oceanic input of organic carbon by continental erosion, *Global Biogeochemical Cycles*, *10*(1), 23-41.

Micinski, E., L. A. Ball, and O. C. Zafiriou (1993), PHOTOCHEMICAL OXYGEN ACTIVATION - SUPEROXIDE RADICAL DETECTION AND PRODUCTION-RATES IN THE EASTERN CARIBBEAN, *Journal of Geophysical Research-Oceans*, *98*(C2), 2299-2306.

Miller, W. L., and R. G. Zepp (1995), PHOTOCHEMICAL PRODUCTION OF DISSOLVED INORGANIC CARBON FROM TERRESTRIAL ORGANIC-MATTER -

SIGNIFICANCE TO THE OCEANIC ORGANIC-CARBON CYCLE, *Geophysical Research Letters*, *22*(4), 417-420.

Miller, W. L., and M. A. Moran (1997), Interaction of photochemical and microbial processes in the degradation of refractory dissolved organic matter from a coastal marine environment, *Limnology and Oceanography*, *42*(6), 1317-1324.

Moffett, J. W., and O. C. Zafiriou (1993), THE PHOTOCHEMICAL DECOMPOSITION OF HYDROGEN-PEROXIDE IN SURFACE WATERS OF THE EASTERN CARIBBEAN AND ORINOCO RIVER, *Journal of Geophysical Research-Oceans*, *98*(C2), 2307-2313.

Mopper, K., and D. J. Kieber (2000), Marine photochemistry and its impact on carbon cycling, in *The effects of UV radiation in the marine environment*, edited by S. J. De Mora, S. Demers and M. Vernet, pp. 101-129, Cambridge University PRess, Cambridge, UK.

Moran, M. A., W. M. Sheldon, and J. E. Sheldon (1999), Biodegradation of riverine dissolved organic carbon in five estuaries of the southeastern United States, *Estuaries*, *22*, 55-64.

Moy, A. D., W. R. Howard, S. G. Bray, and T. W. Trull (2009), Reduced calcification in modern Southern Ocean planktonic foraminifera, *Nature Geoscience*, *2*(4), 276-280.

Osburn, C. L., D. W. O'Sullivan, and T. J. Boyd (2009), Increases in the longwave photobleaching of chromophoric dissolved organic matter in coastal waters, *Limnology and Oceanography*, *54*(1), 145-159.

Ruggaber, R., R. A. Dlugi, and T. Nakajima (1994), Modelling of radiation quantities and photolysis frequencies in the troposphere, *Journal of Atmospheric Chemistry*, 171-210.

Salonen, K., and A. Vahatalo (1994), PHOTOCHEMICAL MINERALIZATION OF DISSOLVED ORGANIC-MATTER IN LAKE SKJERVATJERN, *Environment International*, *20*(3), 307-312.

Shindell, D. T., G. Faluvegi, D. M. Koch, G. A. Schmidt, N. Unger, and S. E. Bauer (2009), Improved Attribution of Climate Forcing to Emissions, *Science*, *326*(5953), 716-718.

Skalski, M. (2006), Seasonal Estimates of Photochemical Production of Dissolved Inorganic Carbon From Terrestrial Organic Matter in an Altantic Canada Coastal Zone Estuary, 74 pp, Dalhousie University, Halifax, Nova Scotia.

Stubbins, A., G. Uher, C. S. Law, K. Mopper, C. Robinson, and R. C. Upstill-Goddard (2006), Open-ocean carbon monoxide photoproduction, *Deep-Sea Research Part Ii-Topical Studies in Oceanography*, *53*(14-16), 1695-1705.

Stubbins, A., V. Hubbard, G. Uher, C. S. Law, R. C. Upstill-Goddard, G. R. Aiken, and K. Mopper (2008), Relating carbon monoxide photoproduction to dissolved organic matter functionality, *Environmental Science & Technology*, *42*(9), 3271-3276.

Tolli, J. D., and C. D. Taylor (2005), Biological CO oxidation in the Sargasso Sea and in Vineyard Sound, Massachusetts, *Limnology and Oceanography*, *50*(4), 1205-1212.

Tolli, J. D., S. M. Sievert, and C. D. Taylor (2006), Unexpected diversity of bacteria capable of carbon monoxide oxidation in a coastal marine environment, and contribution of the Roseobacter-associated clade to total CO oxidation, *Applied and Environmental Microbiology*, *72*(3), 1966-1973.

Valentine, R. L., and R. G. Zepp (1993), FORMATION OF CARBON-MONOXIDE FROM THE PHOTODEGRADATION OF TERRESTRIAL DISSOLVED ORGANIC-CARBON IN NATURAL-WATERS, *Environmental Science & Technology*, *27*(2), 409-412.

Wang, W., C. G. Johnson, K. Takeda, and O. C. Zafiriou (2009), Measuring the Photochemical Production of Carbon Dioxide from Marine Dissolved Organic Matter by Pool Isotope Exchange, *Environmental Science & Technology*, *43*(22), 8604-8609.

Wang, Z. A., W. J. Cai, Y. C. Wang, and H. W. Ji (2005), The southeastern continental shelf of the United States as an atmospheric CO2 source and an exporter of inorganic carbon to the ocean, *Continental Shelf Research*, *25*(16), 1917-1941.

Weishaar, J. L., G. R. Aiken, B. A. Bergamaschi, M. S. Fram, R. Fujii, and K. Mopper (2003), Evaluation of specific ultraviolet absorbance as an indicator of the chemical composition and reactivity of dissolved organic carbon, *Environmental Science & Technology*, *37*(20), 4702-4708.

Wetzel, R. G., P. G. Hatcher, and T. S. Bianchi (1995), Natural photolysis by ultraviolet irradiance of recalcitrant dissolved organic matter to simple substrates for rapid bacterial metabolism, *Limnology and Oceanography*, *40*(8), 1369-1380.

White, E. M., P. P. Vaughan, and R. G. Zepp (2003), Role of the photo-Fenton reaction in the production of hydroxyl radicals and photobleaching of colored dissolved organic matter in a coastal river of the southeastern United States, *Aquatic Sciences*, *65*(4), 402-414.

White, E. M., D. J. Kieber, J. Sherrard, W. L. Miller, and K. Mopper (2010), Carbon dioxide and carbon monoxide photoproduction quantum yields in the Delaware Estuary, *Marine Chemistry*, *118*(1-2), 11-21.

Xie, H. X., O. C. Zafiriou, W. J. Cai, R. G. Zepp, and Y. C. Wang (2004), Photooxidation and its effects on the carboxyl content of dissolved organic matter in two coastal rivers in the Southeastern United States, *Environmental Science & Technology*, *38*(15), 4113-4119.

Xie, H. X., S. Belanger, S. Demers, W. F. Vincent, and T. N. Papakyriakou (2009), Photobiogeochemical cycling of carbon monoxide in the southeastern Beaufort Sea in spring and autumn, *Limnology and Oceanography*, *54*(1), 234-249.

Xie, H. X., S. S. Andrews, W. R. Martin, J. Miller, L. Ziolkowski, C. D. Taylor, and O. C. Zafiriou (2002), Validated methods for sampling monoxide and headspace analysis of carbon in seawater, *Marine Chemistry*, *77*(2-3), 93-108.

Zafiriou, O. C., S. S. Andrews, and W. Wang (2003), Concordant estimates of oceanic carbon monoxide source and sink processes in the Pacific yield a balanced global "blue-water" CO budget, *Global Biogeochemical Cycles*, *17*(1).

Zafiriou, O. C., H. X. Xie, N. B. Nelson, R. G. Najjar, and W. Wang (2008), Diel carbon monoxide cycling in the upper Sargasso Sea near Bermuda at the onset of spring and in midsummer, *Limnology and Oceanography*, *53*(2), 835-850.

Zika, R. G., E. S. Saltzman, and W. J. Cooper (1985), HYDROGEN-PEROXIDE CONCENTRATIONS IN THE PERU UPWELLING AREA, *Marine Chemistry*, *17*(3), 265-275.

Ziolkowski, L. A., and W. L. Miller (2007), Variability of the apparent quantum efficiency of CO photoproduction in the Gulf of Maine and Northwest Atlantic, *Marine Chemistry*, *105*(3-4), 258-270.

CHAPTER 4

BIOLOGICAL RESPONSE TO PHOTOCHEMICALLY ALTERED DISSOLVED ORGANIC CARBON IN A COASTAL ENVIRONMENT[1]

---

[1] Reader, H. E. and W. L. Miller. To be submitted to *Limnology and Oceanography*.

Abstract

Chromophoric dissolved organic matter (CDOM) is the fraction of dissolved organic matter that absorbs solar radiation. Although CDOM is largely biologically refractory in nature, photochemistry has the potential to transform biologically refractory carbon into more biolabile forms. Studies suggest that in marine systems, the effect of UVR on carbon availability and subsequent bacterial production varies widely. To quantify the effects of photochemistry on the biological lability of DOC in a terrestrially influenced system, a quarterly sampling effort was undertaken at three estuarine locations off the coast of Georgia, USA, producing a total of 15 apparent quantum yield (AQY) spectra. Water samples were pre-filtered to remove bacterioplankton and other particulate, irradiated and then re-inoculated with the natural microbial community, isolated from the same sample. Oxygen measurements were made as a proxy for community carbon uptake after a 10-12 day incubation period. Seasonal biolabile carbon photoproduction values ranged from -8.8 to +44.1 μmol C produced/L/irradiation. To compare seasonal and spatial variations in photochemically induced stimulation of bacterial respiration over this large data set, irradiations were set at a photon dose of 9.25×10^{-4} mols photons/cm^2 (under 305 nm cutoff filter, Suntest Solar Simulator). Progressive photon dose experiments showed that irradiation length strongly influenced the total biolabile product as assayed with microbial measurements. A conceptual model is presented to explain this dependence on photon dose. The varying dependence on photon dose is different from other photochemical products such as CO, and further complicates attempts to quantify the effect of photochemistry on the bioavailability of carbon in marine environments.

1. Introduction

Marine dissolved organic carbon (DOC) is one of the largest reactive pools of carbon on earth, totaling 662 Pg of carbon [*Hansell et al.*, 2009]. In the open ocean, much of the DOC comes from in situ biological production, through planktonic exudates, sloppy grazing, and decomposition [*Carlson*, 2002]. In the coastal ocean however, the influence of terrestrial systems on the content of the DOC pool is high. Rivers deliver 200 TgC/year to the ocean, most of which is thought originate in terrestrial soils [*Ludwig et al.*, 1996]. The DOC pool supports the oceanic microbial community by providing substrate for heterotrophic consumption, thereby allowing the microbial community to reshape the nature of the coastal DOC pool [*Azam*, 1998; *Pomeroy*, 1974]. While the microbial community is generally an efficient consumer of labile carbon, the entire pool of carbon is not biologically labile. Recent studies show that the lability of DOC in the ocean falls along a continuum with a small pool of very reactive, or labile carbon and a much larger more refractory pool of carbon [*Carlson*, 2002; *Nagata*, 2008].

Chromophoric dissolved organic matter (CDOM) generally occupies the more refractive end of the lability spectrum. CDOM is the fraction of DOC that absorbs solar radiation in the ocean and is thereby responsible for the majority of ultraviolet radiation (UVR) attenuation in the ocean, especially in the coastal regions where concentrations are high [*Bricaud et al.*, 1981; *Fichot and Miller*, 2010]. Absorption of UVR leads to excited molecular states of DOM that will return to ground state by internal energy conversions, releasing heat or light (as in fluorescence or phosphorescence) or by undergoing chemical transformations [*Mopper and Kieber*, 2000]. These photochemical transformations of CDOM in the ocean have been studied over three decades

[*Johannessen and Miller*, 2001; *Miller and Zepp*, 1995; *Stubbins et al.*, 2006; *Zafiriou et al.*, 1984; *Zika et al.*, 1985]. The photoproduction of easily identifiable low molecular weight organic compounds such as pyruvate and carbon monoxide [*D J Kieber et al.*, 1989; *Wetzel et al.*, 1995], suggested that photochemistry could have an effect on biological production in marine environments. This has been further supported by the identification of carbon monoxide as an effective substrate for certain marine bacteria [*Tolli et al.*, 2006; *Xie et al.*, 2005]. Carbon monoxide is the second largest identifiable photochemical carbon product in the ocean, exceeded only by CO_2 [*Miller and Zepp*, 1995; *Mopper and Kieber*, 2002].

The majority of photochemical carbon products are neither easily identifiable nor universally produced by CDOM, though there is evidence that many are substrates that can support microbial growth. A review by Mopper and Kieber [2002] found that out of 59 total studies on the effect of UVR on DOC in fresh and marine waters, 38 showed increased biological lability of carbon, while 21 showed either no effect, or a negative effect. The range of responses was large, from -75% to 200% change in biological activity. In studies of terrestrially dominated systems, such as the coastal ocean, the effect of UVR on the bioavailabilty of carbon tended to be positive, while open ocean studies tended to have negative responses. Based on these studies, Mopper and Kieber [2002] were able to estimate that the magnitude of indirect mineralization of DOM by formation of BLPs and subsequent respiration by microbial communities is on the order of that of direct mineralization of DOM to CO_2, which is estimated to be as high as 20% of new production in the ocean, yearly [*Hansell and Carlson*, 1998]. However, the mechanistic details and spectral dependence have not been considered. The studies reported in Mopper and Kieber [2002] review were based on whole spectrum, or select spectral band irradiations, in both natural solar radiations or in laboratory simulated solar radiation set-ups. To date, there has only been one study on the spectral efficiency of photochemical production (i.e. Apparent quantum yield, AQY) of these biologically labile products (BLPs) [*Miller et al.*, 2002]. This study, based on two samples from coastal waters, showed increasing production of BLPs with shorter wavelengths.

The coastal ocean is a dynamic and productive area, both in terms of biological activity and DOC inputs. The study presented here was focused on the photochemical production of BLPs in three inshore sites on the coast of Georgia, USA. Located on the western edge of the South Atlantic Bight, the coast of the state of Georgia is characterized by outflow from the Altamaha River, which drains the largest watershed in the state, as well as large expanses of salt marsh, dominated by the smooth cordgrass, *Spartina alterniflora.* The highly productive salt marsh creates a large non-point source of DOC to the coastal ocean. This region has been well studied in many disciplines, and the only AQYs published for the formation of BLPs [*Miller et al.*, 2002] were determined for waters around Sapelo Island, GA.

Based on previous work, the influence of photochemistry on BLPs was expected to be positive in this region due to the large terrestrial influence on the composition of DOC. To constrain the variability of BLP photochemistry in this region, the three sites were sampled at four distinct periods of the year (Fall 2008 to Summer 2009). The effect of photon dose (i.e. cumulative absorption) on the production of BLPs was also investigated and proved to be a significant factor in evaluating such irradiation experiments.

2. Methods

2.1 Sampling Methods

Samples were collected at three estuarine locations on the coast of Georgia, USA (Figure 4.1). The mouth of the Altamaha Sound (31.314000°N, 81.265333°W) is a strongly river-influenced site. The Doboy Sound (31.376373°N, 81.281718°W) is to the north of Altamaha Sound, and while it is a mostly coastal marine and marsh dominated site, during periods of high flow on the Altamaha River (typically during the spring months), it can experience a significant fresh water influence. The northernmost site, Sapelo Sound (31.537779°N, 81.176860°W) is a coastal marine dominated site and receives little to no freshwater input over the year.

Sample collection for the seasonal study was performed at mid-month spring tide in November 2008, March 2009, May 2009, and August 2009. Samples for additional experiments to examine photon dose dependency on BLP results were taken from the Marsh Landing Dock, Sapelo Island, GA just adjacent to Doboy Sound (31.420556°N, 81.295833°W). Samples were collected in acid-washed and water-rinsed (Milli-Q Gradient system, Millipore) polycarbonate bottles (2 L, Nalgene), and kept on ice until return to the laboratory (<3 hours).

2.2 Photochemical Methods

Upon return to the laboratory, samples were filtered (0.2 μm, Whatman Polycap AS75) directly into fifteen (15) quartz spectrophotometric cells (10 cm path length, ~30mL; Spectrocell), sealed without headspace using Teflon-faced butyl rubber septa (Specialty Silicone Products, SSP) and placed in a chilled aluminum block (held at 15°C), for irradiation under the solar simulator (Suntest model CPS). Duplicates of 7

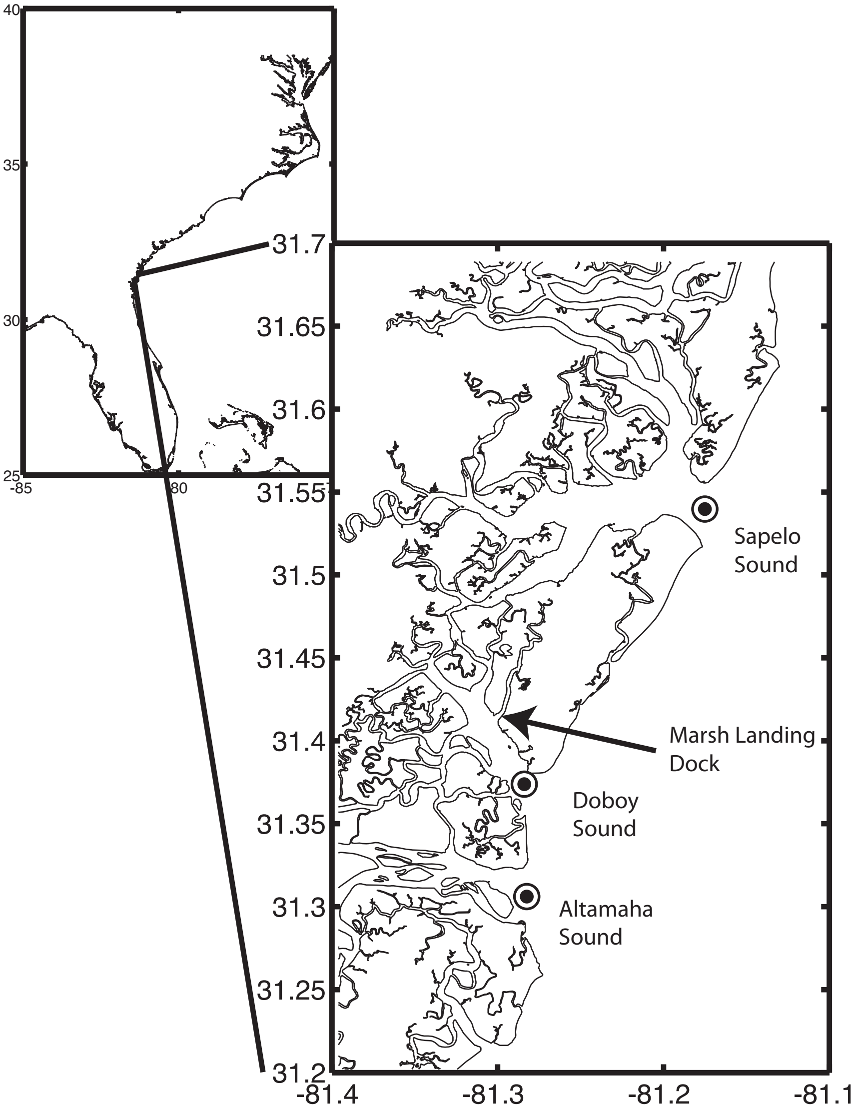

Figure 4.1: Sample sites for the seasonal study and photon dose studies

different Schott-glass cut-off filters (280 nm, 295 nm, 305 nm, 320 nm, 380 nm, 425 nm, 480 nm) were placed over the cells in order to create 14 distinct light fields, and the 15th cell was covered with an opaque disk in order to create a dark treatment. The spectral irradiance under each filter at 1 nm resolution was measured using an Olis 756 spectroradiometer, using a 2-inch integrating sphere, attached with a 60 cm fiber optical cable. The spectroradiometer was calibrated using a OL 752-10 tungsten halogen standard lamp (Figure 4.2). Unless otherwise noted, irradiations were 3 hours long, resulting in a total photon dose of $9.25X10^{-4}$ mols photons/cm^2 under the 305 nm cutoff filter, which provides a spectral shape similar to sunlight. The UV-visible absorbance of the samples was measured directly in the sample cell before and after irradiation (Perkin Elmer Lambda 40) from 250 nm to 700 nm, with 1 nm resolution. Photochemical fading in any sample was minimal (less than 1% at any wavelength) and was accounted for in the AQY calculations, assuming linear photochemical fading, by using the averaged spectrum determined between the starting absorption spectrum and that of each sample after irradiation. In order to account for inner-filter effects (i.e. self-shading) within high CDOM samples, the total photons absorbed by each sample was calculated according to the method described by Hu et al. [2002], and detailed in Chapter 3 of this dissertation.

2.3 Microbial Methods

The natural microbial community was obtained from each sample using a three-stage filtration process. Four litres were pre-filtered was through a 3.0 μm cartridge filter (VWR) to remove larger particulate and detrital matter. Samples were then filtered through a 1.0 μm polycarbonate filter (Whatman) to remove smaller particulates and grazers, and finally the microbial community was captured by filtering on to three 0.2 μm

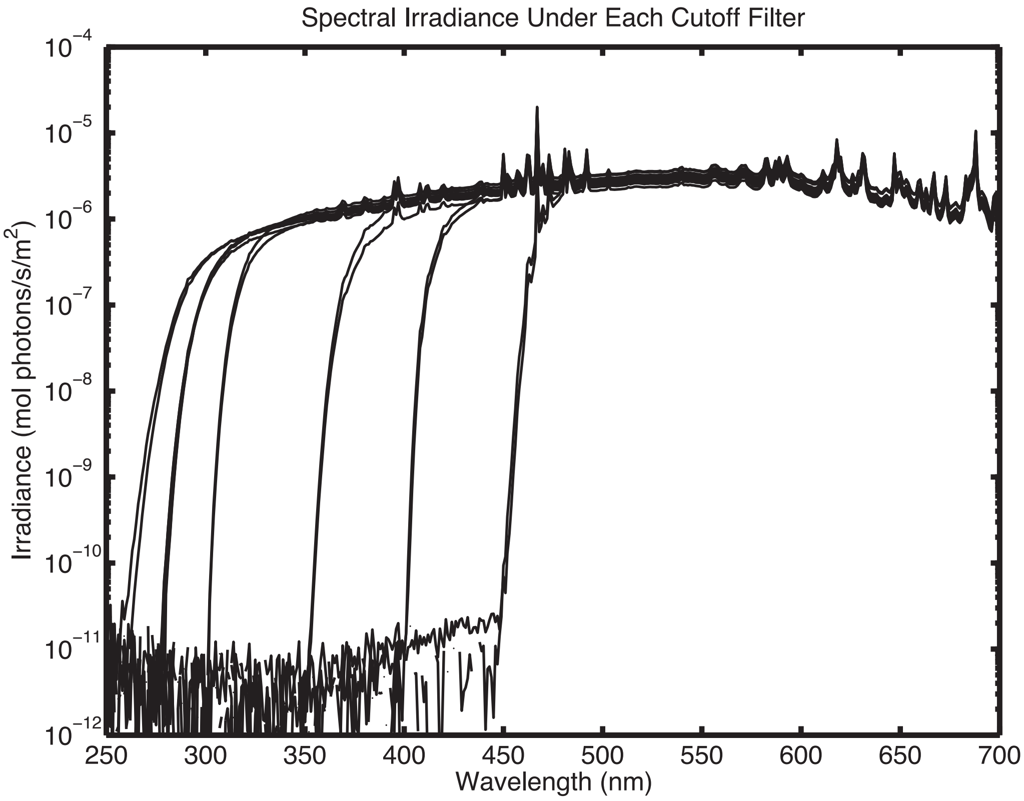

Figure 4.2: Spectral Irradiance under each cutoff filter in the solar simulator

polycarbonate filters (Whatman). The microbial community was re-suspended in 300 mL of 0.2 μm filter-sterilized (Whatman Polycap AS75) sample water, using a shaking table at ambient temperature, with the re-suspended cells in solution for at least 45 minutes. This cell suspension was subsequently used in BLP experiments, without further storage.

After irradiation, samples were poured from the spectrophotometric cells slowly into individual ashed (450°C, 3 hours) glass beakers to reestablish O_2 equilibrium with room air and were then inoculated with 300 μL of the microbial community suspension. Inorganic nutrients, NH_4Cl, $NaNO_3$, NaH_2PO_4 (all Fisher Scientific) were added to a final concentrations of 5 μM NH_4^+, 5 μM NO_3^-, and 1 μM PO_4^{3-}, in order to ensure an excess of nutrients and that carbon would eventually limit growth [*Miller et al.*, 2002]. The 15 irradiated samples were then each transferred to three clean, ashed (450°C, 3 hours) 7 mL vials and sealed without headspace using Teflon-faced butyl rubber septa (1 mm thick, Specialty Silicone Products, SSP). One vial from each was sacrificed immediately in order to establish initial (t = 0) O_2 concentrations, while the remaining vials were placed in a rack and incubated under water in the dark at 30°C and measured after 10 days.

Oxygen consumption was used as a proxy for community microbial carbon consumption, assuming a ratio of 1 mol O_2 consumed for every mole of DOC consumed [*Miller et al.*, 2002], thus biologically lability of carbon is operationally defined as the carbon that is consumed over the course of 10 days. O_2 concentration was measured using an Ocean Optics FOXY-R fluorescence based probe inserted through the septa to prevent gas exchange. The probe was calibrated daily using room air (21% O_2) and pure N_2 (0% O_2) (Praxair Zero Grade). Calibrations and measurements were all performed at a known constant temperature (~25°C) using a temperature controlled water bath. The

Ocean Optics FOXY-R probe performance was compared to traditional Winkler oxygen measurements, and was found to have a positive 20 μM offset. This offset was constant over the range of O_2 concentrations seen in all experiments and was accounted for in our calculations. The Ocean Optics FOXY-R probe has a limit of detection of 0.02 ppm O_2. For further details, see Appendix A of this dissertation.

2.4 Mathematical Methods: AQY Determinations

The apparent quantum yield (AQY) represents the efficiency of a photoreaction and is defined as the spectral quantity

$$AQY(\lambda) = \frac{mol\ product\ formed\ or\ lost(\lambda)}{mol\ photons\ absorbed\ by\ CDOM(\lambda)}. \tag{4.1}$$

Most AQY spectra for single chemical photoproducts, such as CO and CO_2, fit an exponential decay function, described in Johannessen [2001]

$$AQY(\lambda) = e^{-(m_1 + m_2(\lambda - 290))} \tag{4.2}$$

where the AQY is unitless, the wavelength (λ) is in meters, m_1 and m_2 are fitting parameters derived from the change in concentration of the chemical in question and photon absorption measurements made during the photochemical experiment. When possible, AQYs were determined using *nlinfit,* a non-linear fitting routine in MATLAB®. The *nlinfit* routine is an iterative fitting routine that requires a defined equation (i.e. Equation 4.2) to fit spectral data, as well as an initial estimate for the fitting constants. In the case of our BLP photochemical experiments, the spectral response did not fit a typical exponential decay function. In order to mathematically determine a spectral equation for BLP AQYs, a wavelength band subtraction was performed to approximate AQY. The wavelength band subtraction method was described in Johannessen and

Miller [2001]. Briefly, the difference between the spectrally integrated photons absorbed in samples from adjacent cutoff filters (e.g. $\text{photons}_{280} - \text{photons}_{295}$) was calculated for each set of wavelength pairs (280-295, 295-305, 305-320, 320-380, 380-425, 425-480). The same was done for the BLP production numbers, and an AQY at the mid-point wavelength (i.e. 288, 300, 313, 350, 403, 453) was determined using Equation 4.3 at 288 nm as an example,

$$AQY_{288} = \frac{mol\ BLP\ produced(295) - mol\ BLP\ produced(280)}{mol\ photon\ absorbed(295) - mol\ photon\ absorbed(280)}\ . \qquad (4.3)$$

With seven distinct cutoff filters, six wavelength-specific AQYs can be defined. The AQYs are then plotted at those wavelengths, and fit to an appropriate equation if possible. The data from the wavelength band subtraction method was fit to various equations in the MATLAB® Curve Fitting Toolbox. This aided in determining a potential spectral shape and starting constants for the more robust iterative fitting routine *nlinfit.* The different equations used to fit the BLP data can be seen in Table 4.1, along with the correlation coefficients of the fits. Because of the density of cutoff filters in the lower wavelengths (i.e. 280, 295, 305, 320), the wavelength band subtraction method has a bias towards overestimating the AQY in the UVR, due to the small difference in absorbed photons in the denominator of the UVR AQYs [*Johannessen and Miller*, 2001].

3. Results

3.1 Production of Biologically Labile Carbon for Full Solar Spectrum Irradiations

For comparison with previously published studies, we examined the photochemical response of BLPs using full solar spectrum irradiations. Figure 4.3 shows the production of BLPs under the 305 nm cutoff filter, sorted by site. Overall, there is no

Table 4.1: Coefficients from the various fits applied to the data using *nlinfit*: Nov = November 2008, Mar = March 2009, May = May 2009, Aug = August 2009, All data (subset) is all data pooled, except for Nov ALT. ALT = Altamaha, SAP = Sapelo, DOB = Doboy. Exponential fits are of the form: $y = ae^{bx}$. Power fits are of the form: $y = ax^{b}$. Double exponential is of the form: $y = ae^{bx} + ce^{dx}$.

Sample	**Fit**	**a**	**b**	**c**	**d**	**e**	**R^2**
Nov ALT	Quadratic	$-9.66X10^{-6}$	$1.07X10^{-2}$	-2.63			-3.51
Nov ALT	Cubic	$-2.49X10^{-8}$	$2.12X10^{-5}$	$-1.76X10^{-3}$	-9.71		-3.46
Nov ALT	Exponential	$1.96X10^{-6}$	$2.33X10^{-2}$				-23.9
Nov SAP	Quadratic	$5.44X10^{-6}$	$-4.23X10^{-3}$	$7.95X10^{-1}$			-1.93
Nov SAP	Cubic	$4.96X10^{-8}$	$-6.01X10^{-5}$	$2.38X10^{-2}$	-3.08		-1.26
Nov DOB	Cubic	$2.27X10^{-8}$	$-3.27X10^{-5}$	$1.52X10^{-2}$	-2.27		-0.25
Mar ALT	4th degree	$-1.61X10^{-9}$	$2.97X10^{-6}$	$2.00X10^{-3}$	$5.82X10^{-1}$	-62.1	-1.37
Mar SAP	Quadratic	$3.41X10^{-6}$	$-2.73X10^{-3}$	$5.33X10^{-1}$			-0.67
Mar SAP	Cubic	$-3.72X10^{-8}$	$5.24X10^{-5}$	$-2.35X10^{-2}$	3.39		-25.6
Mar DOB	Cubic	$-4.40X10^{-8}$	$5.19X10^{-5}$	$-1.97X10^{-2}$	2.44		-8.58
Mar DOB	4th degree	$-1.21X10^{-8}$	$2.20X10^{-5}$	$-1.41X10^{-2}$	4.14	$-4.32X10^{2}$	-0.09
May ALT	Linear	$-1.77X10^{-4}$	$6.33X10^{-2}$				-2.27
May ALT	Power	$3.23X10^{42}$	$-2.02X10^{1}$				$-2.01X10^{13}$
May SAP	Cubic	$4.56X10^{-8}$	$5.43X10^{-5}$	$2.13X10^{-2}$	-2.77		-11.6
May SAP	4th degree	$2.19X10^{-9}$	$-3.81X10^{-6}$	$2.44X10^{-3}$	$-6.82X10^{-1}$	$7.02X10^{1}$	-0.71
May DOB	Quadratic	$3.53X10^{-6}$	$-2.98X10^{-3}$	$6.14X10^{-1}$			-1.26
May DOB	Cubic	$6.79X10^{-8}$	$-7.79X10^{-5}$	$2.91X10^{-2}$	-3.50		-0.30
May DOB	Exponential	$4.02X10^{9}$	$-9.08X10^{-2}$				$-1.08X10^{2}$
Aug ALT	Power	$-5.47X10^{13}$	-5.97	$1.22X10^{-2}$			-1.53
Aug ALT	Double exponential	$-5.09X10^{12}$	$-1.09X10^{-1}$	$3.95X10^{-3}$	$6.45X10^{-3}$		-7.16
Aug SAP	Exponential	$5.12X10^{2}$	$-3.28X10^{-2}$				-3.33
Aug DOB	Quadratic	$1.39X10^{-6}$	$-1.06X10^{-3}$	$2.01X10^{-1}$			-7.62
All Data	Cubic	$-4.44X10^{-8}$	$6.04X10^{-5}$	$-2.64X10^{-2}$	3.24		-8.88
All Data	4th degree	$-2.51X10^{-9}$	$4.67X10^{-6}$	$-3.18X10^{-3}$	$9.35X10^{-1}$	$-1.01X10^{2}$	-0.51
All Data (subset)	Cubic	$-2.87X10^{-8}$	$3.88X10^{-5}$	$-1.70X10^{-2}$	2.40		-5.81
All Data (subset)	4th degree	$-2.46X10^{-9}$	$4.59X10^{-6}$	$-3.13X10^{-3}$	$9.24X10^{-1}$	$-9.99X10^{1}$	-0.07

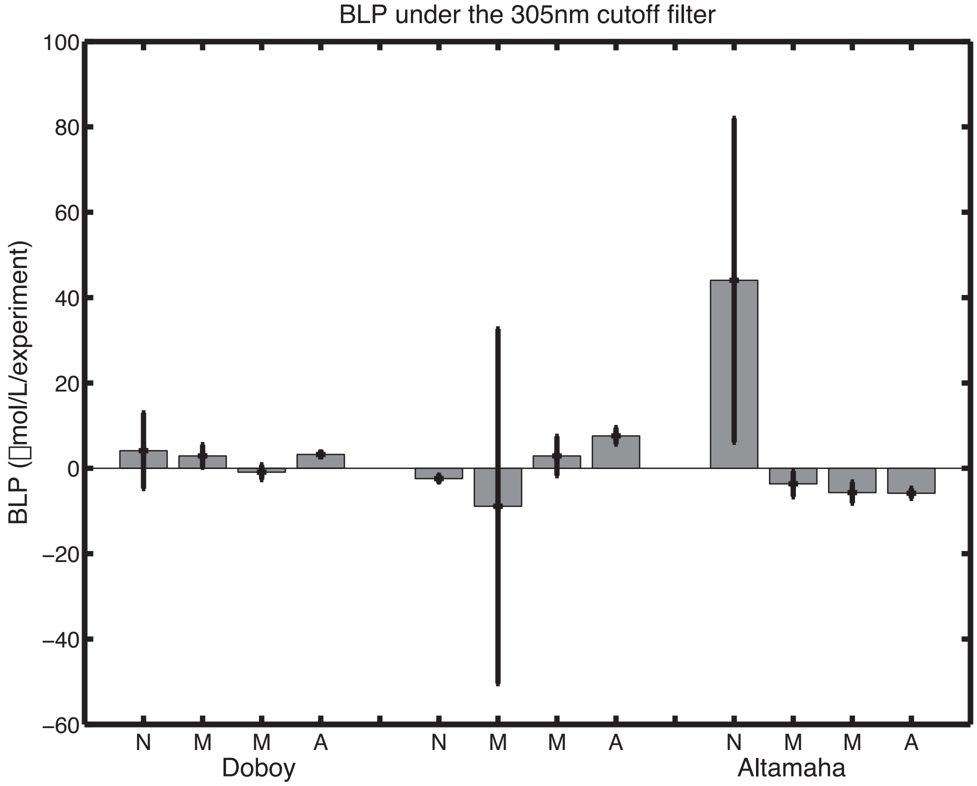

Figure 4.3: Production of BLP under the 305nm cutoff filter per experiment. Order of Months: November 2008, March 2009, May 2009, August 2009

apparent seasonal pattern when considering the three sites together, nor is there any statistically significant seasonal pattern within sites.

Table 4.2 shows relevant characteristics of each sample for comparison. The total range of CDOM concentrations (as determined by a_g320) is small (3.3 – 9.1 m^{-1}). We examined the possibility that differences in production were caused solely by the relative amount of photons absorbed by each sample. BLP production divided by a_g320 resulted in the same patterns of location and season as seen for the non-adjusted production results. In other words, changes in CDOM were not correlated to changes in BLP.

In general, all samples fall within the broad range for microbial growth rate changes due to photochemistry that have been previously reported for similar experiments [*Mopper and Kieber*, 2002]; ranging from -75% to 200% change in lability after exposure.

3.2 Apparent Quantum Yield Spectra

Results revealed a large degree of spectral variability for BLP production. The BLP production under each cutoff filter for the representative AQY determinations can be seen in Figure 4.4, and the entire dataset can be found in Table 4.3. In order to define a spectral AQY in a multispectral irradiation setup such as this, a mathematical equation must be defined, and due to the spectral variability, a single spectral shape was inappropriate for all samples. Table 4.1 summarizes the various fits applied to the experimental data, in an effort to use Matlab's *nlinfit* routine to produce a spectral apparent quantum yield equation for each experiment. The R^2 coefficients are determined for a theoretical 1:1 relationship between the measured and calculated production numbers. A negative R^2 indicates that the equation used to model the AQY

Table 4.2: Characteristics of the seasonal study samples

Month	**Location**	**$a_g(320)$ (m^{-1})**	**Salinity (psu)**
November 2008	Sapelo	3.3	33.2
	Doboy	4.1	33.0
	Altamaha	4.1	32.2
March 2009	Sapelo	4.7	31.7
	Doboy	5.6	29.8
	Altamaha	5.1	31.1
May 2009	Sapelo	9.1	30.2
	Doboy	8.3	30.8
	Altamaha	7.8	1.5
August 2009	Sapelo	5.1	34.0
	Doboy	4.9	32.5
	Altamaha	5.1	33.1

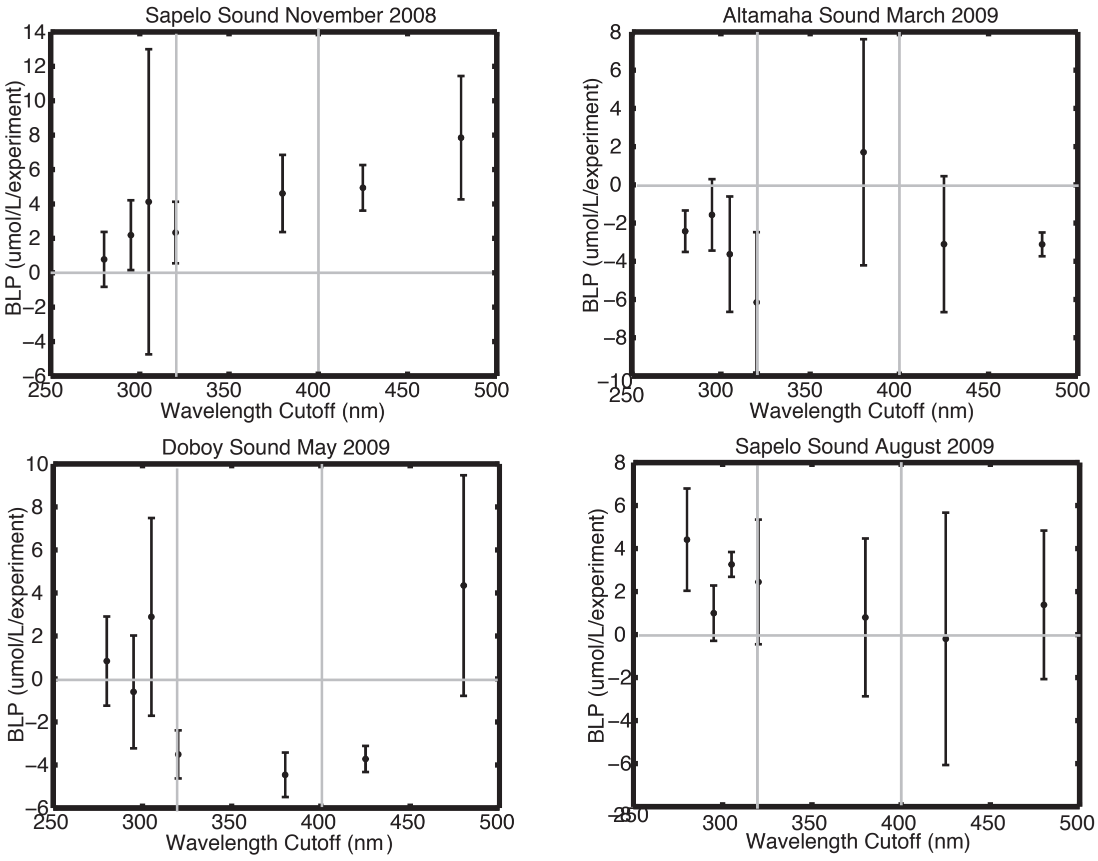

Figure 4.4: BLP production under each cutoff filter for the seasonal study. Representative graphs, for full details see Table 3. Horizontalgrey line represents 0, the two vertical grey lines represent the UVB-UVA cutoff (320 nm) and the UVA-visible cutoff (400 nm).

Table 4.3: Production values under each cutoff filter for the seasonal study.
Units are umol C/L/experiment, Bold values are means and non-bold values are standard deviations.

Month	Site	280nm	295nm	305nm	320nm	380nm	425nm	480nm
November	ALT	**2.43E+01**	**8.47E+00**	**4.41E+01**	**4.57E+01**	**4.60E+01**	**3.85E+01**	**1.82E+01**
		2.25E+01	1.00E+01	3.79E+01	4.01E+01	1.29E+01	4.11E+01	1.51E+01
	SAP	**7.76E-01**	**2.19E+00**	**4.12E+00**	**2.34E+00**	**4.61E+00**	**4.94E+00**	**7.85E+00**
		1.60E+00	2.03E+00	8.87E+00	1.79E+00	2.24E+00	1.32E+00	3.59E+00
	DOB	**2.60E-01**	**1.04E+00**	**-2.40E+00**	**3.87E+00**	**1.47E+00**	**-3.02E+00**	**-6.25E-05**
		9.91E-01	2.04E+00	7.93E-01	1.52E+00	6.12E-01	1.61E+00	1.86E-01
March	ALT	**-2.43E+00**	**-1.57E+00**	**-3.63E+00**	**-6.15E+00**	**1.70E+00**	**-3.10E+00**	**-3.11E+00**
		1.08E+00	1.87E+00	3.02E+00	3.67E+00	5.91E+00	3.56E+00	6.22E-01
	SAP	**3.85E+00**	**1.68E+00**	**2.90E+00**	**8.68E-01**	**2.98E+00**	**8.22E+00**	**-3.02E-02**
		1.18E+01	4.35E+00	2.66E+00	9.56E-01	5.73E+00	1.06E+01	1.75E+00
	DOB	**-2.12E+01**	**-1.76E+01**	**-8.88E+00**	**-1.77E+01**	**-1.69E+01**	**-1.71E+01**	**-1.81E+01**
		2.68E+00	4.83E+00	4.16E+01	1.26E+00	2.14E+00	4.08E+00	2.86E+00
May	ALT	**-5.59E+00**	**-6.15E+00**	**-5.69E+00**	**-6.17E+00**	**-6.32E+00**	**-6.04E+00**	**-5.58E+00**
		3.00E+00	1.81E+00	2.48E+00	2.93E+00	7.68E-01	5.10E+00	5.57E-01
	SAP	**1.41E+00**	**3.03E+00**	**-9.10E-01**	**6.49E+00**	**1.60E+00**	**2.16E-01**	**6.35E+00**
		2.89E+00	1.77E+00	1.74E+00	1.02E+01	1.91E+00	2.00E+00	9.47E+00
	DOB	**8.31E-01**	**-6.03E-01**	**2.89E+00**	**-3.51E+00**	**-4.46E+00**	**-3.72E+00**	**4.34E+00**
		2.07E+00	2.62E+00	4.60E+00	1.12E+00	1.03E+00	6.08E-01	5.13E+00
August	ALT	**1.38E+00**	**-4.27E+00**	**-5.85E+00**	**-2.79E+00**	**1.48E+00**	**3.03E+00**	**-5.12E-01**
		1.48E+01	6.07E+00	1.20E+00	4.04E+00	1.92E+00	2.97E+00	7.50E-01
	SAP	**4.41E+00**	**9.95E-01**	**3.26E+00**	**2.45E+00**	**7.98E-01**	**-1.98E-01**	**1.38E+00**
		2.38E+00	1.29E+00	5.77E-01	2.90E+00	3.67E+00	5.87E+00	3.45E+00
	DOB	**4.86E+00**	**4.82E+00**	**7.60E+00**	**6.91E+00**	**5.34E+00**	**2.86E+00**	**5.49E+00**
		2.86E+00	3.15E+00	1.93E+00	2.43E+00	2.62E+00	2.59E+00	1.78E+00

spectrum is fundamentally inappropriate, rather than just a poor fit. Many of the fits produced negative R^2 values, meaning that the equations applied to the data did not produced a useful AQY spectrum. For some samples, multiple equations were used to determine an AQY with similar results.

Because of the complexity of the BLP spectral response in our experiments, the wavelength band subtraction method of AQY determination for representative samples is presented in Figure 4.5, the entire data set can be found in Table 4.4. This approach showed substantial variation among different samples as well as between differing wavelengths, within the same sample. It is important to note that all of these results represent a net or integrated result of both production and destruction processes over the course of an irradiation.

To further examine the spectral variation and account for the overall complexity of the results, we pooled the data from all 12 experiments and attempted to determine an average AQY spectrum using the wavelength band subtraction method, seen in Figure 4.6.

3.3 Photon Dose Dependency

We examined the photon dose dependency of the effect of photochemical reactions on the biologically labile fraction of DOC in two experiments. The first used a full-spectrum solar simulation (using a window glass filter in the solar simulator), for up to 24 hours equivalent of summertime midday sunlight at 30°N latitude, roughly the same latitude as where the samples were collected. Each hour of irradiation delivered a total of $1.03X10^{-4}$ mol photons/cm^2 to the system, in the same proportions as the solar spectrum at the surface of the earth. Figure 4.7 shows that for this experiment, the highest net

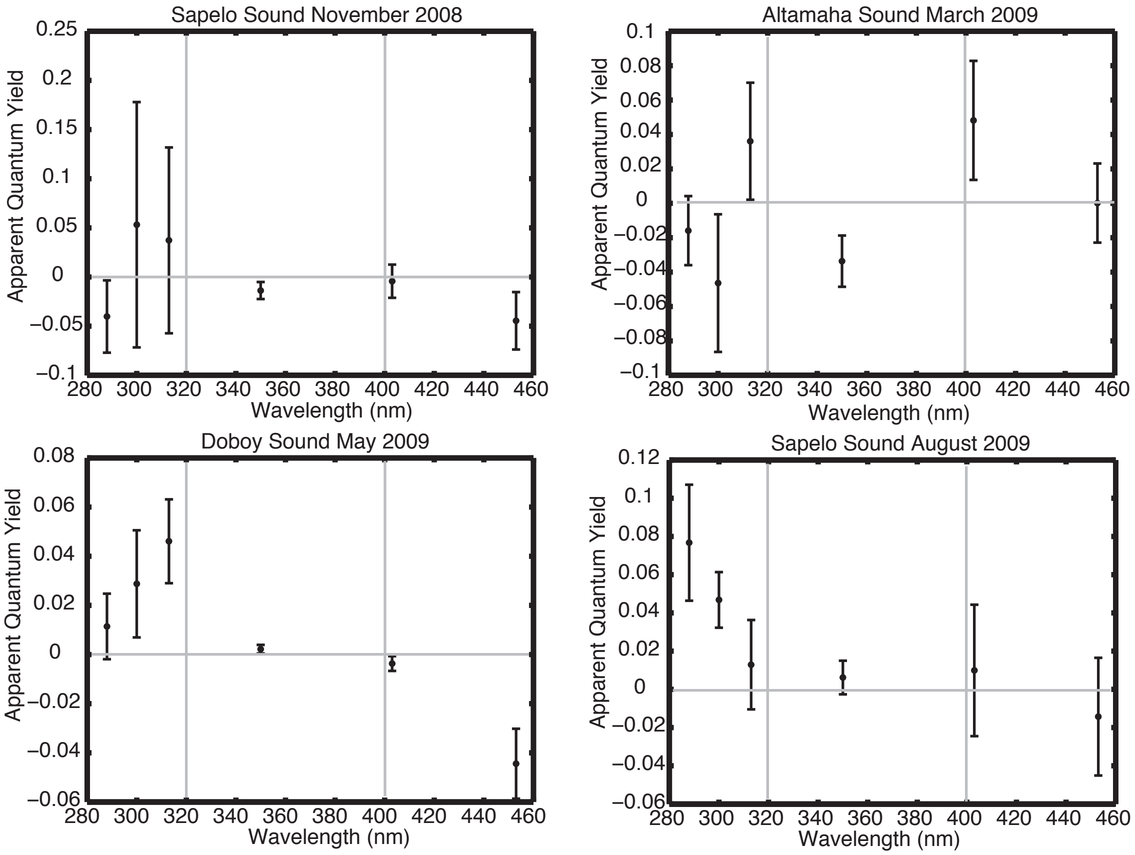

Figure 4.5: AQY by band subtraction method for seasonal study. Representative graphs, for full details see Table 4. Horizontal grey line represents 0, the two vertical grey lines represent the UVB-UVA cutoff (320 nm) and the UVA-visible cutoff (400 nm).

Table 4.4: Full AQY data by band subtraction method

Month	Site	288nm	300nm	313nm	350nm	403nm	453nm
November	Altamaha	4.10E-01 +/-3.19E-01	9.06E-01 +/-5.00E-01	-3.11E-02 +/-5.32E-01	-1.59E-03 +/-1.16E-01	8.57E-02 +/-2.48E-01	2.73E-01 +/-2.95E-01
	Sapelo	-4.02E-02 +/-3.68E-02	5.32E-02 +/-1.25E-01	3.73E-02 +/-9.45E-02	-1.37E-02 +/-8.68E-03	-4.28E-03 +/-1.69E-02	-4.45E-02 +/-2.92E-02
	Doboy	-2.81E-02 +/-4.11E-02	-8.14E-02 +/-2.59E-02	-9.61E-02 +/-1.31E-02	1.05E-02 +/-3.60E-03	3.02E-02 +/-5.80E-03	-3.01E-02 +/-8.10E-03
March	Altamaha	-1.59E-02 +/-2.01E-02	-4.64E-02 +/-4.00E-02	3.61E-02 +/-3.40E-02	-3.36E-02 +/-1.49E-02	4.82E-02 +/-3.46E-02	1.46E-04 +/-2.30E-02
	Sapelo	3.12E-02 +/-9.03E-02	2.39E-02 +/-4.99E-02	4.29E-02 +/-2.99E-02	-8.91E-03 +/-1.22E-02	-5.91E-02 +/-6.78E-02	1.11E-01 +/-7.17E-02
	Doboy	-6.57E-02 +/-5.04E-02	1.35E-01 +/-3.24E-01	2.55E-01 +/-6.02E-01	-3.71E-03 +/-5.64E-03	3.22E-03 +/-3.37E-02	1.41E-02 +/-3.60E-02
May	Altamaha	9.03E-03 +/-2.81E-02	3.34E-03 +/-1.12E-02	2.76E-03 +/-1.11E-02	4.15E-04 +/-4.02E-03	-1.63E-03 +/-1.48E-02	-2.92E-03 +/-1.64E-02
	Sapelo	-1.65E-02 +/-1.73E-02	-6.76E-02 +/-2.12E-02	-1.23E-01 +/-8.60E-02	9.43E-03 +/-1.00E-02	6.33E-03 +/-6.33E-03	-3.28E-02 +/-2.59E-02
	Doboy	1.14E-02 +/-1.33E-02	2.88E-02 +/-2.18E-02	4.61E-02 +/-1.71E-02	+/-2.18E-03 1.75E-03	-3.68E-03 +/-3.00E-03	-4.44E-02 +/-1.42E-02
August	Altamaha	-3.17E-01 +/-4.49E-01	8.89E-02 +/-1.74E-01	-4.99E-02 +/-3.44E-02	-1.58E-02 +/-8.28E-03	-1.13E-02 1.29E-02	3.35E-02 +/-1.45E-02
	Sapelo	7.67E-02 +/-3.03E-02	4.68E-02 +/-1.46E-02	1.29E-02 +/-2.34E-02	6.20E-03 +/-8.79E-03	9.90E-03 +/-3.44E-02	-1.43E-02 +/-3.08E-02
	Doboy	9.04E-04 +/-4.79E-02	4.97E-02 +/-3.30E-02	1.04E-02 +/-2.35E-02	5.81E-03 +/-6.62E-03	2.26E-02 +/-1.67E-02	-2.23E-02 +/-1.32E-02

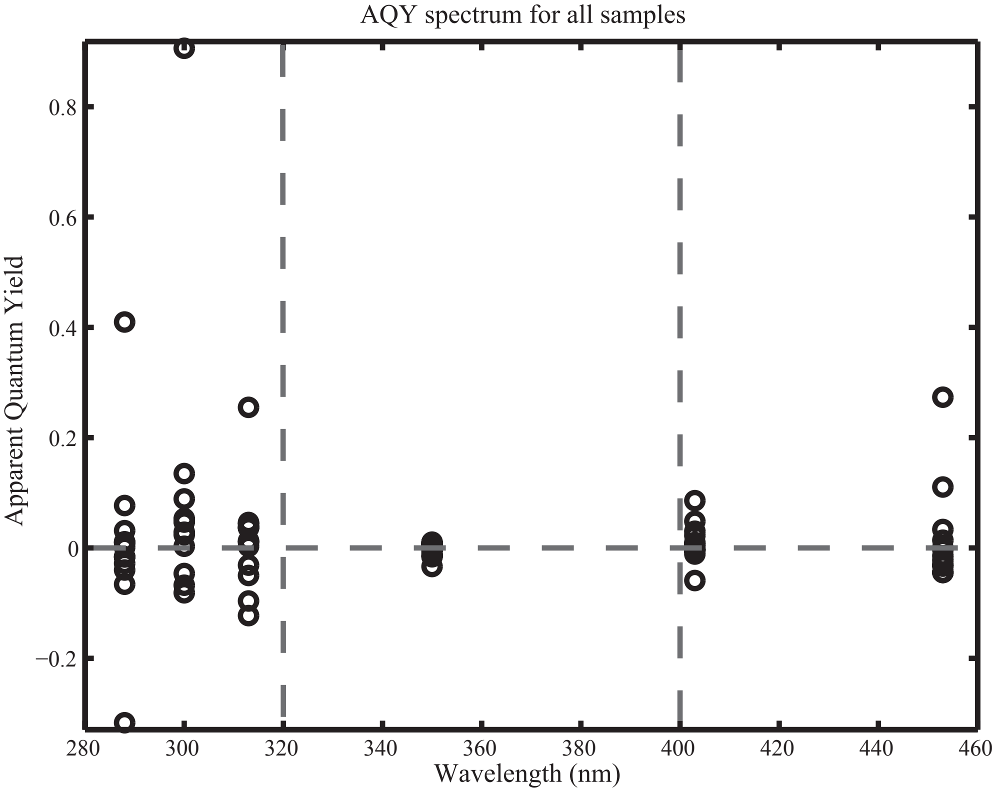

Figure 4.6: AQY by band subtraction for all seasonal data. Horizontal grey line represents 0, the two vertical grey lines represent the UVB-UVA cutoff (320 nm) and the UVA-visible cutoff (400 nm).

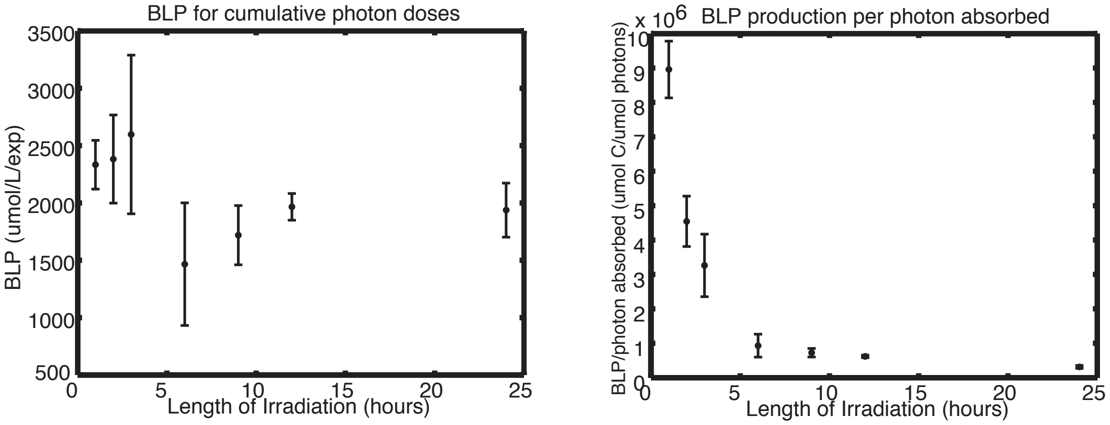

Figure 4.7: BLP production and AQY for cumulative photon doses under the 305nm cutoff filter.

production of BLPs, as determined by whole community respiration after 10 days, occurred after the shortest period of irradiation (1 hour, 1.03×10^{-4} mol photons/cm^2). The net BLP production dropped off quickly with increasing photon dose. The 9 hour time point is an equivalent photon dose to that received under the 305 nm cutoff filters in the AQY experiments. Consequently, AQY results should be considered a conservative estimate of the effect of photochemistry on the biological lability of carbon in this system. Again, it is important to note that these results represent a net effect of both photochemical production and photochemical destruction processes, and it is not necessarily the non-biological production of BLPs that drops off with increasing photon dose, but that BLP removal processes are also included in these data. The sharp decline in net BLP production with increasing photon dose suggests that photochemical destruction processes may become significant early in these types of irradiation experiments.

To investigate the spectral characteristics of BLP production as a function of photon dose, three successive AQY experiments were performed on the same sample (under the 305 nm cutoff filter: 3 hours = 3.08×10^{-4} mol photons/cm^2, 6 hours = 6.17×10^{-4} mol photons/cm^2, 9 hours = 9.25×10^{-4} mol photons/cm^2). Not only does the total BLP response under the 305nm cutoff filters change with increasing photon dose, as was seen in the previous experiment, but the spectral shape of the AQY changes as well, as can be seen in Figure 4.8. These AQY spectral response results suggest that the photochemical production and photochemical destruction processes that together result in the net BLP result observed for all full spectrum experiments are controlled by different

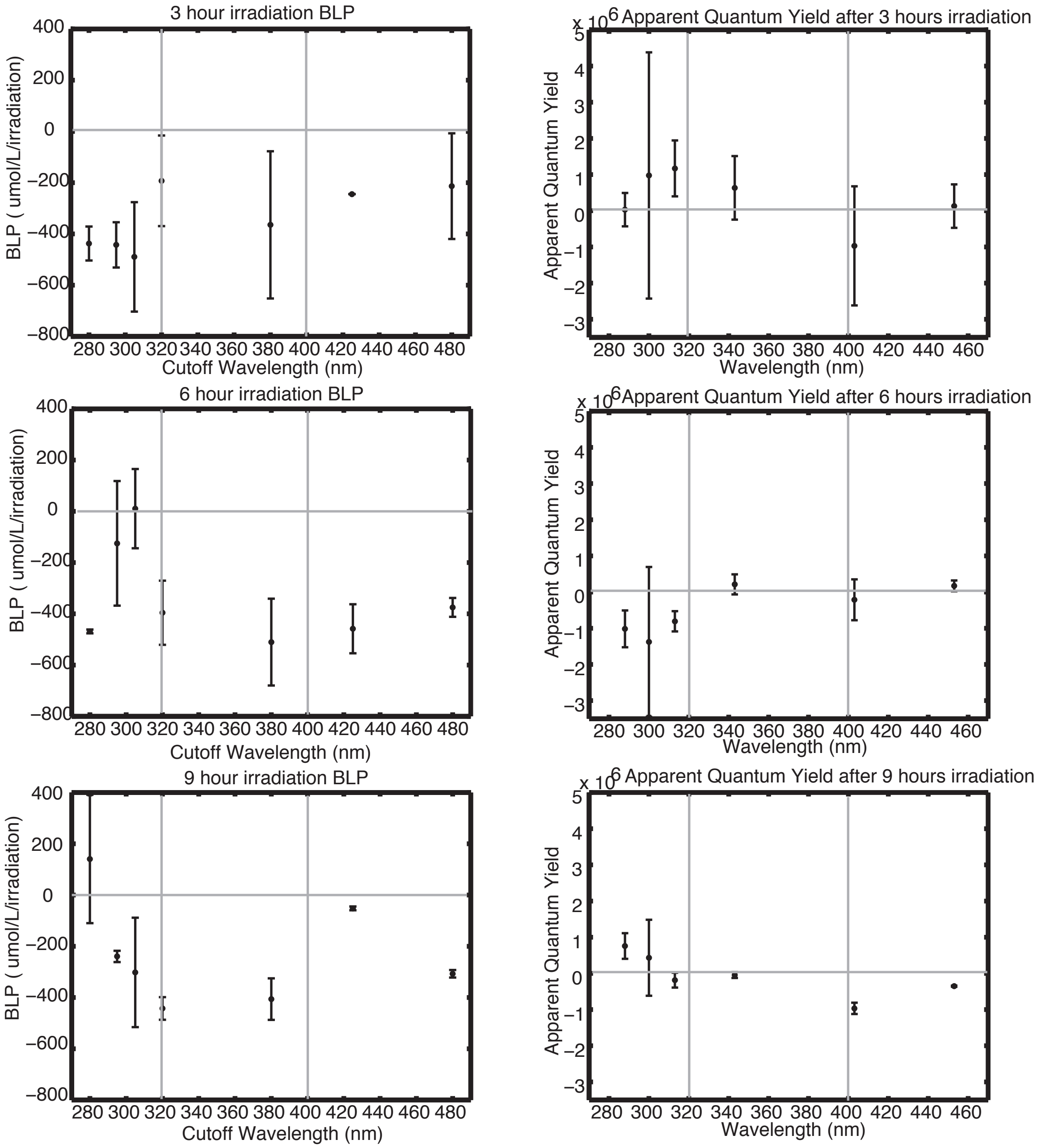

Figure 4.8: Spectral production and AQY for increasing photon dose. Left hand column is the production under each cutoff filter. Right hand column is the AQY by band subtraction. Error bars are standard deviation for production and standard error for AQY. Horizontal grey line represents 0, the two vertical grey lines represent the UVB-UVA cutoff (320 nm) and the UVA-visible cutoff (400 nm).

portions of the spectrum, and also that they evolve over time with the total number of photons available to the system.

4. Discussion

The results of this study are a clear reminder that these types of experiments show a net result of photochemical activity with respect to biological lability of DOC. With most well-studied and well-defined photochemical products (e.g. carbon monoxide, formaldehyde, hydrogen peroxide, carbon dioxide), the spectral AQY can be described by a relatively simple exponential decay function where the higher energy wavelengths of the UV are more efficient than the longer, lower energy wavelengths in the visible. [*Johannessen and Miller*, 2001; *R J Kieber et al.*, 1990; *Zafiriou et al.*, 2003]. In the situation where a single photochemical product is not subsequently photochemically labile, the definition of an apparent quantum yield is relatively straightforward. In the present study, the resulting photoproduct is not a single molecule, but rather a whole host of compounds, which may or may not be photochemically active. When the components of the biologically labile carbon pool are themselves also photochemically labile, irradiation can lead to the destruction of these compounds. Because this, and almost every other study, treats of BLPs as a single product (i.e. using a measurable microbial response as a proxy for the amount of biologically labile carbon in the system), the results in this study must be viewed as a net balance between photochemical production and destruction processes. Figure 4.9 presents a conceptual model of DOC in the surface ocean, and the potential transfer between pools. This is a complicated system with many overlapping processes. The total photochemical mineralization of CDOM to CO and CO_2 has been widely reported in the literature [*Johannessen and Miller*, 2001; *Miller and*

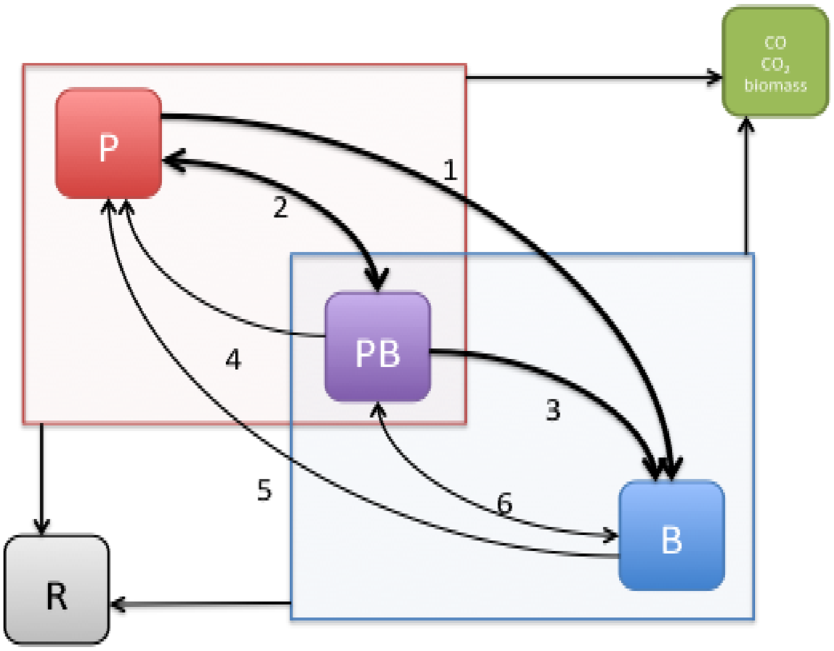

Figure 4.9: Box model of DOC in the surface ocean. P is the photochemically labile pool, B is the biologically labile pool, PB is the photochemically and biologically labile pool, R is the refractory pool. Pathways 1, 2, and 3 are photochemically mediated pathways, while pathways 4, 5, and 6 are biologically mediated.

Zepp, 1995; *Stubbins et al.*, 2006; *White et al.*, 2010; *Zafiriou et al.*, 2003; *Ziolkowski and Miller*, 2007] and therefore is fairly well constrained. Such processes are relatively straightforward to quantify, because there is only one product being considered and its production is not a "net" result since no removal processes are involved. Therefore only one "arrow" must be considered. For BLPs however, the analytical approach of this and many other studies consolidate pathways 1, 2 and 3 together, and thereby assess their net effect.

4.1 Implications of varying spectral shape of apparent quantum yields

The varying shape of net AQY spectra seen in this study means that the most efficient BLP production is measured in some cases when the UVR is removed from the irradiation spectrum. In the ocean, the amount of UVR available decreases exponentially with depth. The major source of UVR attenuation in the water column is its absorption by CDOM, which accounts for up to 70% of attenuation at 320nm, with an increasing percentage as the energy of the photons increases further into the UVB wavelengths [*Fichot and Miller*, 2010]. Because of this, the higher energy wavelengths of the UVR are diminished at subsurface depths. For a photochemical product with no photochemical loss term and an AQY where UVR wavelengths have the highest efficiency of production, the depth of highest the production rate is the very surface layer of the ocean, and production decreases with depth [*Fichot and Miller*, 2010]. A non-exponential AQY representing the net result of photoproduction and consumption as seen with this study could lead to the possibility of subsurface maxima of BLP photoproduction. For example, if BLP removal mechanisms are weighted towards the shorter UVR wavelengths, then as they are attenuated, the destruction processes will necessarily attenuate as well, and the net result will tend towards production.

Many studies of microbial response to open ocean photochemistry in the literature show either no production or show removal of BLPs [*Mopper and Kieber*, 2002]. These studies were largely carried out using ship deck incubations or with solar simulation, both of which produced results meant to be applicable to the full solar spectrum in the surface layer of the ocean. In these clear water cases, the results can be misleading, since they always include the higher energy wavelengths that are, in reality, strongly attenuated in the surface ocean. At depth, without these high-energy wavelengths, the possibility of BLP production rates being larger than photochemical removal rates becomes a possibility when considering differing AQY spectral shapes for BLP efficiency, as seen in our study. This spectral complexity does not appear to be consistent among coastal samples and adds a considerable challenge to modeling the effect of photochemistry on the biological availability of carbon in real marine systems.

4.2 Implications of photon dose dependency

Aside from the complex spectral structure of the AQYs, the dependence on photon dose for the observed bet production of BLPs provides an additional challenge for determining the true effect of photochemistry on the availability of carbon to the biological community in the ocean. In a laboratory setting, the spectral quality and total dose of photons can be controlled. As seen in Figure 4.7, the competition between photochemical production and destruction appears to begin at relatively low photon doses. This particular problem has not been addressed in the literature. While the concept of competing processes, and DOC pools of mixed lability [*Obernosterer and*

Benner, 2004] have been proposed, the experiments that are performed to determine the effect of photochemistry on the biological lability of carbon are rarely quantitative with respect to total photon absorption by the sample, much less the spectral dependence of the response [*Miller and Moran*, 1997; *Mopper and Kieber*, 2002; *Obernosterer and Benner*, 2004; *Vahatalo and Wetzel*, 2004]. One notable exception to this is the paper by Miller et al. [2002], which presented two AQY spectra that inherently contain photon dose information. The total quantity of photons absorbed by a system is clearly important not only with respect to the total integrated result (i.e. Figure 4.7) but also to the spectral distribution of active wavelengths (Figure 4.8) producing the observed response by the microbial community. Without knowing the number of photons absorbed by a sample, in light of the competing processes that may be occurring, it is impossible to quantitatively extrapolate current results to a real ocean situation.

Some studies have attempted to examine the transfer of DOC between labile pools, as well as estimate total pool size by performing successive photodegradation and biological degradation experiments [*Obernosterer and Benner*, 2004; *Vahatalo and Wetzel*, 2004] though these also are not quantitative with respect to photon dose. In the current experimental approach, as is the case for many other studies, both the biologically and photochemically labile pool (B-P) and the biologically labile but photochemically refractory pool B (Figure 4.9) are integrated by irradiating a sterile sample with subsequent inoculation of a microbial community after irradiation, with a subsequent dark incubation. It is impossible to distinguish between photochemical transfers from the biologically refractory but photochemically labile (P) pool to the B-P pool or the B pool in this study. The biologically mediated transfer of DOC between pools (i.e.

Pathways 4,5,6; Figure 4.9) is excluded from these types of studies, though this is clearly a possibility when considering biological exudates in the ocean. Some planktonic organisms are known to release photochemically active compounds such as siderophores [*Barbeau et al.*, 2003], and these could clearly have an effect on the transfer between different DOC pools in the real world.

4.3 Competing processes

The competition between photochemical production and destruction suggests that the large differences between experimental designs for published reports of photochemical influence on microbial production preclude a quantitative comparison of literature data on the significance of photochemistry on DOC lability to bacteria. In addition, extrapolating results to the real ocean becomes problematic due to the attenuation of light through the water column, and the differences in attenuation for different water types. Though the daily total photon dose can be estimated with both depth and season from sun rise to sun set, there is a component of mixing that changes the light experienced by each “molecule” of CDOM throughout the day. Combined with the changing spectral distribution of wavelengths with depth (i.e. fraction of UV available, as discussed above), this study suggests that the spectral efficiency for BLP production changes with increasing photon dose. Therefore, applying a single AQY over the course of any irradiation will only provide a rough estimate of the photochemical impacts to the microbial community via altered DOC lability.

Beyond water column dynamics, spectral attenuation and changing photochemical efficiencies, the competition between the destruction of BLPs by photochemical processes and the uptake of BLPs by the microbial community must be considered. In the experimental design employed here (i.e. intense photon dose), the competition between these rates cannot be addressed. However three possible scenarios can be considered for the surface ocean. First, the rate of biological uptake is much slower than that of photochemical breakdown of BLP, and the results of such a situation in the ocean could be very similar to that seen in this study. Second, the rate of biological uptake of BLP could be considerably faster than that of photochemical destruction, in which case a much greater enhancement of microbial activity would result from the photochemical production of BLP than is seen in studies such as the one presented here. Additionally, this would imply that photochemical production is the rate-limiting step for transfer of refractory DOC to the microbial loop. Thirdly, the rates could be approximately equal, and the microbial community would compete directly with the photochemical destruction of BLP. This scenario presents new complexities such as specific compound uptake rates, rates of specific photochemical reactions and the proximity of the new BLP to the microbes. In reality, it is likely that all three of these situations exists due to the complexity of the CDOM mixture and the many DOC molecules that are present in natural systems [*Minor et al.*, 2007; *Stubbins et al.*, 2010], as well as the diverse microbial community present in the surface oceans [*Fuhrman and Hagstrom*, 2008; *Tolli et al.*, 2006].

4.4 Addressing the complexity of DOC lability

The complex nature of competing photochemical rates, when combined with relative microbial uptake rates for BLP produce a situation that is difficult to pull apart and analyze separately. Future attempts to quantify the overall effect of photochemical DOC transformations on the activity of the microbial community may require more integrated approaches. Irradiations that include both DOC and the microbes in the same system might allow uptake of BLP as soon as formed through photochemical reactions. In the current experimental design, as has been the case for other published studies, this cannot be done, because the intensity of the irradiation is such that significant cell damage and death is likely to occur [*Herndl et al.*, 1993; *Huot et al.*, 2000]. Because natural systems have both mixing and complex shading of UVR (due to particulates and CDOM absorption), the biological community is largely protected from high UV doses in the coastal environments such as those examined here. For the irradiation experiment to take place with the microbial community in place, the intensity of irradiation would need to be much lower than seen in the solar simulator used for this study. New approaches that integrate variable photon dose that simulates natural mixing, with realistic light fields should lead to a more holistic understanding but still will not pull apart the variable rates and individual interactions.

The variability seen in this seasonal and spatial study, where the quantity and spectral quality of the photon flux was tightly controlled, suggests that even with improved methods, it is unlikely that applying a single AQY spectrum that is appropriate for all situations can be determined. The carbon source, as well as the microbial communities, very likely have a large effect on the BLP results seen in any given experiment. The challenges to modeling the photochemical effect on the availability of carbon to biological systems are more than just the analytical constraints, but also include the complexity inherent in natural systems.

Acknowledgements

The authors would like to thank the GCE-LTER and M. G. Booth and M. A. Moran.for help with sampling and methods.

References

Azam, F. (1998), Microbial control of oceanic carbon flux: The plot thickens, *Science*, *280*(5364), 694-696.

Barbeau, K., E. L. Rue, C. G. Trick, K. T. Bruland, and A. Butler (2003), Photochemical reactivity of siderophores produced by marine heterotrophic bacteria and cyanobacteria based on characteristic Fe(III) binding groups, *Limnology and Oceanography*, *48*(3), 1069-1078.

Bricaud, A., A. Morel, and L. Prieur (1981), ABSORPTION BY DISSOLVED ORGANIC-MATTER OF THE SEA (YELLOW SUBSTANCE) IN THE UV AND VISIBLE DOMAINS, *Limnology and Oceanography*, *26*(1), 43-53.

Carlson, C. A. (2002), Production and Removal Processes, in *Biogeochemistry of Marine Dissolved Organic Matter*, edited by D. A. Hansell and C. A. Carlson, pp. 91 - 152, Academic Press, San Diego.

Fichot, C. G., and W. L. Miller (2010), An approach to quantify depth-resolved marine photochemical fluxes using remote sensing: Application to carbon monoxide (CO) photoproduction, *Remote Sensing of Environment*, *114*(7), 1363-1377.

Fuhrman, J. A., and A. Hagstrom (2008), Bacterial and Archaeal Community Structure and Its Patterns, in *Microbial Ecology of the Oceans*, edited by D. L.

Kirchman, pp. 45 -90, John Wiley and Sons, Hoboken, New Jersey.

Hansell, D. A., and C. A. Carlson (1998), Net community production of dissolved organic carbon, *Global Biogeochemical Cycles*, *12*(3), 443-453.

Hansell, D. A., C. A. Carlson, D. J. Repeta, and R. Schlitzer (2009), DISSOLVED ORGANIC MATTER IN THE OCEAN A CONTROVERSY STIMULATES NEW INSIGHTS, *Oceanography*, *22*(4), 202-211.

Herndl, G. J., G. Mullerniklas, and J. Frick (1993), MAJOR ROLE OF ULTRAVIOLET-B IN CONTROLLING BACTERIOPLANKTON GROWTH IN THE SURFACE-LAYER OF THE OCEAN, *Nature*, *361*(6414), 717-719.

Hu, C. M., F. E. Muller-Karger, and R. G. Zepp (2002), Absorbance, absorption coefficient, and apparent quantum yield: A comment on common ambiguity in the use of these optical concepts, *Limnology and Oceanography*, *47*(4), 1261-1267.

Huot, Y., W. H. Jeffrey, R. F. Davis, and J. J. Cullen (2000), Damage to DNA in bacterioplankton: A model of damage by ultraviolet radiation and its repair as influenced by vertical mixing, *Photochemistry and Photobiology*, *72*(1), 62-74.

Johannessen, S. C., and W. L. Miller (2001), Quantum yield for the photochemical production of dissolved inorganic carbon in seawater, *Marine Chemistry*, *76*(4), 271-283.

Kieber, D. J., J. McDaniel, and K. Mopper (1989), PHOTOCHEMICAL SOURCE OF BIOLOGICAL SUBSTRATES IN SEA-WATER - IMPLICATIONS FOR CARBON CYCLING, *Nature*, *341*(6243), 637-639.

Kieber, R. J., X. L. Zhou, and K. Mopper (1990), FORMATION OF CARBONYL-COMPOUNDS FROM UV-INDUCED PHOTODEGRADATION OF HUMIC SUBSTANCES IN NATURAL-WATERS - FATE OF RIVERINE CARBON IN THE SEA, *Limnology and Oceanography*, *35*(7), 1503-1515.

Ludwig, W., J. L. Probst, and S. Kempe (1996), Predicting the oceanic input of organic carbon by continental erosion, *Global Biogeochemical Cycles*, *10*(1), 23-41.

Miller, W. L., and R. G. Zepp (1995), PHOTOCHEMICAL PRODUCTION OF DISSOLVED INORGANIC CARBON FROM TERRESTRIAL ORGANIC-MATTER - SIGNIFICANCE TO THE OCEANIC ORGANIC-CARBON CYCLE, *Geophysical Research Letters*, *22*(4), 417-420.

Miller, W. L., and M. A. Moran (1997), Interaction of photochemical and microbial processes in the degradation of refractory dissolved organic matter from a coastal marine environment, *Limnology and Oceanography*, *42*(6), 1317-1324.

Miller, W. L., M. A. Moran, W. M. Sheldon, R. G. Zepp, and S. Opsahl (2002), Determination of apparent quantum yield spectra for the formation of biologically labile photoproducts, *Limnology and Oceanography*, *47*(2), 343-352.

Minor, E. C., B. L. Dalzell, A. Stubbins, and K. Mopper (2007), Evaluating the photoalteration of estuarine dissolved organic matter using direct temperature-resolved mass spectrometry and UV-visible spectroscopy, *Aquatic Sciences*, *69*(4), 440-455.

Mopper, K., and D. J. Kieber (2000), Marine photochemistry and its impact on carbon cycling, in *The effects of UV radiation in the marine environment*, edited by S. J. De Mora, S. Demers and M. Vernet, pp. 101-129, Cambridge University PRess, Cambridge, UK.

Mopper, K., and D. J. Kieber (2002), Photochemistry and the Cycling of Carbon, Sulfur, Nitrogen and Phosphorus, in *Biogeochemistry of Marine Dissolved Organic Matter*, edited by D. A. Hansell and C. A. Carlson, pp. 456 - 508, Academic Press, San Diego.

Nagata, T. (2008), Organic Matter-Bacteria Interactions In Seawater, in *Microbial Ecology of the Oceans, Second Edition*, edited by D. L. Kirchman, pp. 207-241, John Wiley and Sons, Inc.

Obernosterer, I., and R. Benner (2004), Competition between biological and photochemical processes in the mineralization of dissolved organic carbon, *Limnology and Oceanography*, *49*(1), 117-124.

Pomeroy, L. R. (1974), OCEANS FOOD WEB, A CHANGING PARADIGM, *Bioscience*, *24*(9), 499-504.

Stubbins, A., G. Uher, C. S. Law, K. Mopper, C. Robinson, and R. C. Upstill-Goddard (2006), Open-ocean carbon monoxide photoproduction, *Deep-Sea Research Part Ii-Topical Studies in Oceanography*, *53*(14-16), 1695-1705.

Stubbins, A., R. G. M. Spencer, H. M. Chen, P. G. Hatcher, K. Mopper, P. J. Hernes, V. L. Mwamba, A. M. Mangangu, J. N. Wabakanghanzi, and J. Six (2010), Illuminated darkness: Molecular signatures of Congo River dissolved organic matter and its photochemical alteration as revealed by ultrahigh precision mass spectrometry, *Limnology and Oceanography*, *55*(4), 1467-1477.

Tolli, J. D., S. M. Sievert, and C. D. Taylor (2006), Unexpected diversity of bacteria capable of carbon monoxide oxidation in a coastal marine environment, and contribution of the Roseobacter-associated clade to total CO oxidation, *Applied and Environmental Microbiology*, *72*(3), 1966-1973.

Vahatalo, A. V., and R. G. Wetzel (2004), Photochemical and microbial decomposition of chromophoric dissolved organic matter during long (months-years) exposures, *Marine Chemistry*, *89*(1-4), 313-326.

Wetzel, R. G., P. G. Hatcher, and T. S. Bianchi (1995), Natural photolysis by ultraviolet irradiance of recalcitrant dissolved organic matter to simple substrates for rapid bacterial metabolism, *Limnology and Oceanography*, *40*(8), 1369-1380.

White, E. M., D. J. Kieber, J. Sherrard, W. L. Miller, and K. Mopper (2010), Carbon dioxide and carbon monoxide photoproduction quantum yields in the Delaware Estuary, *Marine Chemistry*, *118*(1-2), 11-21.

Xie, H. X., O. C. Zafiriou, T. P. Umile, and D. J. Kieber (2005), Biological consumption of carbon monoxide in Delaware Bay, NW Atlantic and Beaufort Sea, *Marine Ecology-Progress Series*, *290*, 1-14.

Zafiriou, O. C., S. S. Andrews, and W. Wang (2003), Concordant estimates of oceanic carbon monoxide source and sink processes in the Pacific yield a balanced global "blue-water" CO budget, *Global Biogeochemical Cycles*, *17*(1).

Zafiriou, O. C., J. Joussotdubien, R. G. Zepp, and R. G. Zika (1984), PHOTOCHEMISTRY OF NATURAL-WATERS, *Environmental Science & Technology*, *18*(12), A358-A371.

Zika, R. G., E. S. Saltzman, and W. J. Cooper (1985), HYDROGEN-PEROXIDE CONCENTRATIONS IN THE PERU UPWELLING AREA, *Marine Chemistry*, *17*(3), 265-275.

Ziolkowski, L. A., and W. L. Miller (2007), Variability of the apparent quantum efficiency of CO photoproduction in the Gulf of Maine and Northwest Atlantic, *Marine Chemistry*, *105*(3-4), 258-270.

CHAPTER 5

APPLICATION OF HYPERSPETRAL REMOTE SENSING REFLECTANCE DATA TO PHOTOCHEMICAL RATE CALCULATIONS IN THE DUPLIN RIVER, A TIDAL RIVER ON THE COAST OF GEORGIA, USA[1]

---

[1] Reader, H. E. and W. L. Miller. To be submitted to *Remote Sensing of Environment.*

Abstract

Estuaries are photochemically dynamic environments, with high carbon loads and relatively small areas. The small area poses problems for large-scale satellite based remote sensing calculations, where the resolution is too coarse to distinguish land from water. Airborne remote sensing instruments have potential to reveal the dynamics of these areas with fine-scale resolution. In June 2006, hyperspectral remote sensing imagery, using an AISA Eagle instrument was collected over the tidal Duplin River, Georgia, USA. A dark-water updated version of the SeaUV algorithm [*Fichot et al.*, 2008] was applied to the AISA remote sensing image to determine diffuse attenuation constants in the ultraviolet, and calculate surface photochemical production rates of two inorganic products, carbon monoxide and carbon dioxide. The photoproduction of carbon dioxide averaged ~ $7X10^{-4}$ mol C/day/m^2, while the photoproduction of carbon monoxide averaged ~ $4X10^{-4}$ mol C/day/m^2 for an average day in June.

1.1 Introduction

Estuaries are dynamic features of the coastal ocean. They are the site of the most direct interaction between the continents and the ocean. River-dominated estuaries deliver 0.2 Pg of carbon per year to the coastal ocean [*Ludwig et al.*, 1996]. Other types of estuaries deliver carbon to the ocean through non-point source mechanisms of terrestrial run off, such as that from tidal marshes [*Clark et al.*, 2008]. Estuaries are also areas where significant in situ production of carbon occurs [*Valiela*, 1995]. Much of this carbon has had little previous exposure to sunlight and when exposed to solar radiation, it can under go photochemical transformations. Photochemically, estuaries are active areas, having been shown to be sources of photochemically produced species such as carbon monoxide [*Law et al.*, 2002; *White et al.*, 2010], carbon dioxide [*Johannessen et al.*, 2007; *White et al.*, 2010] and many other photochemical products [*Minor et al.*, 2007; *Osburn et al.*, 2009]

The major source for carbon monoxide in the surface ocean is photochemical mineralization of chromophoric dissolved organic matter (CDOM), the light absorbing fraction of the dissolved organic carbon pool. The two major loss terms for CO in the surface ocean are air-sea exchange and microbial consumption [*Mopper et al.*, 1991; *Zafiriou et al.*, 2003; *Zafiriou et al.*, 2008]. In the lower atmosphere, CO is an indirect greenhouse gas that competes with methane to scavenge hydroxyl radicals, allowing methane to build up in the atmosphere [*Daniel and Solomon*, 1998] as well as forming precursors to ozone (O_3), a tropospheric pollutant [*Fishman and Seiler*, 1983; *Seiler and Fishman*, 1981]. Microbial studies show that the roseobacter clade is efficient at consuming CO in the surface ocean [*Tolli et al.*, 2006], and may lessen or even prevent the escape of CO into the atmosphere. The efficiency of these two loss terms, together with its photochemical source create CO concentrations in the surface coastal and open ocean around 12 and 2 nM, respectively, with a strong diurnal signal [*Zafiriou et al.*, 2008]. The mineralization of CDOM to CO by photochemistry is potentially a large contributor to the oxidation of dissolved organic carbon in the global carbon cycle [*Mopper and Kieber*, 2002]. Global estimates for the photochemical production of CO in the ocean range from 30 – 84 TgC/year [*Fichot and Miller*, 2010; *Stubbins et al.*, 2006; *Zafiriou et al.*, 2003].

Carbon dioxide is a major component of the oceanic carbonate system. Overall, the ocean acts as a sink for atmospheric CO_2. Some areas of the coastal ocean, such as the inner shelf of the terrestrially influenced South Atlantic Bight and the Pearl River Estuary, China, have been reported as seasonal sources of CO_2 to the atmosphere [*Guo et al.*, 2009; *Jiang et al.*, 2008a; *Jiang et al.*, 2008b] presumably due to heterotrophic production in these regions. Estuaries, in particular, have been shown to be sources of CO_2 to the atmosphere, due to a strong heterotrophic signal in these areas of the ocean [*Cai*, 2011; *Jiang et al.*, 2008a]. Though the total area of estuaries relative to the open ocean is small, they have been shown to be important in the global balance of CO_2 in the atmosphere-ocean system. Several noteworthy studies have found that there is indeed a strong photochemical signal of DIC production in the world's oceans [*Johannessen and Miller*, 2001; *Johannessen et al.*, 2007; *Miller and Zepp*, 1995; *White et al.*, 2010] Many of these studies concentrate on estuarine and coastal ocean waters.

Since estuaries have been shown to be strong photochemical sources of these two trace gases in the ocean, it is useful to be able to make large-scale predictions of the influence of photochemistry in these relatively small areas on the global carbon cycle. Satellite-based remote sensing has allowed large scale estimations of oceanic characteristics and processes, such as sea surface temperatures and salinity [*Jorda et al.*, 2011], primary production [*Carder et al.*, 1999; *Carder et al.*, 1991], and even photochemical processes [*Fichot and Miller*, 2010]. Until recently, the coverage for satellite remote sensing of the ocean system has been confined to open ocean areas. Resolution of satellite-based instruments have been relatively coarse (SeaWiFS and MODIS), and estuaries, with their small scale land-water structure are difficult for these sensors to resolve. Coastal areas are also areas that experience weather systems that manifest themselves in large amounts of cloud cover, which makes remote sensing of these systems difficult. Passive ocean color satellite systems (such as SeaWiFS and MODIS) cannot retrieve data from beneath clouds. To collect reliable remote sensing information in these environments, airborne remote sensing instruments with much higher resolution must be used. While airborne hyperspectral instruments have been used in lake based studies, where the areas are too small to be reliably imaged by satellites [*Bukata et al.*, 2001; *Kallio et al.*, 2001], they have not been applied to the coastal ocean, with as much frequency. In this paper, using an extensive photochemical apparent quantum yield study that was performed in the area around Sapelo Island, Georgia USA from November 2008 to September 2009 [*Reader and Miller*, 2011] (see Chapter 3 for details), we present the adaptation of AISA hyperspectral airborne remote sensing imagery to estimate photochemical production in the tidal Duplin River, USA.

2. Methods

2.1 Adaptation of Hyperspectral Imagery for Remote Estimates of Photochemical Processes

In June 2006, airborne hyperspectral imagery was collected over the Duplin River, a tidal tributary to Doboy Sound on the coast of Georgia, USA (Figure 5.1). The imagery was collected by the University of Nebraska-Lincoln's Center for Advanced Land Management Information Technologies (CALMIT), using an AISA Eagle Visible-Near-Infrared imaging instrument, with 1 m^2 resolution along the length of the Duplin River. Data collection occurred during mid-day conditions at low-water tidal conditions. The AISA Eagle instrument is a pushbroom sensor with a spectral range of 400 nm to 970 nm, and can collect up to 244 spectral bands at once with a spectral resolution of up to 2.9 nm. Atmospheric corrections were performed by CALMIT using the Environment for Visualizing Images' Quick Atmospheric Correction (QUAC, ENVI, ITT Visual Information Systems). The 6 bands that overlapped most closely with the 6 corresponding bands of the SeaWiFS satellite were extracted from the entire data set for further processing, using ENVI, see Table 5.1 for waveband details. Simultaneous ocean colour measurements were taken in the Duplin River and Doboy Sound using a modified MicroSAS Ocean Colour Radiometer (Satlantic) which includes above surface downwelling ultraviolet sensors (305, 325, 340 and 380 nm) as well as upwelling and downwelling visible sensors (412, 443, 490, 510, 555, 670 and 683 nm), during the hyperspectral flyover. The brightness of the corrected imagery was scaled by 10 to ensure that the remote sensing data was in the same order of magnitude as the in situ ocean color measurements.

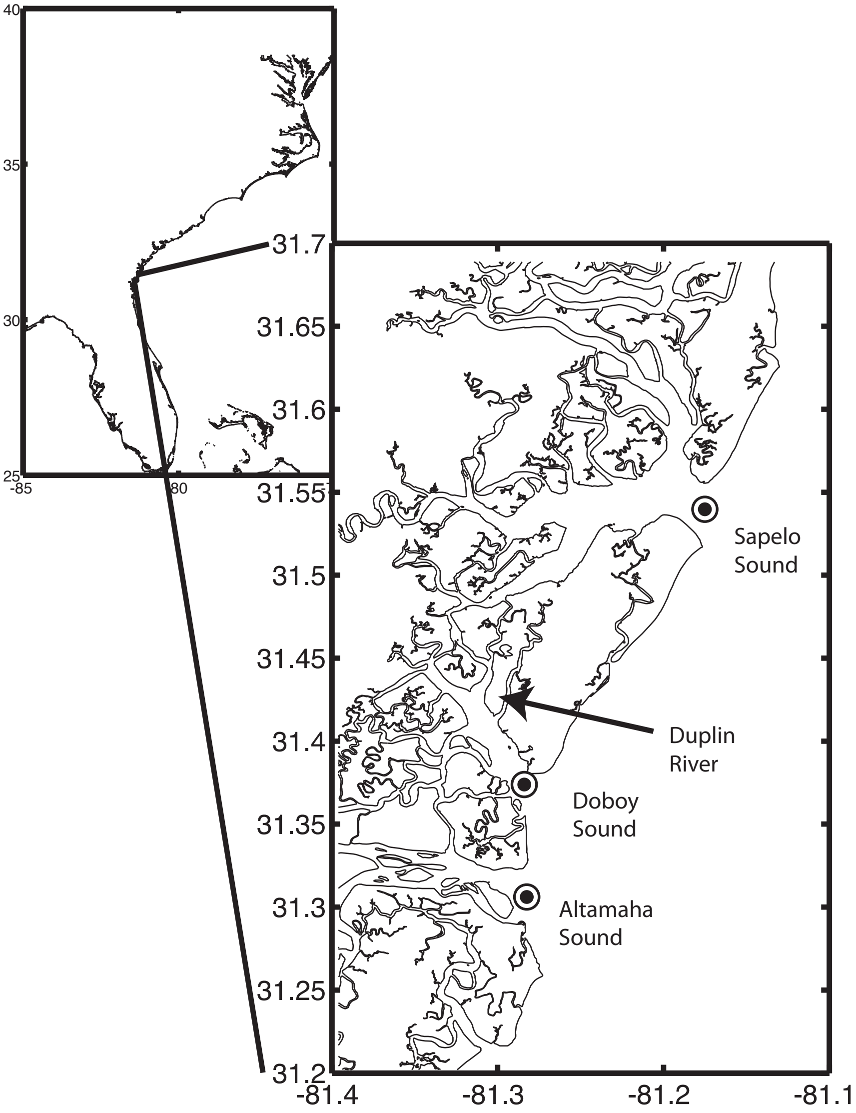

Figure 5.1: Sample sites for the seasonal study

Table 5.1: Wavebands and bandwidths (Full width half maximum) for both the SeaWiFS and AISA sensor used in the SeaUV algorithm.

SeaWiFS wave band (nm)	**Sea WiFS bandwidth**	**AISA wave band (nm)**	**AISA bandwidth (nm)**
412	20	409.910004	8.760000
443	20	445.230011	9.040000
490	20	490.420013	9.040000
510	20	508.500000	9.040000
555	20	553.890015	9.280000
670	20	666.390015	9.400000

The SeaUV algorithm [*Fichot et al.*, 2008] retrieves the attenuation of light in the water column from visible remote sensing reflectance data, using a principle component analysis approach. The algorithm was originally developed for use with SeaWiFS satellite data, using a large data set of coastal and open ocean waters. In order to adapt the algorithm for use in darker estuarine waters, it was adapted with a dark water data set, compiled from samples collected in the vicinity of Sapelo Island, GA [*Cao et al.*, 2010; *Miller and Fichot*, 2009]. Briefly, the addition of the dark water dataset changed the coefficients of the linear regression of the principle components used to determine attenuation, improving the retrieval of K_D in dark waters, see Figure 5.2. The original linear regression coefficients used derive K_D from the 4 first principle components of SeaUV as well as the newly derived coefficients can be seen in Table 5.2 for comparison. After updating the PC values, the subset 6 bands from the hyperspectral data set were processed using the dark-corrected SeaUV algorithm to determine the downwelling attenuation (K_D) at 320 nm. Absorption by CDOM accounts for 68% of attenuation at 320 nm [*Fichot and Miller*, 2010], and from this the absorption coefficient of CDOM at 320 nm can be calculated. The UV CDOM absorption spectrum important for photochemical calculations is derived using the equation

$$a_g(\lambda) = a_g(320) * e^{-0.00194*(320-\lambda)}. \tag{5.1}$$

The slope coefficient used here (i.e. 0.00194) was derived over the full UV-visible absorption spectrum from a large coastal water data set [*Fichot and Miller*, 2010].

The photochemical production of CO and CO_2 in the surface layer was determined following the methodology of Fichot and Miller [2010], using the photoproduction equation

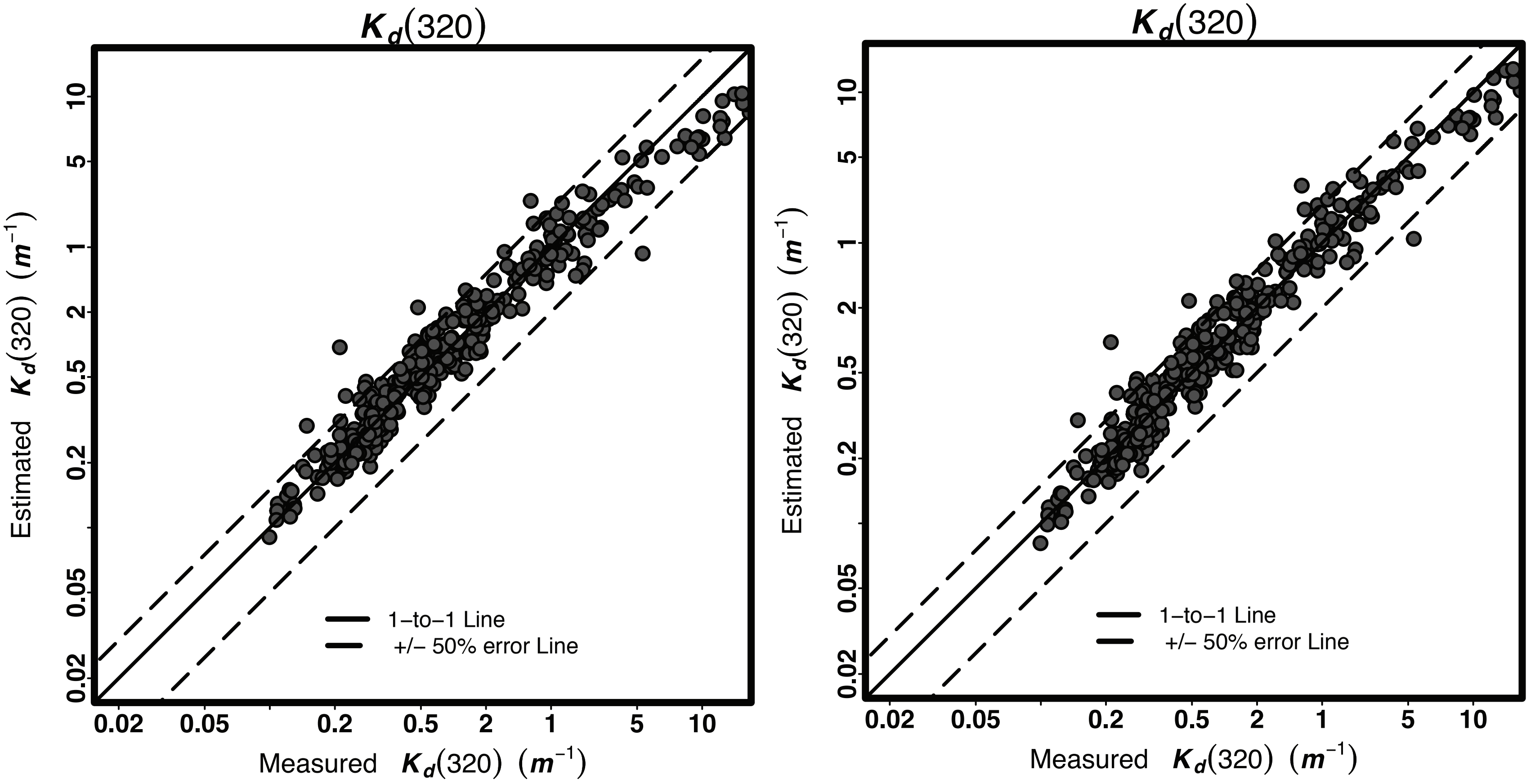

Figure 5.2: K_d320 for the original SeaUV algorithm (Left) and for the dark-waterupdated algorithm (Right).

Table 5.2: Regression coefficients used in SeaUV for the original data set [*Fichot et al.*, 2008] and for the dark water updated data set [*Cao et al.*, 2010; *Miller and Fichot*, 2009]

		α	**β**	**γ**	**δ**	**ε**
Original SeaUV	ln[K_D(320)]	-0.5764	0.0750	-0.7197	-0.4112	1.2952
	ln[K_D(340)]	-0.8766	00674	-0.7685	-0.3879	1.0123
	ln[K_D(380)]	-1.4305	0.0394	-0.8081	-0.2689	0.4616
	ln[K_D(412)]	-1.7083	0.0357	-0.8256	-0.1311	-0.2447
	ln[K_D(443)]	-1.9117	0.0312	-0.8140	-0.0169	-0.7123
	ln[K_D(490)]	-2.2299	0.0149	-0.7661	0.1780	-0.8206
Dark updated SeaUV	ln[K_D(320)]	0.0743	-0.7658	-0.4335	1.4477	-0.5701
	ln[K_D(340)]	0.07065	-0.80479	0.38721	1.18508	-0.86258
	ln[K_D(380)]	0.004498	-0.85182	-0.26958	0.73362	-1.41074
	ln[K_D(412)]	0.04526	-0.86931	-0.13252	-0.12886	1.68263
	ln[K_D(443)]	0.042389	-0.857948	0.004547	-0.230141	-1.881223
	ln[K_D(490)]	0.03137	-0.81894	0.16062	-0.25108	-2.18774

$$\int_{290}^{490} P(\lambda) = E_{0d}(\lambda) * a_g(\lambda) * AQY(\lambda) \tag{5.2}$$

where P is photoproduction in mol/m^3/day, E_{0d} is the downwelling scalar irradiance in mol photons/m^2/day, a_g is the absorption coefficient of CDOM in m^{-1}, and the AQY is the unitless apparent quantum yield, defined as

$$AQY(\lambda) = \frac{mol\ CO\ (or\ CO_2)\ formed\ (\lambda)}{mol\ photons\ absorbed\ by\ CDOM\ (\lambda)}\ . \tag{5.3}$$

In order to present reasonable surface layer photochemical rates in these dark waters, the photoproduction was scaled to mol/cm^3/day. Downwelling scalar irradiance was calculated with the STAR model (System for Transfer of Atmospheric Radiance, University of Munich, [*Ruggaber et al.*, 1994]), using a 10 year climatology for the month of June and TOMS data to estimate atmospheric ozone. The methodology for this is detailed in Fichot and Miller [2010].

The AQY spectra used in these calculations were derived by taking the mean of the three fitting coefficients (m_1, m_2, and m_3, Equation 3.6) from the CO and CO_2 AQY data sets, respectively (see Chapter 3 of this dissertation). Briefly, 38 paired CO and CO_2 AQY spectra were compiled from the area around Sapelo Island, Georgia, from November 2008 to September 2009. This data set covers a range of tidal and seasonal conditions, and is the largest paired CO and CO_2 AQY data set to date.

3. Results

3.1 SeaUV Update for Dark Waters

The SeaUV algorithm [*Fichot et al.*, 2008] was originally developed with a wide range of open ocean and coastal water types. Matched in situ measurements of ocean color (remote sensing reflectance, R_{rs}), attenuation (K_D) and CDOM absorption coefficients (a_g) allowed the development of an algorithm that retrieves ultraviolet attenuation in the water column using satellite remote sensing reflectance measurements in the visible spectrum. The algorithm performed well in the waters used to develop the algorithm. When applying the algorithm to darker coastal waters, such as those found in the estuaries and tidal inlets along the South Atlantic Bight, the original algorithm underestimated the attenuation of UV light, see Figure 5.2a. Presumably this was due to a lack of representation of these types of dark water in the original training dataset. Because the SeaUV model is empirical and is based on a principle component analysis, it is straightforward to improve the retrieval of attenuation coefficients, K_D, by retraining with an extended data set containing data for darker waters. This was done by using the original dataset, together with 50 additional samples from within and around the Duplin River estuary, and Doboy Sound (Figure 5.1). Samples were taken both during the period of the hyperspectral flyover and during the following year. The addition of these data to the training dataset improved the retrieval of K_D in darker waters without diminishing the retrieval of K_D from the clearer of the coastal and open ocean. The results of retraining the algorithm can be seen in Figure 5.2.

3.2 Retrieving K_D from airborne remote sensing data

The SeaUV algorithm was originally designed to work with SeaWiFS sensor data which uses a spectrometer with 8 discrete wave bands, as detailed in Table 5.1. While the AISA instrument does not have exactly overlapping wave bands, they were all within 3 nm. The bandwidths of the two detectors ensured that there was overlap between the AISA bands used. By assuming a smooth spectral shape for the remote sensing reflectance spectrum the offsets caused by the small wavelength differences between the paired wave bands of the two instruments are assumed to be negligible. The dark-water updated algorithm was applied to the brightness corrected AISA image, and K_D was successfully retrieved (Figure 5.3). Because of very high attenuation numbers in the Duplin River, light penetration is less than 1m at all sites, and as such, depth resolved photoproduction, as can be done with the SeaUV algorithm in clearer waters, was not calculated. Only $K_D(320)$ was retrieved for use in estimating CDOM absorption at 320 nm according to the methodology in Fichot and Miller [2010]. The map of a_g320 derived from the AISA data can be seen in Figure 5.4.

3.3 Photoproduction of CO and CO_2

The photoproduction calculated from the AISA image with mean AQY spectra determined from Reader and Miller [2011] (Chapter 3, this dissertation) for both products, as can be seen in Figure 5.5. The uncertainty of using a mean AQY for CO adds +/- 12.7% error to the calculation, while the uncertainty of using a mean AQY for CO_2 adds +/- 33.6% error to the calculation. When adding the two photoproduction terms together (5.6) the uncertainty in CO_2 overwhelms that of CO, and errors for the summed carbon transformation can be considered to be the same as CO_2.

4. Discussion

The adaptation of hyperspectral remote sensing imagery to the dark-water updated SeaUV algorithm allows for the estimation of photochemical production in estuarine environments. Spectral AQY accuracy remains a critical component in the accurate prediction of photochemical reaction rates from optical data. While the AQY for CO is fairly well constrained for these waters and the error is relatively minimal (12.7%), the AQY for CO_2 is less well constrained [*Reader and Miller*, 2011]. Analytical difficulties

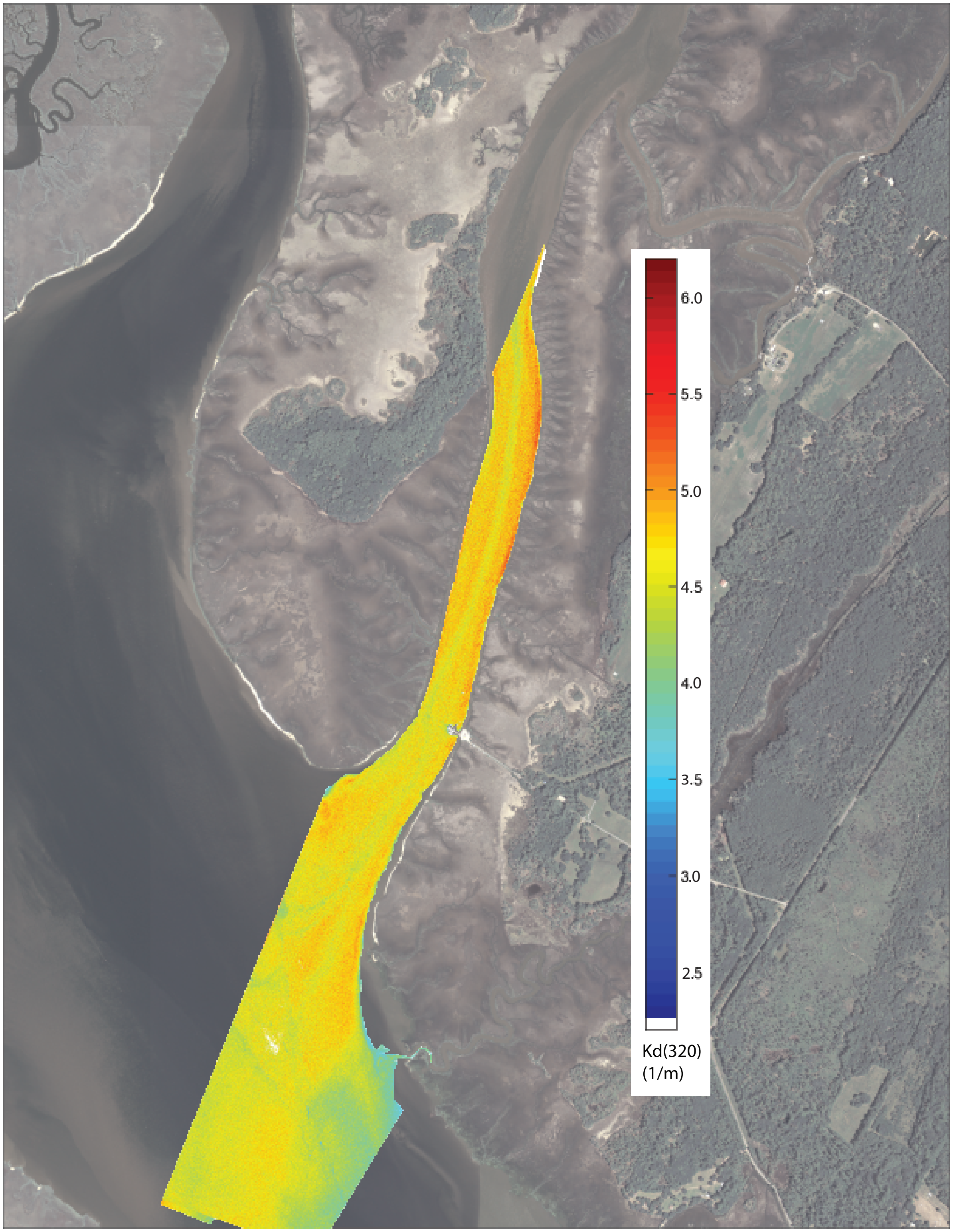

Figure 5.3: Diffuse attenuation at 320nm for the Duplin River

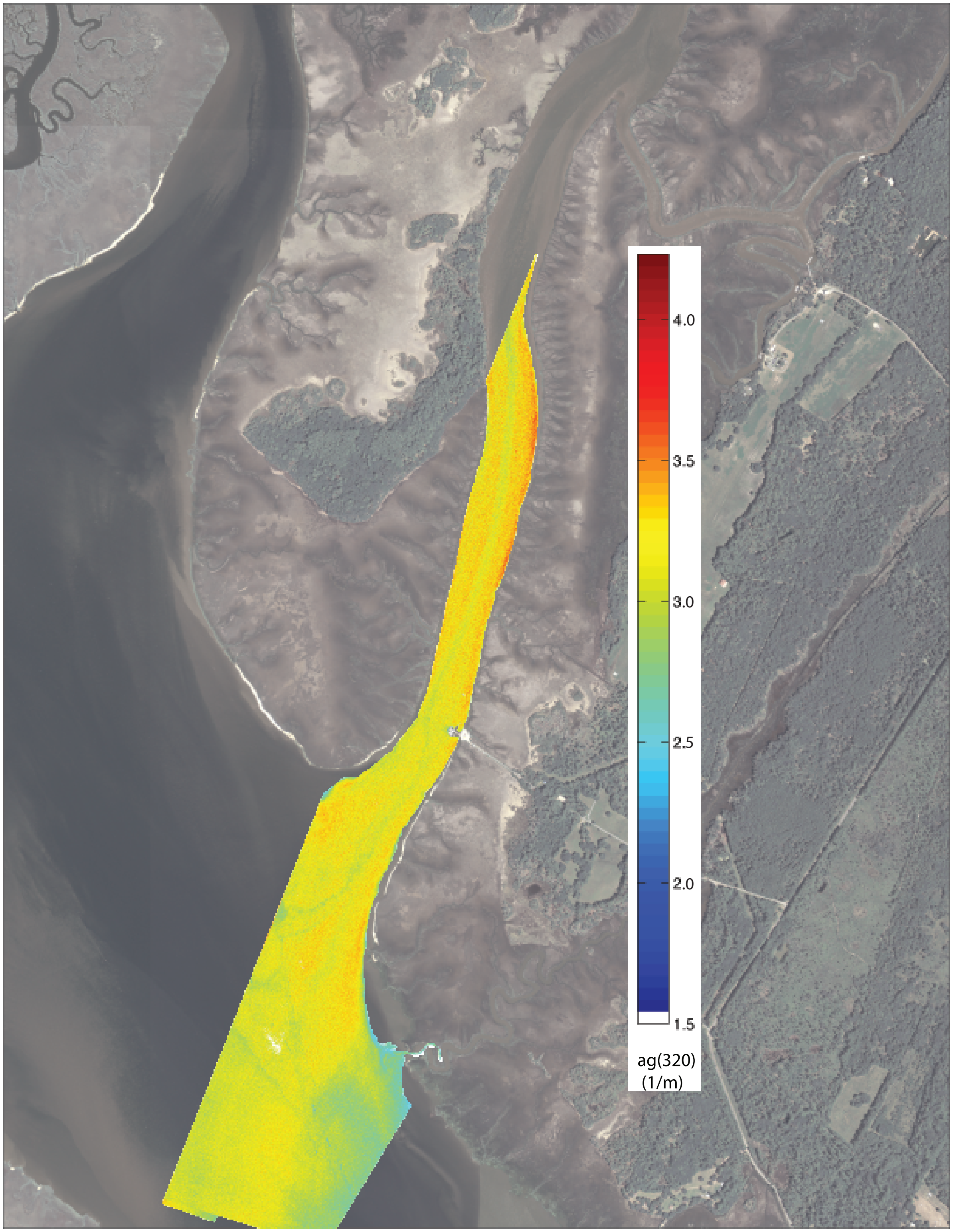

Figure 5.4: Map of $a_g(320)$ for the Duplin River

in measuring photochemically produced CO_2 has contributed to a higher uncertainty for extrapolated photochemical calculations in this and other work [*Johannessen and Miller*, 2001; *White et al.*, 2010]. The CO2 AQY data set contained in this dissertation is the most extensive available anywhere, and as such can be used to calculate CO_2 photoproduction with the best constraints for the seasonal and spatial variability of AQY to date.

Estuarine environments, while relatively small, are particularly dynamic and the use of airborne remote sensing methods allows measurements to be made across large areas, potentially capturing multiple scenes within short timeframes. With the recent retirement of the multiband SeaWiFS instrument, multiband algorithms such as SeaUV will require adaptation to accomodate the recent shift towards hyperspectral imagery, a trend that will further increase the spectral information obtained by remote sensing instruments. Increased resolution such as is available with the aircraft operated AISA Eagle and other such instruments will further increase information on the variability of coastal systems. Spaceborne radiometers have been developed with higher spectral and spatial resolution, such as the Hyperspectral Imager for the Coastal Ocean (HICO) aboard the International Space Station (124 spectral bands and 100 m^2 spatial resolution), and will soon be common in ocean color data collection particularly in coastal waters. The increase in optical information in the coastal ocean is likely to reveal small-scale structure relevant to photochemical processes that previously was not available to remote sensing studies.

With the increase of information, especially small-scale structure, the current in situ ocean color data coverage will be lacking. It will become increasingly important to

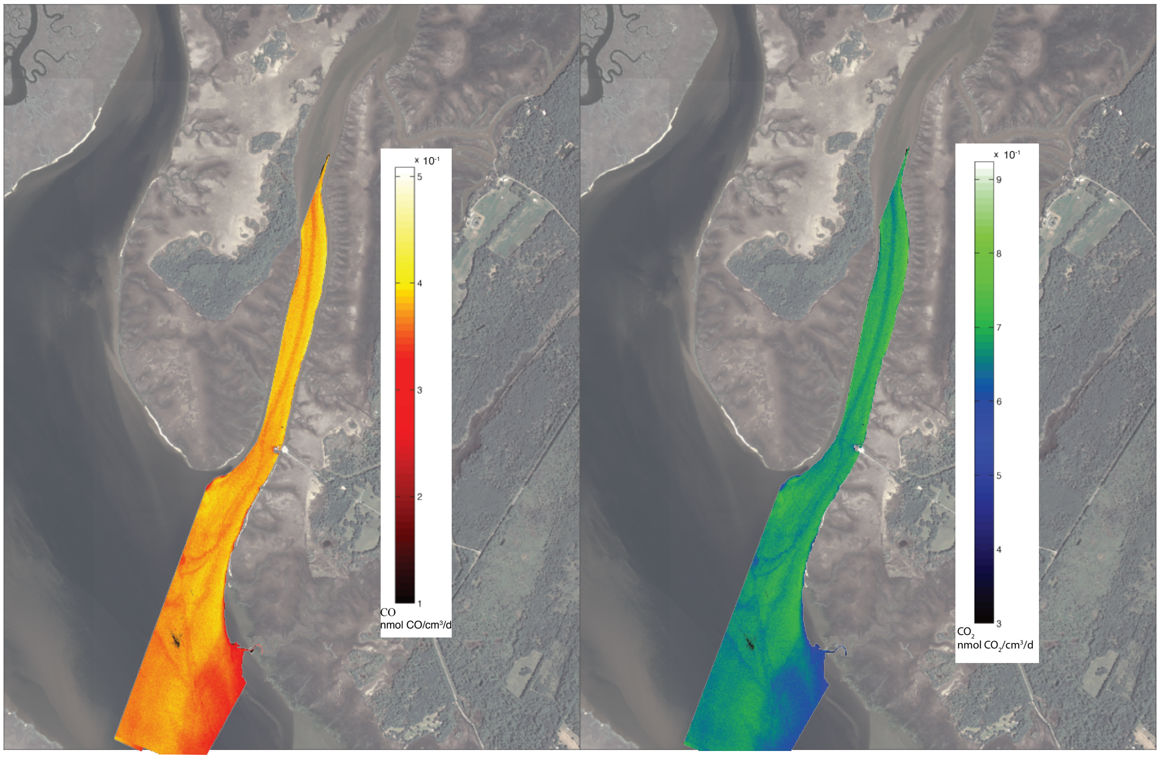

Figure 5.5 CO and CO_2 surface layer photoproduction in the Duplin River

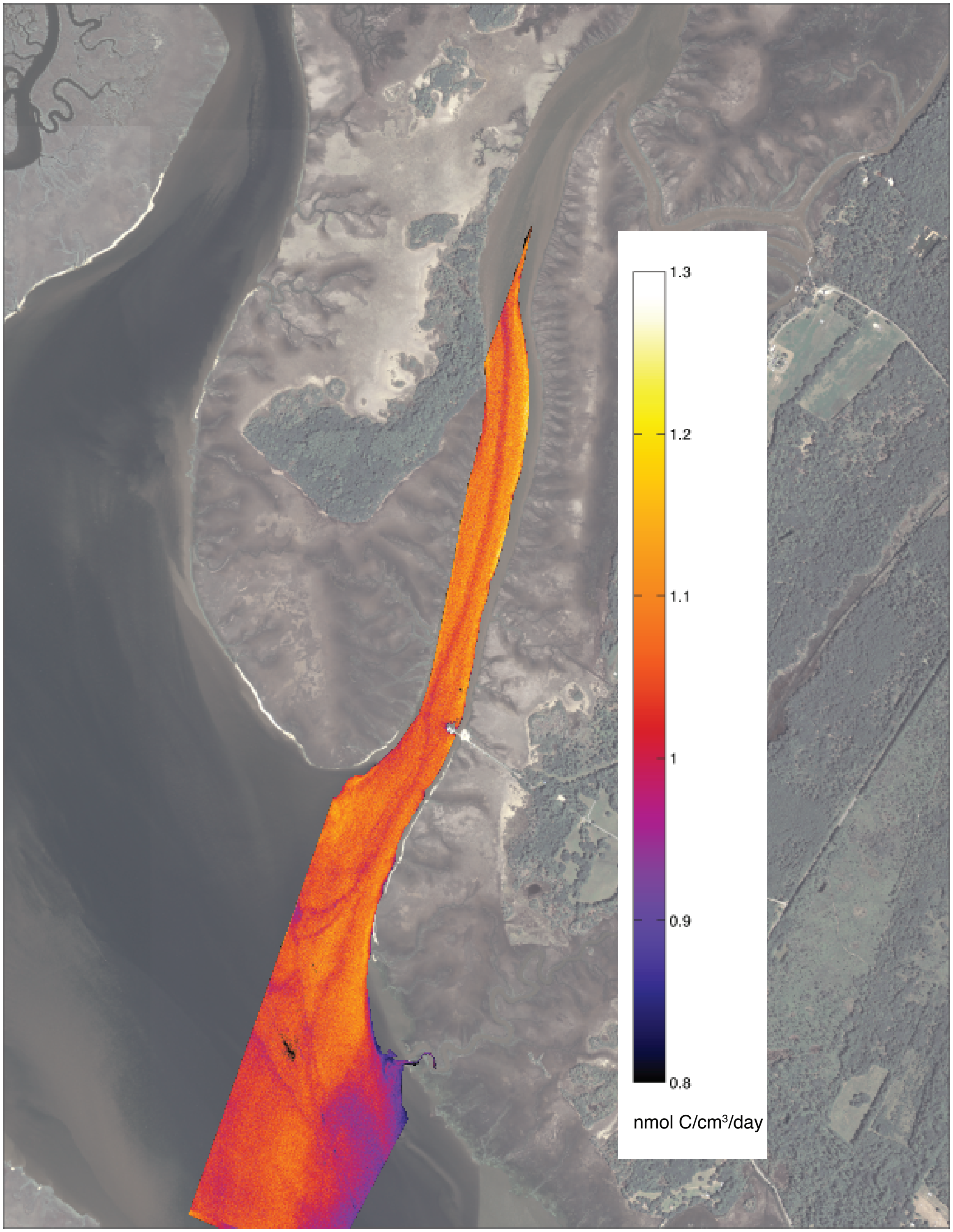

Figure 5.6: Total CO and CO_2 surface layer photoproduction in the Duplin River

ground truth hyperspectral formats with fine scale spatial and temporal data. As can be seen from the maps in Figures 5,3, 5.4, 5.5, and 5.6 the hydrodynamic structure of the Duplin River on an outgoing tide is apparent in the high resolution AISA imagery. For photochemical products such as CO, published evidence suggests that the apparent quantum yield spectra will show relatively little variability across water types [*Reader and Miller*, 2011; *Ziolkowski and Miller*, 2007] (see Chapter 3, this dissertation) but this does not seem to be the case for CO_2 [*Johannessen and Miller*, 2001; *Reader and Miller*, 2011; *White et al.*, 2010] (see Chapter 3, this dissertation) which appears to vary greatly. In a situation such as remote sensing of the open ocean with kilometer scale resolution, such variability may not pose a large problem for estimating the magnitude of photochemical processes. In smaller scale areas with fine resolution remote sensing data, however, this variability will become increasingly important.

The increased spectral information available with hyperspectral instruments is also likely to reveal intricacies in the coastal system that previously were difficult, if not impossible to sense remotely. Because the interaction of CDOM with solar radiation is the driver for most photochemical reactions in the ocean, the increased spectral resolution will likely lead to deeper insight concerning the variability of photochemical processes and their drivers in coastal systems, provided the effort to collect appropriate in situ data is also made. The potential of hyperspectral imagery is great, and will be harnessed in the next round of remote sensing algorithm development required for modeling coastal processes.

Acknowledgements

The authors would like to thank J. F. Schalles for the hyperspectral imagery.

References

Bukata, R. P., D. V. Pozdnyakov, J. H. Jerome, and F. J. Tanis (2001), Validation of a radiometric color model applicable to optically complex water bodies, *Remote Sensing of Environment*, *77*(2), 165-172.

Cai, W. J. (2011), Estuarine and Coastal Ocean Carbon Paradox: CO2 Sinks or Sites of Terrestrial Carbon Incineration?, *Annual Review of Marine Science*, *3*, 123-145.

Cao, F., H. E. Reader, and W. L. Miller (2010), RETRAINING THE SEAUV/SEAUVC MODEL FOR IMPROVED ALGORITHM OF DARK, INSHORE WATERS FROM THE GEORGIA COAST, USA, paper presented at Ocean Optics XX, Anchorage, Alaska, USA.

Carder, K. L., F. R. Chen, Z. P. Lee, S. K. Hawes, and D. Kamykowski (1999), Semi-analytic MODIS algorithms for chlorophyll a and absorption with bio-optical domains based on nitrate depletion temperatures, *Journal of Geophysical Research-Oceans*, *104*(C3), 5403-5421.

Carder, K. L., S. K. Hawes, A. Baker, R. C. Smith, R. G. Steward, and B. G. Mitchell (1991), Relectrance model for quantifying chlorophyll a in the presence of productivity degradation products, *Journal of Geophysical Research*, *96*(20599-20611).

Clark, C. D., L. P. Litz, and S. B. Grant (2008), Salt marshes as a source of chromophoric dissolved organic matter (CDOM) to Southern California coastal waters, *Limnology and Oceanography*, *53*(5), 1923-1933.

Daniel, J. S., and S. Solomon (1998), On the climate forcing of carbon monoxide, *Journal of Geophysical Research-Atmospheres*, *103*(D11), 13249-13260.

Fichot, C. G., and W. L. Miller (2010), An approach to quantify depth-resolved marine photochemical fluxes using remote sensing: Application to carbon monoxide (CO) photoproduction, *Remote Sensing of Environment*, *114*(7), 1363-1377.

Fichot, C. G., S. Sathyendranath, and W. L. Miller (2008), SeaUV and SeaUV(C): Algorithms for the retrieval of UV/Visible diffuse attenuation coefficients from ocean color, *Remote Sensing of Environment*, *112*(4), 1584-1602.

Fishman, J., and W. Seiler (1983), CORRELATIVE NATURE OF OZONE AND CARBON-MONOXIDE IN THE TROPOSPHERE - IMPLICATIONS FOR THE TROPOSPHERIC OZONE BUDGET, *Journal of Geophysical Research-Oceans and Atmospheres*, *88*(NC6), 3662-3670.

Guo, X. H., M. H. Dai, W. D. Zhai, W. J. Cai, and B. S. Chen (2009), CO2 flux and seasonal variability in a large subtropical estuarine system, the Pearl River Estuary, China, *Journal of Geophysical Research-Biogeosciences*, *114*.

Jiang, L. Q., W. J. Cai, and Y. C. Wang (2008a), A comparative study of carbon dioxide degassing in river- and marine-dominated estuaries, *Limnology and Oceanography*, *53*(6), 2603-2615.

Jiang, L. Q., W. J. Cai, R. Wanninkhof, Y. C. Wang, and H. Luger (2008b), Air-sea CO2 fluxes on the US South Atlantic Bight: Spatial and seasonal variability, *Journal of Geophysical Research-Oceans*, *113*(C7).

Johannessen, S. C., and W. L. Miller (2001), Quantum yield for the photochemical production of dissolved inorganic carbon in seawater, *Marine Chemistry*, *76*(4), 271-283.

Johannessen, S. C., M. A. Pena, and M. L. Quenneville (2007), Photochemical production of carbon dioxide during a coastal phytoplankton bloom, *Estuarine Coastal and Shelf Science*, *73*(1-2), 236-242.

Jorda, G., D. Gomis, and M. Talone (2011), The SMOS L3 Mapping Algorithm for Sea Surface Salinity, *Ieee Transactions on Geoscience and Remote Sensing*, *49*(3), 1032-1051.

Kallio, K., T. Kutser, T. Hannonen, S. Koponen, J. Pulliainen, J. Veps‰l‰inen, and T. Pyh‰lahti (2001), Retrieval of water quality from airborne imaging spectrometry of various lake types in different seasons, *The Science of The Total Environment*, *268*(1-3), 59-77.

Law, C. S., T. N. Sjoberg, and R. D. Ling (2002), Atmospheric emission and cycling of carbon monoxide in the Scheldt Estuary, *Biogeochemistry*, *59*(1-2), 69-94.

Ludwig, W., J. L. Probst, and S. Kempe (1996), Predicting the oceanic input of organic carbon by continental erosion, *Global Biogeochemical Cycles*, *10*(1), 23-41.

Miller, W. L., and R. G. Zepp (1995), PHOTOCHEMICAL PRODUCTION OF DISSOLVED INORGANIC CARBON FROM TERRESTRIAL ORGANIC-MATTER - SIGNIFICANCE TO THE OCEANIC ORGANIC-CARBON CYCLE, *Geophysical Research Letters*, *22*(4), 417-420.

Miller, W. L., and C. G. Fichot (2009), Training the SeaUV/SeaUVc algorithms for improved inshore estimates of UV optics and photochemical and photobiological rate calculations, in *ASLO Aquatic Sciences*, edited, Nice, France.

Minor, E. C., B. L. Dalzell, A. Stubbins, and K. Mopper (2007), Evaluating the photoalteration of estuarine dissolved organic matter using direct temperature-resolved mass spectrometry and UV-visible spectroscopy, *Aquatic Sciences*, *69*(4), 440-455.

Mopper, K., and D. J. Kieber (2002), Photochemistry and the Cycling of Carbon, Sulfur, Nitrogen and Phosphorus, in *Biogeochemistry of Marine Dissolved Organic Matter*, edited by D. A. Hansell and C. A. Carlson, pp. 456 - 508, Academic Press, San Diego.

Mopper, K., X. L. Zhou, R. J. Kieber, D. J. Kieber, R. J. Sikorski, and R. D. Jones (1991), PHOTOCHEMICAL DEGRADATION OF DISSOLVED ORGANIC-CARBON AND ITS IMPACT ON THE OCEANIC CARBON-CYCLE, *Nature*, *353*(6339), 60-62.

Osburn, C. L., L. Retamal, and W. F. Vincent (2009), Photoreactivity of chromophoric dissolved organic matter transported by the Mackenzie River to the Beaufort Sea, *Marine Chemistry*, *115*(1-2), 10-20.

Reader, H. E., and W. L. Miller (2011), Variability of carbon monoxide and carbon dioxide apparent quantum yield spectra in three coastal estuaries of the South Atlantic Bight, *In Prep*.

Ruggaber, R., R. A. Dlugi, and T. Nakajima (1994), Modelling of radiation quantities and photolysis frequencies in the troposphere, *Journal of Atmospheric Chemistry*, 171-210.

Seiler, W., and J. Fishman (1981), THE DISTRIBUTION OF CARBON-MONOXIDE AND OZONE IN THE FREE TROPOSPHERE, *Journal of Geophysical Research-Oceans and Atmospheres*, *86*(NC8), 7255-7265.

Stubbins, A., G. Uher, C. S. Law, K. Mopper, C. Robinson, and R. C. Upstill-Goddard (2006), Open-ocean carbon monoxide photoproduction, *Deep-Sea Research Part Ii-Topical Studies in Oceanography*, *53*(14-16), 1695-1705.

Tolli, J. D., S. M. Sievert, and C. D. Taylor (2006), Unexpected diversity of bacteria capable of carbon monoxide oxidation in a coastal marine environment, and contribution of the Roseobacter-associated clade to total CO oxidation, *Applied and Environmental Microbiology*, *72*(3), 1966-1973.

Valiela, I. (1995), *Marine Ecological Processes*, 686 pp., Springer, New York.

White, E. M., D. J. Kieber, J. Sherrard, W. L. Miller, and K. Mopper (2010), Carbon dioxide and carbon monoxide photoproduction quantum yields in the Delaware Estuary, *Marine Chemistry*, *118*(1-2), 11-21.

Zafiriou, O. C., S. S. Andrews, and W. Wang (2003), Concordant estimates of oceanic carbon monoxide source and sink processes in the Pacific yield a balanced global "blue-water" CO budget, *Global Biogeochemical Cycles*, *17*(1).

Zafiriou, O. C., H. X. Xie, N. B. Nelson, R. G. Najjar, and W. Wang (2008), Diel carbon monoxide cycling in the upper Sargasso Sea near Bermuda at the onset of spring and in midsummer, *Limnology and Oceanography*, *53*(2), 835-850.

Ziolkowski, L. A., and W. L. Miller (2007), Variability of the apparent quantum efficiency of CO photoproduction in the Gulf of Maine and Northwest Atlantic, *Marine Chemistry*, *105*(3-4), 258-270.

CHAPTER 6

CONCLUSIONS

The coastal ocean is a dynamic area with high in situ production, and serves as the transition zone between the continents and the open ocean. Much of the dissolved organic carbon (DOC) reaching the coastal ocean has not been previously been exposed to strong sunlight and its potential for photochemical reactivity is high. To properly assess the contribution of organic photochemistry to DOC cycles in the coastal ocean, a thorough understanding of the variability in photochemical efficiency and the related contributing factors is required.

1. Optics and Photochemical Efficiency

The first law of photochemistry states that a photon must be absorbed in order for a photochemical reaction to occur. Accordingly, to perform quantitative photochemical calculations, the total absorption of photons at all wavelengths active for photochemistry must be known exactly. Ultraviolet radiation (UVR) generally drives most photochemical processes in the surface ocean. The main UV absorber in these waters, chromophoric dissolved organic matter (CDOM), is most often considered to be a single absorbing moiety when, in fact, it is an optical measurement that integrates all dissolved substances absorbing sunlight. While the UV-visible absorption spectrum of CDOM can be easily measured in the laboratory for discrete samples, large-scale calculations generally require the entire CDOM absorption spectrum to be modeled from limited optical information. The exponential shape most often used to describe CDOM in the literature results in modeling of the spectrum with data from a specified range of wavelengths. If the wavelength range used to model the CDOM absorption spectrum is significantly different from the active wavelengths for photochemistry (i.e. using only visible wavelengths) significant error can be introduced into photochemical calculations. Using a spectral slope determined over UV wavelengths is preferable when modeling CDOM absorption for use in photochemical calculations, as seen in Chapter 2 of this dissertation. When visible data is the only data available, such as when using CDOM absorption values in the blue wavelengths, such as those obtained using remote sensing techniques, the hyperbolic model discussed in Chapter 2 helps to minimize error in the UVR because the hyperbolic shape has an inherently sharper inflection towards the UV than the exponential model that is often applied in the literature.

After the initial photon absorption by the CDOM, one must also know the efficiency of the photochemical reaction, in order to model it. The efficiency of a photochemical reaction in natural waters is defined by its Apparent Quantum Yield (i.e. AQY). Direct oxidation of DOC to CO and CO_2 are two relatively efficient photochemical pathways. In the Georgia estuaries studied in this dissertation, photochemical production of CO is enhanced relative to previous studies. Because of this enhanced photochemical efficiency of CO, the ratio of CO_2 to CO photoproduction seen in this study (Chapter 3) is lower than previous reports suggest. Together, these two photochemical species can account for up to 4% of the loss of DOC as it transits the estuaries and inner shelf of the South Atlantic Bight, each year. While the AQY spectra were not entirely invariable throughout the course of the study, the variability in both CO and CO_2 AQYs was not driven by the optical indicators of CDOM characteristics used in this study. The drivers of photochemical efficiency variability appear to be more complex than can be derived through simple optical techniques. This data set is the largest paired CO and CO_2 AQY data set to date. The extensive nature has allowed a more thorough investigation into the variability of both photochemical species. While the drivers of the photochemistry were more complex than the optical methods employed here were able to devolve, the drivers for both CO and CO_2 photochemistry appeared to vary together, as the ratios between the two remained relatively constant for all samples. The added constraints on the CO_2:CO photochemical ratio provided by this extensive data set allow for better constraints on large scale photochemical calculations.

2. Photochemical Effect on Availability of DOC to Bacteria

Indirect photochemical mineralization of DOC can occur by altering the structure of refractory DOC so that it becomes more available to the microbial community. The effect of photochemistry on the biological lability of DOC reveals a complex system. Spectrally, spatially, and seasonally, no clear patterns emerge. Competing photochemical production and photochemical destruction processes means that photon dose and prior irradiation history are important factors to consider when discussing the effect of photochemistry on the biological lability of DOC. The current experimental design (Chapter 4) shows a net response, where over the course of the irradiation photochemically mediated transfers between labile and refractory pools, as well as direct photochemical mineralization of DOC to CO and CO_2 are all integrated together. The total photon dose has a clear effect on what result is seen, not only with spectrally integrated results, but also spectrally resolved results. The reality of changing photon doses in the surface ocean due to mixing processes becomes a relevant issue, when considering that photochemical production and destruction pathways occur at different rates and likely over different portions of the solar spectrum. The variability seen in this seasonal and spatial study, where the quantity and spectral quality of the photon flux was tightly controlled, suggests that even with improved methods, it is unlikely that applying a single AQY spectrum that is appropriate for all situations is possible. Carbon source, as well as the microbial communities, very likely have a large effect on the BLP results seen in any given experiment. The challenges to modeling the photochemical effect on the availability of carbon to biological systems are more than just the analytical constraints, but also include the complexity inherent in natural systems.

3. Estimating Photochemical Rates from Hyperspectral Remote Sensing Imagery

The dynamics of estuarine and coastal environments present challenges to satellite remote sensing instruments. Relatively small-scale changes between land and water, as well as high frequency of cloud cover make satellite remote sensing of these areas difficult. Airborne instruments can provide high spatial resolution and allow measurements across relatively large areas of estuaries, within short time frames, potentially capturing fine scale structure that was previously difficult to detect. Increased resolution such as is available with the aircraft operated AISA Eagle instrument and other such instruments can gather novel information on the optical variability of coastal systems. Spaceborne radiometers have been recently developed with higher spectral and spatial resolution such as the Hyperspectral Imager for the Coastal Ocean (HICO) aboard the International Space Station, and will soon be common in ocean color data collection. The increase in optical information in the coastal ocean is likely to reveal small scale structure relevant to photochemical processes that previously was not available to remote sensing systems.

With the recent retirement of the SeaWiFS multiband instrument, multiband algorithms will require adaptation to accommodate this recent shift towards hyperspectral imagery. With the increase of information, especially small-scale structure, current in situ ocean color coverage will be lacking. It will become increasingly important to ground truth hyperspectral formats with fine scale special and temporal data. As was evidenced in Chapter 5 of this dissertation, hydrodynamic structure of systems can easily be seen with such high resolution systems. While the photochemical evidence suggests that the AQY for CO does not vary greatly within this type of system, the CO_2 AQY does appear to exhibit greater variability (Chapter 3). In open ocean remote sensing with kilometer scale resolution, this variability may not pose a great problem for estimating the magnitude of photochemical processes. In smaller scale areas, with fine resolution remote sensing data, however, this variability will become increasingly important.

This increased spectral information available with hyperspectral instruments is also likely to reveal intricacies in the coastal system that were previously difficult, if not impossible to sense remotely. Because the interaction of CDOM with solar radiation is the driver for photochemical reactions, the increased spectral resolution could lead to deeper insight into the variability of photochemical processes and their drivers in coastal systems, provided the effort to collect appropriate in situ data is also made. The potential of hyperspectral imagery is great and will be harnessed in the next round of remote sensing algorithm development required for modeling coastal processes.

4. Future Directions

In all, for a robust assessment of the impact on photochemistry on the cycling of carbon in the coastal ocean, it is crucial to know all aspects of the system accurately. While the total area of estuaries is small compared to the total area of the open ocean, these systems are very dynamic, and influence the coastal ocean through the cycling of DOC. While the direct photochemical oxidation of DOC to CO and CO_2 can be relatively well constrained, the influence of photochemical alterations of DOC on the biological lability of DOC is a more complex problem. Future efforts should be made to assess the influence of photochemistry on BLP using a more holistic approach, by irradiating samples with the microbial community intact. This sort of approach would require less intense irradiation than used in the current study, and also would require allowing the microbial community and the DOC the opportunity to experience changing light fields, such as mixing in the open ocean allows. The emergence of techniques such as electrospray ionization Fourier transform ion cyclotron resonance mass spectrometry allow for molecular formula level characterization of DOC. Using these high resolution characterization techniques allows for a deeper understanding of what types of compounds exist in the DOC mixture. Using these techniques to probe photochemical reactions will lead to insight into the mechanisms that drive these reactions and characterize the photochemical turnover of DOC. Combining this with successive photochemical and biological degradation experiments will lead to a deeper understanding of what types of photochemical carbon transformations increase biological lability in DOC, and with that, a better understanding of the efficiency with which photochemistry makes and destroys certain types of compounds.

With improved remote sensing methods, more of the variability in the coastal system will become apparent. High spectral and spatial resolution remote sensing techniques, such as the hyperspectral instruments that are rapidly becoming more available will greatly increase the amount of information available to scientists. While carbon drivers for photochemistry beyond the absorption of CDOM are impossible to ascertain from multiband data, the possibility of more complex spectral variations in hyperspectral reflectance data being caused by different types of carbon will allow for further refining of photochemical models. Currently, the application of mean AQYs from different data sets for photochemical calculations allows for a certain amount of constraint limited to that of the data set used. With more information about the molecular-level composition of DOC, the drivers of variations of photochemical processes, and their optical signals, the potential to more accurately select an appropriate AQY for application to a remote sensing scene exists, but only with appropriate ground truth data. Combining high resolution laboratory techniques for characterization of DOC, along with high resolution techniques for remote sensing of carbon systems will provide insight into the mechanisms that drive photochemical processes in ocean, and allow for better constraints on photochemical models.

APPENDIX A

COMPARISON OF DISSOLVED OXYGEN MEASUREMENTS USING THE OCEAN OPTICS FOXY-R PROBE AND WINKLER TITRATIONS

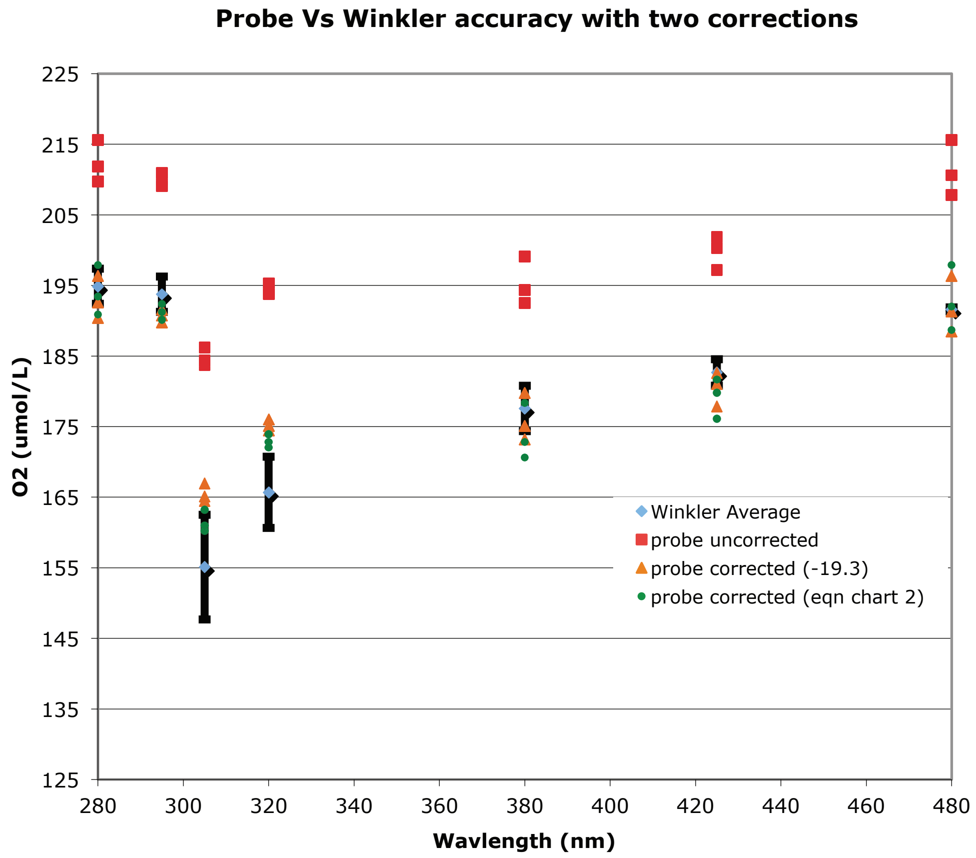

Figure A1: FOXY-R and Winkler Titration Oxygen measurements made for the same irradiation experiment. The error bars represent 1 standard deviation on the Winkler titrations. Orange triangles represent FOXY-R probe data corrected with a constant offset of -19.3 umol O_2/L, and the green circles represent the FOXY-R probe corrected with a the linear equation y =1.1801x-56.697 ($R^2 = 0.9299$) derived from the differences between each paired measurement. The constant offset was used for the calculations in this dissertation.